

# Physical Layer Cooperation: Theory and Practice

THÈSE N° 6500 (2015)

PRÉSENTÉE LE 29 MAI 2015

À LA FACULTÉ INFORMATIQUE ET COMMUNICATIONS  
LABORATOIRE D'ALGORITHMIQUE POUR L'INFORMATION EN RÉSEAUX  
PROGRAMME DOCTORAL EN INFORMATIQUE ET COMMUNICATIONS

ÉCOLE POLYTECHNIQUE FÉDÉRALE DE LAUSANNE

POUR L'OBTENTION DU GRADE DE DOCTEUR ÈS SCIENCES

PAR

Ayan SENGUPTA

acceptée sur proposition du jury:

Prof. E. Telatar, président du jury  
Prof. C. Fragouli, directrice de thèse  
Prof. S. Diggavi, rapporteur  
Prof. R. Urbanke, rapporteur  
Prof. I.-H. Wang, rapporteur



ÉCOLE POLYTECHNIQUE  
FÉDÉRALE DE LAUSANNE

Suisse  
2015



*To my father...*

*...and to all who have made me smile.*



# Acknowledgements

I begin by extending my heartfelt gratitude and respect to my adviser, Professor Christina Fragouli. In addition to her academic and research excellence, it has been her ever-enthusiastic, positive-thinking and supportive personality that has made this research experience memorable. I have been really lucky to have an adviser like Christina.

I have also had the privilege of working with Professor Suhas Diggavi on various occasions, and I have had the most enriching experiences in the process. His way of thinking about and approaching research problems is something that has really inspired me. I have learnt a lot from Suhas, and like Christina, he is one of the kindest and most supportive people I have come across.

During my Ph.D, I have also had the opportunity to collaborate with two outstanding postdoctoral scholars—Dr. I-Hsiang Wang and Dr. Melissa Duarte, who have since gone on to excel in acclaimed academia and industry positions. The countless number of times I would knock on I-Hsiang’s door to ask even the most trivial of questions, and the patience and encouragement with which he would help me along, is something I will always remember. Working with Melissa on the systems projects has surely been a highlight of my research experience at EPFL. Her unmatched skills with software radios, outstanding organization, a bounty of kindness and a heart of gold, made for an experience that is truly one-of-a-kind.

Then, of course, there is Siddhartha Brahma. My friend, philosopher, guide, collaborator—perhaps a lot more that escapes my mind at this moment. Ever since we started work at EPFL together, he has been someone I have always turned to: a pillar of support, an absorber and filter for my oftentimes inchoate and naive ideas (research and otherwise), the most wonderful companion for my nomadic sojourns, a bank of knowledge that never ceases to fascinate, and most of all, a human being par excellence—he is more than words can describe. He will always be a part of my best memories in life.

I would also like to thank the outstanding people at IPG and ARNI in EPFL, who help to nurture a stimulating and congenial research environment. Professor Emre Telatar, Professor Rüdiger Urbanke, Dr. Olivier Leveque and Dr. Nicolas Macris are among the most knowledgeable academicians in their fields; yet, they are also the nicest and most helpful people around. I will always miss this great work environment at EPFL, no matter where my life takes me.

IPG and ARNI are indeed blessed with the most amazing people in Françoise, Muriel and Damir. I have rarely come across someone as helpful and nice as Françoise, and

## Acknowledgements

---

Damir's skills with computers (and other geeky stuff!) is second-to-none. I will miss going upstairs and having a chat with these amazing people from time to time.

I had a wonderful time sharing office with Saeid Haghighatshoar over the last 4 years, and found a really close friend in him. As inspired as I was with his brilliance, his insights on diverse topics ranging from psychology to world-affairs made office time something to look forward to.

I also enjoyed interacting with the vastly talented and friendly researcher colleagues in IPG. My special thanks to Marc D. (and Dr. Nicolas Macris) for their help with the French translation of the thesis abstract.

Over the years, we had developed into a very close-knit group at ARNI, and each and every one of the ARNI members, past and present, share a very close bonding among themselves. I had a great time knowing and getting to be friends with Mahdi, Lorenzo, Javad, Shirin, Marios and Laszlo.

Of course, there are two more people from ARNI who I wish to make special mentions of. Emre Atsan and Iris Safaka. They are among the very best friends I have ever made in life. There is so much I have shared with Emre and Iris, so much unconditional support I have received, the wonderful times I have been part of, and so so much more that I will forever be thankful for. Wherever life takes us, I hope we will always get to meet, and relive the wonderful times we shared.

In the course of my 4 years at EPFL, I have been very privileged to meet and become friends with the most amazing people from Greece—Christina, Sofia, Manos, Matt, Panagiotis, Iraklis and others would always have a welcoming smile on their face whenever I met them, and the warmth, closeness and lively spirit associated with their culture has left a lasting impression on me.

I also take this opportunity to thank my best friends from school and college—Riddhiman, Praveen, Diptesh and Arnab. In my best times and worst, in joys and sorrow, in confusion and clarity, they have always stood by me and never let me feel alone; never let me feel down. Over these years, I have rediscovered my childhood best friend Riddhiman in so many ways: he has been my confidante, one of my biggest supports in my toughest hours, and in stark contrast to our childhood, my greatest source of (extra-academic) advice. I am indeed blessed to have such wonderful friends in my life. My family has been a pillar of strength for me right from my childhood, and words can hardly be enough to thank them for their contribution—my mother, for her unending care, affection and sacrifices; my late maternal grandmother and late aunt for always having the utmost faith in my abilities and for the gift of a memorable childhood; my maternal grandfather, for being one of the most inspirational teachers and role-models in life; and my cousin, for being so much more than a brother and best friend.

Before I end, there still remains one last person that I wish to thank, perhaps for the very first time in my life. A person who understood me the best in this world. A person to whom I would not have to explain any situation explicitly, yet it would almost nonchalantly be deciphered. A person who would unconditionally support me in every venture of life, while maintaining an almost unimaginably high degree of faith in me. A

person who took me by the hand and showed me the world. A person who taught me so many things without ever posing as a teacher. A person who made me what I am, but never for once took the slightest credit for it. A person who treated human beings with the utmost love, care and respect. This person was the closest thing to me that I had in this world. It so happened, that he was my father. I will forever miss him.

*Kharagpur, 12 January 2015*

A. Sg.



# Abstract

Information theory has long pointed to the promise of physical layer cooperation in boosting the spectral efficiency of wireless networks. Yet, the optimum relaying strategy to achieve the network capacity has till date remained elusive. Recently however, a relaying strategy termed Quantize-Map-and-Forward (QMF) was proved to achieve the capacity of arbitrary wireless networks *within a bounded additive gap*. This thesis contributes to the design, analysis and implementation of QMF relaying by optimizing its performance for small relay networks, proposing low-complexity iteratively decodable codes, and carrying out over-the-air experiments using software-radio testbeds to assess real-world potential and competitiveness.

The original QMF scheme has each relay performing the same operation, agnostic to the network topology and the channel state information (CSI); this facilitates the analysis for arbitrary networks, yet comes at a performance penalty for small networks and medium SNR regimes. In this thesis, we demonstrate the benefits one can gain for QMF if we optimize its performance by leveraging topological and channel state information. We show that for the  $N$ -relay diamond network, by taking into account topological information, we can exponentially reduce the QMF additive approximation gap from  $\Theta(N)$  bits/s/Hz to  $\Theta(\log N)$  bits/s/Hz, while for the one-relay and two-relay networks, use of topological information and CSI can help to gain as much as 6 dB. Moreover, we explore what benefits we can realize if we jointly optimize QMF and half-duplex scheduling, as well as if we employ hybrid schemes that combine QMF and Decode-and-Forward (DF) relay operations.

To take QMF from being a purely information-theoretic idea to an *implementable* strategy, we derive a structure employing Low-Density-Parity-Check (LDPC) ensembles for the relay node operations and message-passing algorithms for decoding. We demonstrate through extensive simulation results over the full-duplex diamond network, that our designs offer a robust performance over fading channels and achieves the full diversity order of our network at moderate SNRs.

Next, we explore the potential real-world impact of QMF and present the design and experimental evaluation of a wireless system that exploits relaying in the context of WiFi. We deploy three main competing strategies that have been proposed for relaying, Amplify-and-Forward (AF), DF and QMF, on the WarpLab software radio platform. We present experimental results—to the best of our knowledge, the first ones—that compare QMF, AF and DF in a realistic indoor setting. We find that QMF is a competitive scheme

## Abstract

---

to the other two, offering in some cases up to 12% throughput benefits and up to 60% improvement in frame error-rates over the next best scheme.

We then present a more advanced architecture for physical layer cooperation (termed QUILT), that seamlessly adapts to the underlying network configuration to achieve competitive or better performance than the best current approaches. It combines on-demand, opportunistic use of DF or QMF followed by interleaving at the relay, with hybrid decoding at the destination that extracts information from even potentially undecodable received frames. We theoretically quantify how our design choices affect the system performance. We also deploy QUILT on WarpLab and show through over-the-air experiments up to 5 times FER improvement over the next best cooperative protocol.

Key words: Physical Layer Cooperation; Quantize-Map-and-Forward; Optimization; Low-Density Parity-Check Codes; Software-Defined Radio.

# Résumé

La théorie de l'information a longtemps pointé dans la direction de la coopération avec la couche physique pour augmenter l'efficacité spectrale des réseaux sans fil. Cependant, la stratégie de relai optimale pour atteindre la capacité du réseau demeure évasive. Récemment, on a démontré qu'une stratégie de relai appelée Quantize-Map-and-Forward (QMF) atteint la capacité d'un réseau sans fil arbitraire si l'on admet un *trou (gap) additif borné*. La thèse qui suit contribue au design, à l'analyse et à l'implémentation du relai QMF en optimisant sa performance pour de petits réseaux, en proposant des codes à faible complexité itératifs et en exécutant des expériences avec des radios logicielles pour évaluer le potentiel et la compétitivité dans un cadre d'utilisation réaliste.

Le schéma de transmission d'origine QMF impose à chaque relai de performer les mêmes opérations, indépendamment de la topologie du réseau ou de l'information sur l'état du canal (CSI); ceci facilite l'analyse pour un réseau arbitraire, mais vient avec un coût pour de petits réseaux et un SNR de taille moyenne. Dans cette thèse, nous démontrons les bénéfices possibles pour QMF lorsque l'on optimise pour la topologie du réseau et le CSI. Nous montrons que pour le réseau en diamant avec  $N$  relais, nous pouvons diminuer le trou approximatif de QMF exponentiellement, de  $\Theta(N)$  bits/s/Hz à  $\Theta(\log N)$  bits/s/Hz. Pour les réseaux à un et deux relais, l'utilisation des informations topologiques et du CSI peut faire gagner jusqu'à 6 dB. De plus, nous explorons les bénéfices possibles si l'on optimise le QMF et l'ordonnance half-duplex simultanément, ou si l'on emploie un schéma hybride combinant le QMF et Decode-and-Forward (DF). Pour passer du QMF comme idée de pure théorie de l'information à une stratégie implémentable, nous dérivons une structure basée, sur les ensembles à contraintes de parité diluées (Low-Density-Parity-Check ensembles:LDPC) pour les opérations aux nœuds de relais, et basée sur les algorithmes de propagation de messages pour le décodage. Nous démontrons à travers des simulations extensives sur le réseau full-duplex en diamant, que notre conception possède une performance robuste sur les canaux à évanouissement et atteint l'ordre de diversité maximal pour notre réseau avec rapport signal-sur-bruit (SNR) modéré.

Ensuite, nous explorons l'impact potentiel dans le monde réel du QMF et présentons une conception ainsi qu'une évaluation expérimentale d'un système sans fil exploitant des relais dans le contexte du WiFi. Nous déployons et comparons trois stratégies qui ont été proposées pour le relai, l'Amplification-et-Forward (AF), Décode-et-Forward (DF) et QMF, sur la plateforme du logiciel WarpLab pour la software radio. Nous présentons des

résultats expérimentaux – à notre connaissance les premiers – qui comparent QMF, AF et DF dans une situation réaliste intérieure (intra-muros). Nous trouvons que QMF est un schéma compétitif par rapport aux deux autres, offrant dans certains cas jusqu'à 12% de bénéfice pour le débit et jusqu'à 60% d'amélioration dans le taux d'erreur de trame (frame error rate: FER) par rapport au prochain meilleur schéma.

Nous présentons finalement une architecture plus avancée pour la coopération sur la couche physique (appelée QUILT), qui s'adapte sans problème à la configuration sous-jacente du réseau pour réaliser une performance compétitive ou meilleure par rapport aux meilleures approches courantes. Celle-ci combine, à la demande, l'utilisation opportuniste de DF ou QMF, suivie de l'entrelacement au relai, avec un décodage hybride à la destination qui extrait l'information même pour des trames (frames) recues mais non-décodables. Nous quantifions théoriquement comment notre conception affecte la performance du système. Nous déployons aussi QUILT sur WarLab et montrons à travers des expériences de transmission en direct (over the air) une amélioration du taux d'erreur FER pouvant aller jusqu'à un facteur 5 par rapport au prochain meilleur protocole avec coopération.

Mots clefs: la coopération sur la couche physique; Quantize-Map-and-Forward; optimisation; Low-Density Parity-Check codes; software-defined radio.

# Contents

<b>Acknowledgements</b>	<b>i</b>
<b>Abstract (English/Français)</b>	<b>v</b>
<b>List of figures</b>	<b>xiii</b>
<b>List of tables</b>	<b>xv</b>
<b>Glossary</b>	<b>xvii</b>
<b>Introduction</b>	<b>1</b>
<b>I Theory</b>	<b>7</b>
<b>1 Finite-SNR QMF Optimizations for Single-Relay Networks</b>	<b>9</b>
1.1 Model and Metrics . . . . .	9
1.1.1 System Model . . . . .	9
1.1.2 Outage Performance in Slow Fading Environment . . . . .	10
1.1.3 Limited CSI constraints . . . . .	11
1.2 Rate Expressions and Upper Bounds . . . . .	11
1.2.1 QMF Achievable Rates . . . . .	12
1.2.2 DF and DDF Achievable Rates . . . . .	12
1.2.3 Upper Bounds on Capacity . . . . .	13
1.3 Full-Duplex Single Relay Network . . . . .	13
1.3.1 Global CSI at the Relay . . . . .	14
1.3.2 Local CSI at the Relay . . . . .	15
1.3.3 CSIR at the Relay . . . . .	15
1.3.4 CSIR limited Hybrid DF/QMF . . . . .	17
1.3.5 Numerical Evaluation . . . . .	19
1.4 Half-Duplex Single Relay network . . . . .	19
1.4.1 Global CSI at the Relay: . . . . .	20
1.4.2 CSIR at the Relay . . . . .	21
1.4.3 CSIR-limited hybrid QMF/DDF . . . . .	21
	<b>ix</b>

## Contents

---

1.4.4	Numerical Evaluations . . . . .	23
<b>2</b>	<b>Finite-SNR QMF Optimizations for Multiple-Relay Networks</b>	<b>25</b>
2.1	System Model . . . . .	25
2.2	Rate Expressions and Upper Bounds . . . . .	26
2.2.1	QMF Achievable Rates . . . . .	26
2.2.2	DF Achievable Rates . . . . .	27
2.2.3	Upper Bounds on Capacity . . . . .	27
2.3	Achieving Capacity within $\Theta(\log(N))$ Bits . . . . .	27
2.4	Global CSI-aware Quantizer Optimization . . . . .	29
2.4.1	Solution for the 2-Relay Network . . . . .	30
2.4.2	Solution for the Symmetric $N$ -Relay Network . . . . .	31
2.5	CSIR limited Hybrid DF/QMF Relaying . . . . .	32
2.6	Numerical Evaluations . . . . .	34
	<b>Related Work</b>	<b>35</b>
<b>II</b>	<b>Low-Complexity Codes</b>	<b>37</b>
<b>3</b>	<b>Graph-based Codes for QMF Relaying</b>	<b>39</b>
3.1	Model and Metrics . . . . .	39
3.1.1	2-Relay Diamond Network . . . . .	39
3.1.2	Traditional Cooperative Strategies . . . . .	40
3.1.3	Outage Framework . . . . .	41
3.2	QMF System Design . . . . .	41
3.2.1	Encoding and Relaying . . . . .	41
3.2.2	Iterative QMF Decoder . . . . .	42
3.2.3	Non-binary signaling . . . . .	45
3.3	Numerical Evaluations . . . . .	46
	<b>Related Work</b>	<b>49</b>
<b>III</b>	<b>Testbed Implementation</b>	<b>51</b>
<b>4</b>	<b>QMF Relaying: First Experimental Study</b>	<b>53</b>
4.1	Model and Preliminaries . . . . .	53
4.1.1	Signal Model . . . . .	54
4.1.2	Network Operation . . . . .	55
4.2	Relaying Schemes . . . . .	57
4.2.1	Relay Operation . . . . .	57
4.2.2	System Design . . . . .	57
4.3	System Implementation . . . . .	60

4.3.1	Frame Structure and Operation . . . . .	61
4.3.2	Timing and Carrier Synchronization . . . . .	62
4.3.3	Estimation of Effective Noise . . . . .	64
4.4	Experimentation . . . . .	66
<b>5</b>	<b>QUILT: An Advanced Architecture for PHY-layer cooperation</b>	<b>71</b>
5.1	QUILT System Overview . . . . .	71
5.1.1	Source Operation . . . . .	72
5.1.2	On Demand Relaying: Two Phase Operation . . . . .	72
5.1.3	Relay Operation in Phase 2 . . . . .	72
5.1.4	Hybrid Decoding at the Destination . . . . .	74
5.2	Theoretical Analysis . . . . .	74
5.2.1	Performance Metric: Outage Probability . . . . .	74
5.2.2	Benefits of Interleaving . . . . .	75
5.2.3	Benefits of Hybrid Decoding . . . . .	76
5.2.4	Benefits of Opportunistic Decoding or Quantization . . . . .	76
5.3	System Implementation . . . . .	76
5.3.1	Cooperative Schemes Implemented . . . . .	76
5.3.2	Frame Structure . . . . .	77
5.4	Experimental evaluation . . . . .	78
5.4.1	Performance Metrics . . . . .	78
5.4.2	Testbed . . . . .	78
5.4.3	Evaluation of Interleaving . . . . .	80
5.4.4	Evaluation of Hybrid Decoding . . . . .	80
5.4.5	Evaluation of Opportunistic Decoding or Quantizing . . . . .	81
5.4.6	Putting it All Together: Evaluation of QUILT . . . . .	81
	<b>Related Work</b>	<b>83</b>
<b>A</b>	<b>Appendices</b>	<b>85</b>
A.1	Optimal Quantizer for Asymmetric Fades . . . . .	85
A.2	Proof of Lemma 2.4.1 . . . . .	86
A.2.1	$\Delta_2 \geq \delta_2$ . . . . .	87
A.2.2	$\Delta_2 < \delta_2$ . . . . .	88
A.2.3	Proof of Claim 1 . . . . .	90
A.2.4	Proof of Claim 2 . . . . .	90
A.3	Proof of Theorem 2.4.2 . . . . .	91
A.4	Proof of Lemmas 2.4.3, 2.4.4 and 2.4.5 . . . . .	93
A.4.1	Proof of Lemma 2.4.3 . . . . .	93
A.4.2	Proof of Lemma 2.4.4 . . . . .	93
A.4.3	Proof of Lemma 2.4.5 . . . . .	94
	<b>Bibliography</b>	<b>95</b>

## Contents

---

Curriculum Vitae	99
------------------	----

# List of Figures

1	Increase in mobile data requirements. . . . .	2
2	Figure illustrating the QMF scheme, where each relay quantizes and directly (randomly) maps its quantized sequence to the transmit codebook. . . . .	2
1.1	Single Relay Communication Model . . . . .	9
1.2	Illustration of the integration region for computing $Q(\Delta)$ . . . . .	16
2.1	Diamond Network Communication Model . . . . .	26
2.3	$R_i(\Delta)$ 's as a function of $\Delta$ for a 5-Relay symmetric network with $ h  = 1$ and $ g  = 3.16$ . . . . .	32
2.4	The cut in the above diagram depicts the information transfer across nodes for a given choice of $\Gamma$ . $I_D(\Omega)$ is the minimum of all such cut values computed over every possible choice of $\Gamma$ . . . . .	33
3.1	QMF Strategy for the 2-Relay Diamond Network . . . . .	40
3.2	Decoding Graph for binary signaling with 1-bit scalar quantizers . . . . .	42
4.1	The 3-node network considered in this work: the source $S$ communicates with the destination $D$ with the help of the relay $R$ . . . . .	54
4.2	LDPC-based joint decoder for QMF . . . . .	60
4.3	Node and host PC configuration . . . . .	61
4.4	Time-slot frame structure for LS and LC. . . . .	62
4.5	Radio board receiver path . . . . .	65
4.7	Average measured RSSI values per scenario. . . . .	67
4.8	Frame error rates. . . . .	68
4.9	Throughput in bps/Hz. . . . .	69
4.10	Distribution of percentage of frames that fail in $T_2$ . . . . .	69
5.1	Schematic diagram of QUILT illustrating the various components of the system. $T_1$ and $T_2$ indicate the first and second phase, respectively. . . . .	72
5.2	Outage performance of different relaying schemes. . . . .	75
5.3	Node placement illustrating the topologies considered. . . . .	78
5.4	RSSIs for the different settings considered. . . . .	79
5.5	FER benefits of interleaving, hybrid decoding, and opportunistic decoding. . . . .	79

## List of Figures

---

5.6	Throughput benefits of interleaving, hybrid decoding, and opportunistic decoding/quantizing. . . . .	79
5.7	Performance of QUILT. . . . .	82

# List of Tables

4.1	Schedule for Link Switching . . . . .	56
4.2	Schedule for Link Cooperation . . . . .	56
4.3	Transmitted signals from source and relay per subcarrier for DFLL . . . .	58
4.4	Transmitted signals from source and relay per subcarrier for AFLC . . . .	58
4.5	Implemented schemes when the relay is active. The network modes (rows) are described in Section 4.1.2 and the relaying strategies (columns) in Section 4.2.1. . . . .	61
A.1	Limiting values of $\alpha_1, \alpha_2, \alpha'_1$ and $\alpha'_2$ . . . . .	85



# Glossary

CSI	Channel-State Information
DMT	Diversity-Multiplexing Tradeoff
SNR	Signal-to-Noise Ratio
QMF	Quantize-Map-and-Forward
DF	Decode-Forward
DDF	Dynamic Decode-Forward
AF	Amplify-Forward
LDPC	Low-Density Parity-Check
MAP	Maximum A posteriori Probability
LLR	Log Likelihood Ratio
BP	Belief Propagation
AWGN	Additive White Gaussian Noise
FER	Frame Error Rate
OFDM	Orthogonal Frequency Division Multiplexing
QAM	Quadrature Amplitude Modulation
DT	Direct Transmission
DTHR	Direct Transmission at Half Rate
LS	Link Switching
LC	Link Cooperation
MAC	Medium Access Control
CRC	Cyclic Redundancy Check
MISO	Multiple Input Single Output
CFO	Carrier Frequency Offset
FFT	Fast Fourier Transform
AGC	Automatic Gain Control
FPGA	Field-Programmable Gate Array
ADC	Analog-to-Digital Converter
DAC	Digital-to-Analog Converter
RF	Radio Frequency
RSSI	Received Signal Strength Indicator
SDR	Software-Defined Radio
BPSK	Binary Phase-Shift Keying
ARQ	Automatic Repeat Request



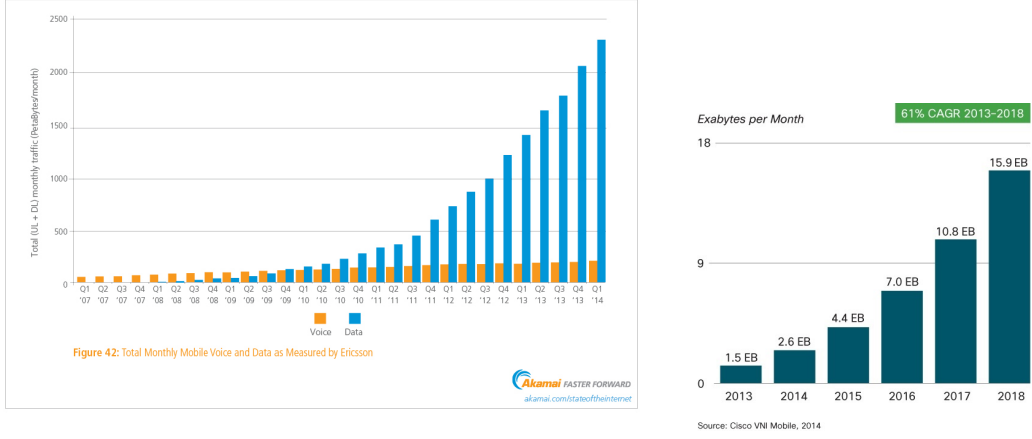
# Introduction

Wireless traffic has been growing exponentially for the past several years (see Fig. 1a) [1] at a pace that is challenging the present infrastructure for meeting the demands to its fullest. Moreover, this demand is only expected to rise exponentially further (see Fig. 1b) in the coming years [2]. Clearly, meeting this ever-increasing demand via releasing bandwidth alone is infeasible. On the other hand, with the advent of wireless-enabled portable equipment such as smartphones and tablets, the number of physical devices accessing the wireless medium is also increasing at a very fast rate [2]. Instead of looking at this as a bane, physical layer cooperation can make a significant impact in next-generation wireless systems by looking at it as an “opportunity”: not all the devices access the medium at the same time, and when idle, they can act as “relays” to assist the communication of other source-destination pairs “in-band”.

Indeed, network information theory has, over the years, pointed to the possible promise of physical layer cooperation techniques in boosting spectral efficiency significantly. However, a key question towards harnessing this promise still remains: which relaying strategy should the relays implement to achieve the network capacity? This has classically proved to be a hard one to resolve: even for very small networks, the network capacity remains unknown. On the upside however, an information theoretic strategy, Quantize-Map-and-Forward (QMF) [3], unlike conventional Decode-and-Forward (DF) and Amplify-and-Forward (AF), was recently proved to achieve the capacity of arbitrary wireless networks *within a bounded additive gap*.

This thesis contributes to the design, analysis and implementation of QMF relaying by optimizing its performance for small relay networks, proposing low-complexity iteratively decodable codes, and carrying out over-the-air experiments using software-radio testbeds to assess real-world potential and competitiveness.

The first design of QMF [3] builds on simple principles that make proofs for arbitrary networks possible. Each relay performs the same operation, independent of its position in the network, and independent of the experienced channel coefficients: it quantizes its received signal at the noise level, (uniformly at random) maps it onto its transmit codebook, and forwards the resulting codeword (see Fig. 2). The destination performs



(a) Increase in mobile data traffic from 2007-2014 [1].

(b) Estimated increase in mobile traffic from 2013-2018 [2].

Figure 1: Increase in mobile data requirements.

a joint decoding operation that together utilizes all the information it receives from the source and the relays to converge on the transmitted source codeword. Unlike conventional Compress-and-Forward [4] however, explicit decoding of the quantized values from the relay is not a requirement for QMF. It was proved that with this simple operation, QMF achieves the capacity of arbitrary networks within a bounded gap. Moreover, in fading channels, where now the relevant performance metrics are outage probability, diversity, and spatial multiplexing, it was proved that QMF can achieve the optimal diversity-multiplexing tradeoff [5] (over arbitrary full-duplex networks [3] as well as the half-duplex single-relay network [6]).

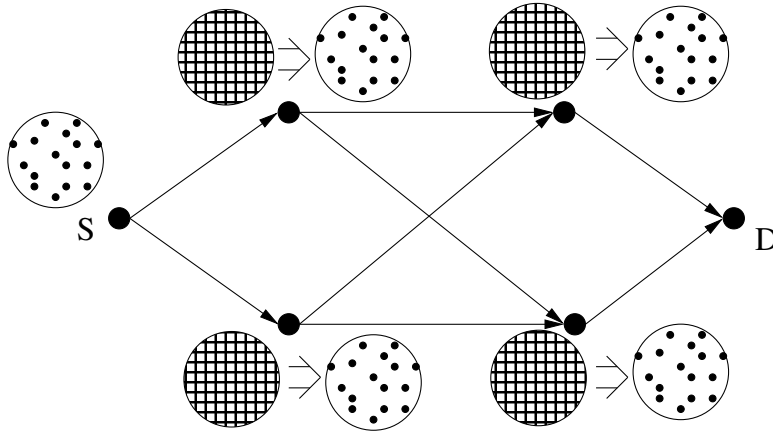


Figure 2: Figure illustrating the QMF scheme, where each relay quantizes and directly (randomly) maps its quantized sequence to the transmit codebook.

However, by making the QMF relay operation agnostic to the network topology and the channel coefficients, we sacrifice performance. In moderate SNR regimes, QMF can have an additive gap from the information-theoretic cut-set upper bound as large as

15N bits/sec/Hz in [3], improved to 1.26N in [7], with  $N$  being the number of nodes in the relay network. Even for small networks, these gaps can be prohibitively large; alternative relaying techniques such as DF and AF, performance of which are not close to the ultimate capacity for arbitrary networks, can still outperform QMF for specific configurations. And in practice, physical layer cooperation will start to get deployed in specific small configurations, such as single-relay or two-relay networks; moreover, these networks will most probably be half-duplex, and operate under slow fading conditions. Is QMF a competitive choice for such configurations? How much benefit can channel state information and topology provide? On the theory front, these are some of the questions we explore in the course of this thesis.

The design and analysis of QMF relaying in [3] was done without regard to computational complexity constraints. A key question to ask for the potential implementation of QMF is whether one can design computationally efficient encoding and decoding strategies that maintain similar advantages over more traditional cooperative communication schemes. In the realm of point-to-point communication, low-density parity-check (LDPC) codes have emerged in the last decade as a class of codes that can exhibit near Shannon-limit performance while admitting low-complexity message-passing decoding algorithms on sparse bipartite graphs. Given the success of iterative codes in point-to-point channels, in this thesis, we also examine the performance of such techniques for the design of QMF-based cooperative strategies.

While QMF possesses a number of potentially attractive theoretical attributes, including simple relay operation, no requirement of forward channel state information, natural scalability (due to independent relay operation) and approximate optimality, it is not *a priori* clear how many of these advantages translate into practical systems. The information-theoretic analysis assumes infinite length coding and no complexity constraints on the transceivers; even then there is a possible gap to information-theoretic capacity; and of course the analysis assumes perfect estimates of the noise and the channel coefficients for decoding. It is well possible that for networks at moderate SNRs these advantages disappear—this is especially so, if we want to operate with backwards compatible coding schemes at the encoder, such as those that IEEE802.11 supports. Somewhat surprisingly, very little experimental results on physical layer cooperation networks exist in the literature—especially ones involving end-to-end error correction coding and broadband modulation techniques like OFDM. It is thus instructive to not only deploy QMF in its implementable flavour on software radio testbeds, but also compare its performance to other state-of-the-art relaying strategies on a level playing field. A significant portion of this thesis is dedicated to the practical implementation of QMF-based relaying strategies.

### Overview of the Chapters

This thesis is organized into three parts: Part I (Chapters 1 and 2) deals with the information theoretic questions regarding QMF operation and optimization in finite SNR regimes, Part II (Chapter 3) provides low-complexity iterative coding solutions for QMF, and Part III (Chapters 4 and 5) is focused on testbed evaluations of QMF and QMF-inspired cooperation strategies.

In Part I, we set out to find how much performance improvement we can gain for QMF, if we optimize its design by taking into account the network configuration, as well as channel state information (CSI), over slow fading channels. We are interested in finding out the benefits we can have for a range of situations, starting from having *only topological information* and no CSI, to having *receiver CSI (CSIR)* where each relay node only knows the realization of the fading channel coefficient of its incoming link (as is the case in practical systems today), to the extreme of the *global CSI* scenario where all relay nodes have full knowledge of the fading coefficients in the entire network. By studying the quantizer optimization, we also came up with a new scheme, that we term hybrid QMF-DF. The idea is the following: if a relay is able to perfectly decode its received signal, it does so, as this operation enables to perfectly remove noise and errors; it then re-encodes the message and forwards the new codeword. If decoding is not possible, then the relay performs QMF relaying. Chapter 1 focusses on the single-relay network, while Chapter 2 extends the ideas to  $N$ -relay diamond networks.

In Part II, we present a low-complexity, structured QMF scheme (for diamond networks, but applicable to general networks) that employs LDPC ensembles for the node operations and message-passing algorithms for decoding. We describe how the non-linearities introduced due to quantization and signal superposition are handled with novel compound graphical models that capture these (nonstandard) operations. The QMF system design introduced in this part plays a pivotal role in the testbed implementation of QMF, to which this iterative decoding framework directly translates.

Part III of the thesis is concerned with testbed implementations of physical layer cooperation techniques, with a special focus on QMF and QMF-inspired strategies. In Chapter 4, we present an experimental study of QMF and other state-of-the-art relaying techniques, and compare their performance for several indoor 802.11 (WiFi) topologies. We focus on the most basic topology: a source sends data to a destination with the help of a relay. In our home, the source could be a WiFi router that streams video to a tablet with the help of a WiFi enabled appliance that boosts the network performance by acting as a relay. We select this setup for several reasons: the simpler the experiment the easier to interpret results; it can serve as a building block towards more complex configurations; this is commonly accepted as the topology that would be used in practice in the immediate future; and surprisingly, even for this small topology, few experimental results have been published.

In Chapter 5, we extend our work in Chapter 4 to develop QUILT, a more advanced system for physical layer cooperation that seamlessly adapts to the underlying network configuration to achieve competitive or better performance as compared to the best current approaches. QUILT combines on-demand, opportunistic use of Decode-Forward (DF) or Quantize-Map-Forward (QMF) followed by interleaving at the relay, with hybrid decoding at the destination that extracts information from received frames even if these are not decodable. We theoretically quantify how our design choices for QUILT affect the system performance, deploy QUILT on the WarpLab software radio platform, and demonstrate the performance benefits through over-the-air experiments.

## Main Contributions

Our main contributions in this thesis are summarized below:

- (i) For the single-relay network, we derive outage-optimal quantizers when the relay is full-duplex, and jointly optimal quantizers and relay schedules when the relay is half-duplex, both for the CSIR and global CSI settings. We report finite-SNR gains (over the standard QMF scheme) ranging from 3 dB for the CSIR setting, to 6 dB for the global CSI setting.
- (ii) For the full-duplex  $N$ -relay diamond network, we show that simply by using topological (and no CSI) information, we can improve the additive approximation gap of QMF from the conventional  $\Theta(N)$  [3] [7] to within  $\Theta(\log N)$  bits/s/Hz—an exponential improvement.
- (iii) In the CSIR settings, we prove that suitable hybridizations of optimized QMF with DF (Dynamic DF for half-duplex) universally outperform the outage performance of the individual schemes for the single relay network. For the diamond network, we show that hybrid schemes can also improve the performance of QMF, with simulations demonstrating a 5 dB gain over QMF, and a diversity order gain over DF in asymmetric diamond networks.
- (iv) We develop a compound graphical representation of QMF network operation using LDPC codes that takes into account the wireless multiple access and broadcast, as well as the processing at various nodes such as quantization, modulation and mapping. We devise an efficient scheduling and message passing algorithm on this graph and evaluate the performance of our codes to demonstrate that our design and implementation of QMF retains several of the advantages over competing strategies.
- (v) We design and deploy the first QMF relaying system, as well as *coded* Amplify-and-Forward (AF) and Decode-and-Forward (DF) relaying systems on WARP radio testbeds. We report a number of experiments that compare the three schemes, and

evaluate the utility of relaying in the context of WiFi. We also find that QMF is a competitive scheme to DF and AF, offering in some cases up to 12% throughput benefits and up to 60% improvement in Frame Error Rates (FER) over the next best scheme.

- (vi) We design QUILT, an on-demand physical layer cooperation scheme of a source with a relay, where the relay retrieves the source sequence by opportunistically decoding or quantizing, interleaves it and transmits it synchronously with the source, while the destination benefits from hybrid decoding. We deploy QUILT on a WARPLAB testbed and present exhaustive performance comparisons with DF and QMF protocols through over-the-air experiments. Our experimental results demonstrate benefits up to a factor of 5 for FER as compared to the next best scheme and two orders of magnitude over the FER of traditional point-to-point transmissions.

# Theory **Part I**



# 1 Finite-SNR QMF Optimizations for Single-Relay Networks

In QMF-based networks, there are two obvious places where topological and CSI information can immediately help in boosting performance. First, at the QMF quantizer, that essentially reflects the amount of useful information each relay can capture and forward: we can have each relay utilize a different quantization level depending on its position in the network and the CSI. Second, in half duplex networks, where relays cannot listen and transmit at the same time, we can use this information to optimize the half-duplex schedules. Clearly these two parameters are not independent: in half duplex networks, we achieve the optimal performance by *jointly* optimizing the quantizers and the scheduling. We show that such optimizations can indeed offer very significant benefits. We also demonstrate the benefits of employing a hybrid relaying strategy involving DF and QMF and show how it provably outperforms the individual schemes.

## 1.1 Model and Metrics

### 1.1.1 System Model

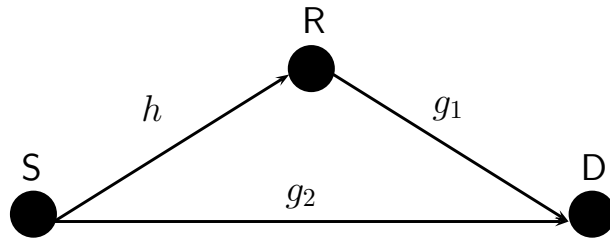


Figure 1.1: Single Relay Communication Model

The single relay channel is depicted in Fig. 1.1. The source S communicates with the destination D with the help of a relay R that is capable of causal signal processing. The signals transmitted by the source and the relay are denoted by  $X$  and  $X_r$  respectively. The received signal at the destination and the relay are denoted by  $Y$  and  $Y_r$  respectively.

In the full-duplex case, the received signals as a function of the transmitted signals are as follows: for  $t \in \{1, 2, \dots, T\}$  where  $T$  is the communication block length,

$$Y_r[t] = hX[t] + Z_r[t], \quad Y[t] = g_1X_r[t] + g_2X[t] + Z[t]. \quad (1.1)$$

The complex channel coefficient from the source to relay is denoted by  $h$  and those from relay to destination and source to destination are denoted by  $g_1$  and  $g_2$  respectively. Additive white Gaussian noises  $Z$  and  $Z_r$  are i.i.d  $\mathcal{CN}(0, 1)$  random variables, i.e., the real and imaginary parts of  $Z$  and  $Z_r$  are each i.i.d zero-mean Gaussian r.v's with a variance of  $1/2$ . The transmitted signals are normalized to have an average power constraint of unity at the source and the relay, i.e.,  $\mathbb{E}(|X|^2) \leq 1$  and  $\mathbb{E}(|X_r|^2) \leq 1$ . For notational convenience, denote the amplitude of the channel coefficients as follows:  $h := |h|, g_1 := |g_1|, g_2 := |g_2|$ .

In the half-duplex scenario, the relay listens for a fraction  $f \in [0, 1]$  of the total communication block length  $N$  and transmits for the fraction  $(1 - f)$ . Without loss of generality, we assume that the relay is in the listening phase during the first  $\lfloor fT \rfloor$  symbols times ( $\lfloor \cdot \rfloor$  denotes the closest rounded integer) and in the transmitting phase during the rest. The source continues its transmission for the entire block of  $T$  symbols, and hence the destination receives a superposition of the source and relay signals when the relay is in transmission mode; in other words, the source and relay transmissions are not orthogonal. The received signals as a function of the transmitted signals are defined as in (1.1) except that due to the half-duplex constraint,  $X_r[t] = 0$  for  $t \in \{1, 2, \dots, \lfloor fT \rfloor\}$  when the relay is listening, and for the remaining time  $Y_r[t] = 0, t \in \{\lfloor fT \rfloor + 1, \dots, T\}$ .

### 1.1.2 Outage Performance in Slow Fading Environment

In the slow fading scenario, the block-fading channel gains are Rayleigh distributed and are independent from link to link, and across blocks.

The outage probability  $P_{\text{out}}(R)$  is the probability that the system cannot support the transmission rate  $R$  from the source. From the static channel capacity bounds, we have the following lower and upper bounds on the outage probability:

$$P_{\text{out}}(R) \geq P_{\text{out, cut}}(R) := \Pr \{R > \bar{C}_{\text{cut}}\}, \quad P_{\text{out}}(R) \leq P_{\text{out, ACH}}(R) := \Pr \{R > R_{\text{ACH}}\}$$

where  $\bar{C}_{\text{cut}}$  denotes the information-theoretic cutset upper bound on network capacity and ACH denotes any achievable scheme, like QMF, DF or DDF.

It is shown as a corollary in [3] that QMF achieves the optimal DMT for arbitrary full-duplex relay networks. In [6], it was shown that even for the single-relay half-duplex channel, QMF relaying with a noise-level quantizer and a fixed  $1/2 - 1/2$  schedule achieves the optimal DMT. At finite SNR however, one can sharpen the upper bound on

the outage probability by optimizing the quantization distortion level (and the schedule  $f$ , for half-duplex networks) at the relay depending on available CSI.

To characterize the finite SNR outage performance corresponding to different *multiplexing gains* on the DMT curve, we demonstrate the performance of our schemes by plotting the outage probabilities as a function of the SNR of one of the links (the SNRs of the other links scale in proportion to the configuration considered) for different rate scalings, i.e, we plot  $P_{\text{out}}(R)$  vs SNR, where instead of a fixed rate  $R$ , we use  $R = r \log(\text{SNR})$  where  $r$  can be thought of as the multiplexing gain. This method of representation allows us to take *finite SNR snapshots* of the DMT for varying multiplexing gains. Also, such a representation serves as a good guideline for most wireless systems that adapt their transmission rates according to channel conditions.

### 1.1.3 Limited CSI constraints

In this work, we are primarily concerned with two settings of available CSI:

- (i) *Global CSI*: In this setting, each relay requires the *magnitudes* of the fading coefficients in the entire network to carry out optimizations on QMF. While each relay can have access to its own forward channels (to the destination) due to reciprocity of channel magnitudes, for global CSI of *all* channels, there needs to be coordination among the relays to exchange channel information. In that regard, the global CSI optimal QMF is more of theoretical interest and is to be treated as an *upper bound* to the performance of schemes based on more practical CSI assumptions that we discuss in the chapter.
- (ii) *CSIR*: when only receiver CSI (CSIR) is available at the relay (both magnitude and phase information), as is the most practical scenario for typical wireless systems.

We derive QMF optimizations and optimal combinations with other schemes for both settings for the single relay network. We consider both the full-duplex as well as the half-duplex problem.

While arriving at the CSIR-optimal relaying schemes, we also provide optimizations for the single relay network where the relay has access to *local* CSI, i.e., the instantaneous knowledge of its incoming and outgoing channels.

## 1.2 Rate Expressions and Upper Bounds

To consolidate the development of our optimization framework, in this section we provide the expressions of the information-theoretic cutset upper bound and achievable rates of the QMF relaying scheme as well as other relaying schemes (DF and DDF)

considered in this work. The explicit derivation of these expressions follows straightforwardly from the literature [3] [7] [4]. For notational convenience, in the rest of this chapter, logarithm is of base 2.

### 1.2.1 QMF Achievable Rates

The achievable rate for QMF relaying is given by the following single-letter characterization [7]: for a given probability distribution  $p(X)p(X_r)p(\hat{Y}_r|Y_r,X_r)$ ,

$$R_{\text{QMF}} = \min \left\{ I(X, X_r; Y) - I(Y_r; \hat{Y}_r | X, X_r, Y), I(X; \hat{Y}_r, Y | X_r) \right\}.$$

Here  $\hat{Y}_r$  denotes the quantizer output of the relay. We pick  $X \sim \mathcal{CN}(0, 1)$ ,  $X_r \sim \mathcal{CN}(0, 1)$  and a Gaussian vector quantization codebook generated by the single-letter probability distribution

$$\hat{Y}_r = Y_r + \hat{Z}_r, \quad \hat{Z}_r \sim \mathcal{CN}(0, \Delta), \quad (1.2)$$

independent of everything else. The parameter  $\Delta$  determines the *quantization distortion level*: the larger  $\Delta$  is, the coarser the quantization is [7]. With this choice, the QMF achievable rates are as follows:

**Full-Duplex:**  $R_{\text{QMF}}(\Delta) = \lceil \min \{I_1, I_2\} \rceil^+$ , where

$$I_1(\Delta) = \log \left( 1 + \frac{h^2}{1 + \Delta} + g_2^2 \right), \quad I_2(\Delta) = \log(1 + g_1^2 + g_2^2) - \log \left( \frac{1 + \Delta}{\Delta} \right) \quad (1.3)$$

The notation  $\lceil x \rceil^+$  represents  $\max\{x, 0\}$ .

**Half-Duplex:**  $R_{hd, \text{QMF}}(\Delta; f) = \lceil \min \{I_{hd,1}, I_{hd,2}\} \rceil^+$ , where

$$\begin{aligned} I_{hd,1}(\Delta, f) &= f \log \left( 1 + \frac{h^2}{1 + \Delta} + g_2^2 \right) + (1 - f) \log(1 + g_2^2) \\ I_{hd,2}(\Delta, f) &= (1 - f) (\log(1 + g_1^2 + g_2^2)) + f \left\{ \log(1 + g_2^2) - \log \left( \frac{1 + \Delta}{\Delta} \right) \right\} \end{aligned} \quad (1.4)$$

### 1.2.2 DF and DDF Achievable Rates

**Full-Duplex:**  $R_{\text{DF}} = \max \{ \log(1 + g_2^2), \min \{ \log(1 + h^2), \log(1 + g_1^2 + g_2^2) \} \}$ .

DF is also DMT optimal for the single relay full-duplex network, and the DF achievable rate is within 1 bit/sec/Hz of the cutset bound. It is to be noted that in the expression above, we assume that the relays do not know the phases of the forward channels and hence, in the last term there is no coherent combining gain. This assumption is

true throughout this chapter. Also note that we shall use point-to-point transmission if  $h^2 < g_2^2$ .

**Half-Duplex:** For the half-duplex network, the dynamic decode-forward (DDF) protocol [8] is the appropriate variant of DF. In this protocol, the relay adjusts its schedule (the fraction of time it listens) in accordance with the received channel strength to decide how long it needs to listen for it to be able to decode, or whether at all it can decode the transmission from the source. The achievable rate as a function of the relay schedule is given by

$$R_{\text{DDF}}(f) = \{\log(1 + g_2^2), R_1(f)\}, \text{ where}$$

$$R_1(f) = \min \left\{ f \log(1 + h^2), (1 - f) \log(1 + g_1^2 + g_2^2) + f \log(1 + g_2^2) \right\}.$$

The optimal rate achievable (over all possible schedules) is given by:

$$R_{\text{DDF}}^* = \max_{f \in [0,1]} R_{\text{DDF}}(f)$$

. It is important to note that for the half-duplex network, none of the schemes (including DDF) other than QMF is DMT optimal for the entire range of multiplexing gains [6].

#### 1.2.3 Upper Bounds on Capacity

The cutset upper bound on the capacity of the full-duplex single relay channel is given by  $\bar{C}_{\text{cut}} = \min\{C_1, C_2\}$  where

$$C_1 = \log(1 + h^2 + g_2^2), \quad C_2 = \log(1 + (g_1 + g_2)^2).$$

For the half-duplex case, the cutset bound expression for a given schedule  $f$  is given by  $\bar{C}_{\text{hd, cut}}(f) = \min\{C_{\text{hd},1}(f), C_{\text{hd},2}(f)\}$  where

$$\begin{aligned} C_{\text{hd},1}(f) &= f \log(1 + h^2 + g_2^2) + (1 - f) \log(1 + g_2^2), \\ C_{\text{hd},2}(f) &= f \log(1 + g_2^2) + (1 - f) \log(1 + (g_1 + g_2)^2). \end{aligned} \tag{1.5}$$

### 1.3 Full-Duplex Single Relay Network

In this section we focus on the full-duplex single-relay network. We study the ways in which the full-duplex relay can utilize the available CSI to optimize and improve the performance of QMF in slow fading scenarios. As mentioned in Section 2.2, we focus on

QMF with Gaussian random codebooks and Gaussian vector quantizers as shown in (1.2). Hence, the optimization parameter that the relay can choose is the quantization level  $\Delta$  used in (1.2).

We assume that the relay knows the probability distributions of the three links  $\{h, g_1, g_2\}$ , but has limited access to the realizations of them in each transmission block. Recall that the channels are Rayleigh-faded and are independent from link to link, and across blocks:

$$h \sim \mathcal{CN}(0, 1/\rho), \quad g_1 \sim \mathcal{CN}(0, 1/\lambda_1), \quad g_2 \sim \mathcal{CN}(0, 1/\lambda_2)$$

where  $1/\rho, 1/\lambda_1, 1/\lambda_2$  denote the signal-to-noise ratios in the Source-Relay link, the Relay-Destination link, and the Source-Destination link respectively.

In the rest of this section, we study the following CSI scenarios:

- The relay has global CSI, i.e., the instantaneous realizations of  $h, g_1$  and  $g_2$ .
- The relay has local CSI, that is, the instantaneous realizations of  $h$  and  $g_1$ .
- The relay has CSI at the receiver (CSIR) only, that is the realization of  $h$ .

In the global CSI setting, the optimization problem is equivalent to *rate maximization*. In the other cases, we formulate the objective function as the outage probability, *conditioned* on the known channel gain realizations at the relay. For the CSIR-limited case, we also prove that a hybridization of QMF (using optimized quantizers) with DF provides a strictly better outage performance than either one of the two schemes for all channel configurations.

### 1.3.1 Global CSI at the Relay

When the relay has access to the instantaneous channel gain realizations  $h, g_1$  and  $g_2$ , it will choose a quantizer distortion  $\Delta^*$  that maximizes  $R_{\text{QMF}}(\Delta)$ . Hence using (1.3), the optimization problem can be stated as a max min problem as follows:

$$R_{\text{QMF}}^* = \max_{\Delta > 0} \{ \lceil \min \{I_1, I_2\} \rceil^+ \}$$

and the optimizing  $\Delta$  is denoted by  $\Delta^*$ .

We note that  $I_1$  is *monotonically decreasing* in  $\Delta$  and  $I_2$  is *monotonically increasing* in  $\Delta$ . Also, at the boundary points of the admissible range of  $\Delta$ , we have,

$$\begin{aligned} I_1(0) &= \lim_{\Delta \rightarrow 0^+} I_1 = \log(1 + h^2 + g_2^2) & I_1(\infty) &= \lim_{\Delta \rightarrow \infty} I_1 = \log(1 + g_2^2) \\ I_2(0) &= \lim_{\Delta \rightarrow 0^+} I_2 = -\infty & I_2(\infty) &= \lim_{\Delta \rightarrow \infty} I_2 = \log(1 + g_1^2 + g_2^2) \end{aligned}$$

The properties  $I_1 > 0 \quad \forall \Delta > 0$ ,  $I_2(0) < I_1(0)$  and  $I_2(\infty) > I_1(\infty)$ , together with the above mentioned monotonicity properties ensure that the optimum quantizer distortion is given by

$$\Delta^* = \arg_{\Delta} \{I_1 = I_2\} = \frac{1 + h^2 + g_2^2}{g_1^2}$$

### 1.3.2 Local CSI at the Relay

The goal here is to find a quantizer distortion based on the available channel knowledge that minimizes the conditional probability of outage at a given rate  $R$ , denoted by  $P_{\text{out}|h,g_1}(R;\Delta)$ . Since the fading channel coefficients  $\{h, g_1, g_2\}$  are mutually independent, we have

$$\begin{aligned} 1 - P_{\text{out}|h,g_1}(R;\Delta) &= 1 - \Pr\{R > R_{\text{QMF}}(\Delta)\} = \Pr\{R \leq R_{\text{QMF}}(\Delta)\} \\ &= \Pr\left\{R \leq \log\left(1 + \frac{h^2}{1+\Delta} + g_2^2\right), R \leq \left\lceil \log(1 + g_1^2 + g_2^2) - \log\left(\frac{1+\Delta}{\Delta}\right) \right\rceil^+\right\} \\ &= \Pr\left\{g_2^2 \geq \left\lceil \underbrace{2^R - \frac{h^2}{1+\Delta}}_{\beta_1} - 1 \right\rceil^+, g_2^2 \geq \left\lceil \underbrace{2^R \left(\frac{1+\Delta}{\Delta}\right) - g_1^2 - 1}_{\beta_2} \right\rceil^+\right\} \\ &= \Pr\{g_2^2 \geq \max\{\lceil \beta_1 \rceil^+, \lceil \beta_2 \rceil^+\}\} = e^{-\lambda_2 \max\{\lceil \beta_1 \rceil^+, \lceil \beta_2 \rceil^+\}}. \end{aligned}$$

The problem of finding the optimal  $\Delta^*$  that minimizes  $P_{\text{out}|h,g_1}(R;\Delta)$  can then be stated as

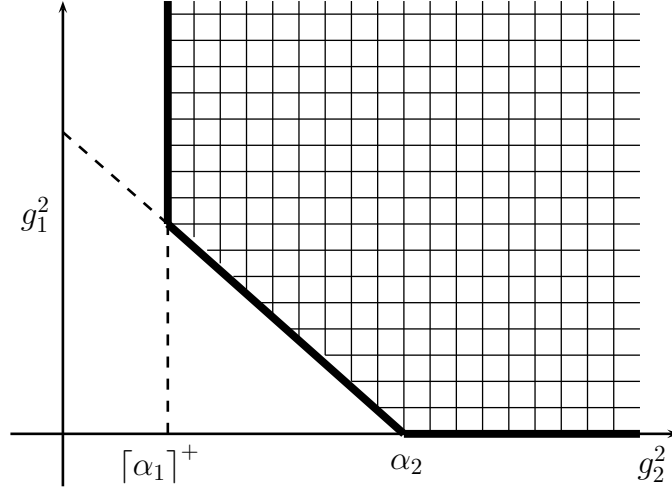
$$\Delta^* = \arg \max_{\Delta > 0} e^{-\lambda_2 \max\{\lceil \beta_1 \rceil^+, \lceil \beta_2 \rceil^+\}} = \arg \min_{\Delta > 0} \max\{\lceil \beta_1 \rceil^+, \lceil \beta_2 \rceil^+\}.$$

Now,  $\lceil \beta_1 \rceil^+$  is *non-decreasing* in  $\Delta$  and  $\lceil \beta_2 \rceil^+$  is *non-increasing* in  $\Delta$ . The properties that  $\lceil \beta_2 \rceil^+(0) > \lceil \beta_1 \rceil^+(0)$  and  $\lceil \beta_2 \rceil^+(\infty) < \lceil \beta_1 \rceil^+(\infty)$ , together with the monotonicity conditions ensure that the optimum quantizer distortion is given by

$$\begin{aligned} \Delta^* &= \arg_{\Delta > 0} \{\beta_1 = \beta_2\} = \arg_{\Delta > 0} \{g_1^2 \Delta^2 + (g_1^2 - h^2 - 2^R) \Delta - 2^R = 0\} \\ &= \frac{\sqrt{(g_1^2 - h^2 - 2^R)^2 + 4g_1^2 2^R} - (g_1^2 - h^2 - 2^R)}{2g_1^2}. \end{aligned}$$

### 1.3.3 CSIR at the Relay

To obtain an outage-optimal quantizer in this setting, the metric to minimize is again the conditional probability of outage, but this time conditioned *only* on  $h$ . Proceeding in a


 Figure 1.2: Illustration of the integration region for computing  $Q(\Delta)$ .

similar fashion as in the local CSI case, we have,

$$Q(\Delta) \triangleq 1 - P_{\text{out}|h}(R; \Delta) = \Pr \left\{ g_2^2 \geq \underbrace{\left[ 2^R - \frac{h^2}{1+\Delta} - 1 \right]^+}_{\alpha_1}, g_1^2 + g_2^2 \geq \underbrace{2^R \left( \frac{1+\Delta}{\Delta} \right) - 1}_{\alpha_2} \right\}.$$

We note that in contrast to the local CSI setting where only  $g_2^2$  was treated as a random variable, both  $g_1^2$  and  $g_2^2$  are to be treated as random variables in the optimization for the CSIR setting. With regards to  $\alpha_1$  and  $\alpha_2$ , note that  $\alpha_2 > \alpha_1$  and  $\lceil \alpha_1 \rceil^+ = \alpha_1$  for  $\Delta > \Delta_t = \frac{h^2}{2^R - 1} - 1$ .

By integrating the joint density of the two independent exponentially distributed random variables corresponding to  $g_1^2$  and  $g_2^2$  over the shaded region in the 2-D plane (as shown in Fig. 1.2), the above probability is computed as follows

$$Q(\Delta) = \begin{cases} \frac{\lambda_2}{\lambda_2 - \lambda_1} e^{-(\lambda_1 \alpha_2 + (\lambda_2 - \lambda_1) \lceil \alpha_1 \rceil^+)} - \frac{\lambda_1}{\lambda_2 - \lambda_1} e^{-(\lambda_2 \alpha_2)} & \lambda_1 \neq \lambda_2 \\ e^{-\lambda_1 \alpha_2} (1 + \lambda_1 \alpha_2 - \lambda_1 \lceil \alpha_1 \rceil^+) & \lambda_1 = \lambda_2 \end{cases}.$$

Hence the problem of choosing the optimal quantizer distortion can be stated as follows:

$$\Delta^* = \arg \max_{\Delta > 0} Q(\Delta).$$

For simplicity, we focus on the case where  $\lambda_1 = \lambda_2$ . The case where  $\lambda_1 \neq \lambda_2$  is treated in Appendix A.1. When  $\lambda_1 = \lambda_2$ ,

$$Q'(\Delta) = \lambda_1 (\lceil \alpha_1 \rceil^+ - \alpha_2) \alpha_2' - \lceil \alpha_1 \rceil^{+'}$$

where all derivatives are with respect to  $\Delta$ .

To derive the optimal  $\Delta^*$ , we first assume that  $\alpha_1 > 0$  and solve the optimization problem. With this assumption, we note that  $Q'(0) = +\infty$ , i.e.  $Q(\Delta)$  is increasing at  $\Delta = 0$ . Also, the solution to  $Q'(\Delta) = 0$  is given by the solution of a cubic equation with *exactly one* positive root (this can easily be seen from the Descartes' sign scheme), which we denote by  $\Delta^\dagger$

$$\Delta^\dagger = \arg_{\Delta>0} \left\{ \left( \frac{h^2}{\lambda_1} \right) \Delta^3 - (2^R (2^R + h^2)) \Delta^2 - (2^R (2^{R+1} + h^2)) \Delta - (2^{2R}) = 0 \right\},$$

where  $\Delta^\dagger$  can be evaluated analytically using the properties of cubic equations.

Since  $Q'(0) = +\infty$ , and  $\Delta^\dagger$  is the *only* critical point of  $Q(\Delta)$ , the maximizing  $\Delta^* = \Delta^\dagger$ , provided our initial assumption of  $\alpha_1 > 0$  is correct, which translates to  $\Delta^\dagger > \Delta_t = \frac{h^2}{2^R - 1} - 1$  being satisfied.

If however,  $\Delta^\dagger \leq \Delta_t$ , our initial assumption is invalid, and we set  $\lceil \alpha_1 \rceil^+ = 0$  in the  $Q(\Delta)$  expression. We also note that in this case, the maximizing  $\Delta^*$  will lie in the interval  $(0, \Delta_t]$ . In such a case,  $Q'(\Delta) = -\lambda_1 \alpha_2 \alpha'_2 > 0 \quad \forall \Delta \in (0, \Delta_t]$ , i.e.,  $Q(\Delta)$  is monotonically increasing in  $\Delta$ . Hence, the maximizing  $\Delta^* = \Delta_t$ .

Thus, combining the above cases, we have,

$$\Delta^* = \max \{ \Delta^\dagger, \Delta_t \} \quad \text{for} \quad \lambda_1 = \lambda_2$$

### 1.3.4 CSIR limited Hybrid DF/QMF

In this strategy, we let the relay perform a DF operation if it is able to decode the codeword sent from the source. However, if it cannot decode, it will go into QMF mode, whereby it will use the CSIR-optimal quantizer distortion to quantize the received signal and subsequently map and forward it to the destination. The relay will also transmit a 1-bit flag to the destination letting it know the relaying scheme it has used, i.e., DF or QMF. We next show that the outage performance of this hybrid scheme (denoted by HYB) is superior to the outage performance of both the DF and CSIR-optimal QMF schemes individually.

We write the outage probabilities at a given rate  $R$  for the relaying schemes using the total probability theorem by conditioning on whether the relay can decode the source transmission. Thus, for the relaying schemes DF, QMF and HYB, we have:

$$P_{\text{out,DF}}(R) = \left\{ \begin{array}{l} \Pr \{R > \log(1 + g_1^2 + g_2^2)\} \cdot \Pr \{R < \log(1 + h^2)\} \\ + \Pr \{R > \log(1 + g_2^2)\} \cdot \Pr \{R \geq \log(1 + h^2)\} \end{array} \right\} \quad (1.6)$$

$$P_{\text{out,QMF}}(R) = \left\{ \begin{array}{l} \Pr \{R > R_{\text{QMF}}(\Delta^*)\} \cdot \Pr \{R < \log(1 + h^2)\} \\ + \Pr \{R > R_{\text{QMF}}(\Delta^*)\} \cdot \Pr \{R \geq \log(1 + h^2)\} \end{array} \right\} \quad (1.7)$$

$$P_{\text{out,HYB}}(R) = \left\{ \begin{array}{l} \Pr \{R > \log(1 + g_1^2 + g_2^2)\} \cdot \Pr \{R < \log(1 + h^2)\} \\ + \Pr \{R > R_{\text{QMF}}(\Delta^*)\} \cdot \Pr \{R \geq \log(1 + h^2)\} \end{array} \right\} \quad (1.8)$$

An important point to note for the above expressions is that in terms involving  $R_{\text{QMF}}(\Delta^*)$ , the probability must be computed by further conditioning on the source-to-relay channel  $h$ , and then using the total probability theorem. This is because in CSIR-optimized QMF, the distortion  $\Delta^*$  depends on the channel realization  $h$ .

To show that  $P_{\text{out,HYB}}(R) < P_{\text{out,QMF}}(R)$ , from equations (1.7) and (1.8) we have to show:

$$\Pr \{R > \log(1 + g_1^2 + g_2^2)\} < \Pr \{R > R_{\text{QMF}}(\Delta^*)\}$$

where  $\Delta^*$  is the CSIR-optimal quantizer distortion derived previously.

From the QMF rate expression in (1.3), we see that

$$R_{\text{QMF}}(\Delta^*) < \log(1 + g_1^2 + g_2^2) - \log\left(\frac{1 + \Delta^*}{\Delta^*}\right) \implies R_{\text{QMF}}(\Delta^*) < \log(1 + g_1^2 + g_2^2)$$

which proves that  $P_{\text{out,HYB}}(R) < P_{\text{out,QMF}}(R)$ .

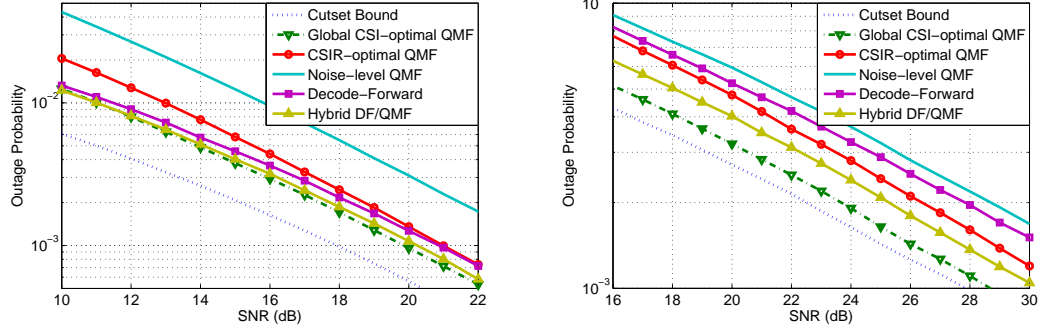
Next, to show that  $P_{\text{out,HYB}}(R) < P_{\text{out,DF}}(R)$ , from equations (1.6) and (1.8) we have to show:

$$\Pr \{R > R_{\text{QMF}}(\Delta^*)\} < \Pr \{R > \log(1 + g_2^2)\}.$$

From the definition of  $\Delta^*$ , the CSIR-optimal quantizer distortion, we know that it minimizes the outage probability  $\Pr \{R > R_{\text{QMF}}(\Delta)\}$  for every realization  $h$  of the source to relay channel. Hence, if we pick any  $\Delta = \Delta_1$  irrespective of  $h$  (in other words, we pick the same quantizer distortion  $\Delta_1$  for all realizations  $h$  instead of using optimized distortions for every realization), we have:  $\Pr \{R > R_{\text{QMF}}(\Delta^*)\} < \Pr \{R > R_{\text{QMF}}(\Delta_1)\}$ . Picking  $\Delta_1 = \infty$  gives us:

$$\Pr \{R > R_{\text{QMF}}(\Delta^*)\} < \Pr \{R > \log(1 + g_2^2)\}$$

which proves that  $P_{\text{out,HYB}}(R) < P_{\text{out,DF}}(R)$ .



(a) All channels are i.i.d. The rate scales as:  $R = 0.3 \log_2(\text{SNR})$ .  
 (b)  $\mathbb{E}\{|g_1|^2\} = \mathbb{E}\{|g_2|^2\} = 10\mathbb{E}\{|h|^2\}$ .  $x$ -axis:  $\mathbb{E}\{|h|^2\}$ .  
 The rate scales as  $R = 0.7 \log_2(\text{SNR})$ .

Figure 1.3: Outage Performance in Rayleigh faded channels over the full-duplex single-relay network.

### 1.3.5 Numerical Evaluation

In Fig. 1.3, the outage performance of the relaying schemes are plotted for different rate scalings and channel configurations. In the setting shown in Fig. 1.3a with i.i.d. channels and a multiplexing gain of 0.3, the CSIR-optimized QMF is shown to provide a 3 dB gain over the baseline noise-level scheme. The global CSI optimal QMF roughly offers an additional 2 dB gain over the CSIR-optimal QMF. Similar optimization gains are also observed for the setting in Fig. 1.3b with a higher rate scaling and more asymmetric channels.

Another interesting point observed from simulations is that the performance of the *local* CSI-optimal QMF is numerically indistinguishable from that of the global CSI variant for all channel configurations we tested. This possibly indicates that the S – D direct link does not influence the performance of QMF significantly as far as relay parameter choices are concerned.

From Fig. 1.3a, we also see that for i.i.d. channels, in CSIR limited settings, DF marginally outperforms CSIR-optimal QMF (by about 1 dB), but the (CSIR limited) hybrid scheme outlined in section 1.3.4 outperforms both DF and CSIR-optimal QMF. For the setting shown in Fig. 1.3b on the other hand, where the source-to-relay link is weaker in comparison to the other links, CSIR-optimal QMF outperforms DF by about 2 dB. The hybrid again outperforms them both, providing an additional 1 dB benefit over CSIR-optimal QMF.

## 1.4 Half-Duplex Single Relay network

To extend our framework to half-duplex QMF relaying, we have two parameters – the schedule (fraction of listening time)  $f$ , and the quantizer distortion  $\Delta$ , that we have to

*jointly* optimize depending on the CSI available to the relay. This problem is significantly more involved than the full-duplex QMF problem. In fact it turns out that it is difficult to provide clean analytical characterizations for most of the CSI conditions that we have tackled in this work.

### 1.4.1 Global CSI at the Relay:

With global CSI, the equivalent rate-maximization problem can be stated using (1.4) as:

$$R_{\text{QMF}}^* = \max_{f \in (0,1); \Delta > 0} \left\{ \lceil \min \{I_{hd,1}, I_{hd,2}\} \rceil^+ \right\}.$$

From the expressions above, it is evident that

- $I_{hd,1}$  is *monotonically increasing* in  $f$  and *monotonically decreasing* in  $\Delta$
- $I_{hd,2}$  is *monotonically increasing* in  $\Delta$

To proceed, let us first fix an  $f$ , and find the optimal  $\Delta = \Delta^*(f)$  corresponding to that fixed value of  $f$ . The equivalent representation of the original optimization problem then becomes

$$R_{\text{QMF}}^* = \max_{f \in (0,1)} \{R_{\Delta}(f)\},$$

where  $R_{\Delta}(f) = \max_{\Delta > 0} \left\{ \lceil \min \{I_{hd,1}, I_{hd,2}\} \rceil^+ \right\}$ , and  $\Delta^*(f) = \arg_{\Delta > 0} R_{\Delta}(f)$ .

For the boundary values, we have

$$\begin{aligned} I_{hd,1}(f, \Delta = 0) &= f \log(1 + h^2 + g_2^2) + (1 - f) \log(1 + g_2^2) \\ I_{hd,1}(f, \Delta = \infty) &= \log(1 + g_2^2) \\ I_{hd,2}(f, \Delta = 0) &= -\infty \\ I_{hd,2}(f, \Delta = \infty) &= f \log(1 + g_2^2) + (1 - f) \log(1 + g_1^2 + g_2^2). \end{aligned}$$

The fact that  $I_{hd,1}(f, \Delta) > 0$  and  $I_{hd,1}(f, \Delta = 0) > I_{hd,2}(f, \Delta = 0)$ , coupled with the above mentioned monotonicity properties of  $I_{hd,1}$  and  $I_{hd,2}$  in the variable  $\Delta$  ensure that for a given  $f$ ,  $\Delta^*(f) = \arg_{\Delta > 0} \{I_{hd,1} = I_{hd,2}\}$ . We can then run a search over  $f \in (0, 1)$  to maximize  $R_{\Delta}(f)$ . The maximising schedule  $f = f^*$  and the distortion  $\Delta^*(f^*)$  is the required optimal.

### 1.4.2 CSIR at the Relay

To obtain a jointly optimal quantizer and relay schedule in this setting, the metric to minimize is again the probability of outage, conditioned only on  $h$ . Proceeding similarly as in the full-duplex case, we have,

$$1 - P_{\text{out}|h}(R; f, \Delta) = \Pr \left\{ \{R < I_{hd,1}\} \cap \{R < I_{hd,2}\} \right\}.$$

We note that both  $g_1^2$  and  $g_2^2$  are to be treated as random variables in the optimization for the CSIR setting. Since  $I_{hd,2}$  now involves *two* random variables, the event  $\{R < I_{hd,1}\} \cap \{R < I_{hd,2}\}$ , for a given  $(f, \Delta)$  pair can equivalently be represented as  $\{(g_1^2, g_2^2) \in \mathcal{G}(f, \Delta)\}$  where  $\mathcal{G}$  is an appropriate open region in the first quadrant of the 2-D plane. The probability is computed numerically and the computation is sped up by taking advantage of the structure of the integration region (isolating rectangular components) and making use of the cumulative distribution function of exponential random variables. The optimal  $(f, \Delta)$  pair is the one that minimizes  $P_{\text{out}|h}(R; f, \Delta)$  thus obtained. One can show that for a given  $f$ ,  $P_{\text{out}|h}(R; f, \Delta)$  increases with  $\Delta$  after a certain threshold  $\Delta_{th}$ . Also, from extensive numerical evaluations, we can conjecture (similar to that in the full-duplex CSIR case for asymmetric fades) that there is exactly one critical point of  $P_{\text{out}|h}(R; f, \Delta)$  in  $(0, \Delta_{th})$  which we can efficiently compute numerically. The optimal over  $f$  can then be found by a sufficiently quantized search over the  $(0, 1)$  interval.

### 1.4.3 CSIR-limited hybrid QMF/DDF

Similar to the full-duplex case, we outline a hybrid strategy for the CSIR-limited half-duplex network that combines the benefits of the CSIR-optimal QMF and the dynamic decode forward (DDF) strategy proposed in [8]. The relay operation here is more involved than that of the full-duplex relay, as it has to jointly choose a schedule, a quantizer and a relaying scheme (DDF or QMF) using the information available. We next outline the relay operation for this scheme.

Given the received channel  $h$ , the relay essentially runs a scan over all (sufficiently finely quantized) schedules  $f \in [0, 1]$ , and for each such  $f$ , computes the conditional probability of outage. If a schedule  $f$  permits a decoding operation (i.e.,  $R < f \log(1 + h^2)$ ), the outage probability corresponds to that of DDF, whereas, if it does not permit decoding, the outage probability corresponds to that of CSIR-optimized QMF. The schedule  $f^*$  that minimizes the conditional outage probability thus obtained is the required schedule, and the relaying scheme to be used is the one that leads to this minimum outage probability.

However, one can observe that the properties of the rate expressions for DDF allow for a lower complexity equivalent operation at the relay. Consider the quantity  $f_{\text{DDF}} = \frac{R}{\log(1+h^2)}$ . If, for the given  $h$ ,  $f_{\text{DDF}}$  is inadmissible (i.e.,  $f_{\text{DDF}} > 1$ ), the relay will use CSIR-optimized

QMF. For the case when  $f_{\text{DDF}}$  is admissible, the values of  $f$  (in the scan at the relay) for which DDF will be considered to compute the probability of outage lie in the interval  $[f_{\text{DDF}}, 1]$ . Observe that in this regime, the probability of outage is an increasing function of  $f$ , and hence one only needs to run the scan in the interval  $[0, f_{\text{DDF}}]$  with the outage probability corresponding to QMF for  $f \in [0, f_{\text{DDF}})$  and to DDF for  $f = f_{\text{DDF}}$ .

We next prove that the outage performance of the hybrid scheme described above is superior to that of CSIR-optimized QMF as well as DDF schemes taken individually. To do so, we demonstrate that for every schedule  $f \in [0, 1]$ , the outage probability of the hybrid scheme is smaller than that of DDF and CSIR-optimized QMF, which naturally translates to it being better when the optimizing  $f$  is chosen. We denote by  $P_{\text{out}}^{(f)}$ , the probability of outage at a particular schedule  $f$ . Writing out these probabilities for the schemes, we have:

$$P_{\text{out,DDF}}^{(f)}(R) = \left\{ \begin{array}{l} \Pr \{R > (1-f) \log(1+g_1^2+g_2^2) + f \log(1+g_2^2)\} \cdot \Pr \{R < f \log(1+h^2)\} \\ + \Pr \{R > \log(1+g_2^2)\} \cdot \Pr \{R \geq f \log(1+h^2)\} \end{array} \right\} \quad (1.9)$$

$$P_{\text{out,QMF}}^{(f)}(R) = \left\{ \begin{array}{l} \Pr \{R > R_{hd,\text{QMF}}(\Delta^*(f))\} \cdot \Pr \{R < f \log(1+h^2)\} \\ + \Pr \{R > R_{hd,\text{QMF}}(\Delta^*(f))\} \cdot \Pr \{R \geq f \log(1+h^2)\} \end{array} \right\} \quad (1.10)$$

$$P_{\text{out,HYB}}^{(f)}(R) = \left\{ \begin{array}{l} \Pr \{R > (1-f) \log(1+g_1^2+g_2^2) + f \log(1+g_2^2)\} \cdot \Pr \{R < f \log(1+h^2)\} \\ + \Pr \{R > R_{hd,\text{QMF}}(\Delta^*(f))\} \cdot \Pr \{R \geq f \log(1+h^2)\} \end{array} \right\} \quad (1.11)$$

To show that  $P_{\text{out,HYB}}^{(f)}(R) < P_{\text{out,QMF}}^{(f)}(R)$ , we observe from equations (1.10) and (1.11) that we have to show:

$$\Pr \{R > (1-f) \log(1+g_1^2+g_2^2) + f \log(1+g_2^2)\} < \Pr \{R > R_{hd,\text{QMF}}(\Delta^*(f))\}$$

where  $\Delta^*(f)$  is the CSIR-optimal quantizer distortion derived previously.

From the QMF rate expression in (1.4), we see that

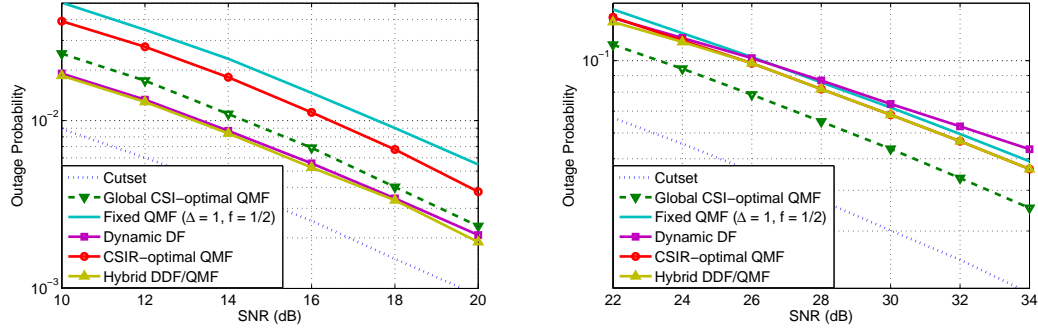
$$\begin{aligned} R_{hd,\text{QMF}}(\Delta^*(f)) &< (1-f) \log(1+g_1^2+g_2^2) + f \log(1+g_2^2) - f \log\left(\frac{1+\Delta^*(f)}{\Delta^*(f)}\right) \\ \implies R_{hd,\text{QMF}}(\Delta^*(f)) &< (1-f) \log(1+g_1^2+g_2^2) + f \log(1+g_2^2) \end{aligned}$$

which proves that  $P_{\text{out,HYB}}^{(f)}(R) < P_{\text{out,QMF}}^{(f)}(R)$ .

Next, to show that  $P_{\text{out,HYB}}^{(f)}(R) < P_{\text{out,DDF}}^{(f)}(R)$ , we observe from equations (1.9) and (1.11) that we have to show:

$$\Pr \{R > R_{hd,\text{QMF}}(\Delta^*(f))\} < \Pr \{R > \log(1+g_2^2)\}$$

where  $\Delta^*(f)$  is the CSIR-optimal quantizer distortion derived previously.



(a) All channels are i.i.d. The rate scales as:  $R = 0.3 \log_2(\text{SNR})$ .  
 (b) All channels are i.i.d. The rate scales as:  $R = 0.7 \log_2(\text{SNR})$ .  
 Figure 1.4: Outage Performance in Rayleigh faded channels over the half-duplex single-relay network.

From the definition of  $\Delta^*(f)$ , we know that it minimizes  $\Pr\{R > R_{hd, \text{QMF}}(\Delta)\}$  for every realization  $h$  of the S – R channel at any given schedule. Hence, if we pick any  $\Delta = \Delta_1$  irrespective of  $h$  and  $f$  (in other words, we pick the same quantizer distortion  $\Delta_1$  for all realizations  $h$  instead of optimized distortions for every realization), we have:

$$\Pr\{R > R_{hd, \text{QMF}}(\Delta^*(f))\} < \Pr\{R > R_{hd, \text{QMF}}(\Delta_1)\}$$

Picking  $\Delta_1 = \infty$  gives us:

$$\begin{aligned} & \Pr\{R > R_{hd, \text{QMF}}(\Delta^*(f))\} \\ & < \Pr\{R > \min\{(1-f) \log(1+g_1^2+g_2^2) + f \log(1+g_2^2), \log(1+g_2^2)\}\} \\ & \implies \Pr\{R > R_{hd, \text{QMF}}(\Delta^*(f))\} < \Pr\{R > \log(1+g_2^2)\} \end{aligned}$$

which proves that  $P_{\text{out, HYB}}^{(f)}(R) < P_{\text{out, DDF}}^{(f)}(R)$ .

#### 1.4.4 Numerical Evaluations

Fig. 1.4a and 1.4b depict the outage performance of the relaying schemes for two different multiplexing gains—0.3 and 0.7 over i.i.d Rayleigh-faded channels<sup>1</sup>. In both cases, we see that using CSIR-optimal QMF provides an improvement of  $\sim 1$  dB over the baseline scheme used in [6] to prove DMT optimality. In addition, the global CSI-optimal provides an additional 3 dB gain over the CSIR optimal in settings where feedback can be exploited.

<sup>1</sup>The schedule for the cutset bound expression in (1.5) is optimized using global CSI, similar to Sec. 1.4.1

$$\text{and is given by } f^* = \arg_f \{C_{hd,1} = C_{hd,2}\} = \frac{\log\left(\frac{1+(g_1+g_2)^2}{1+g_2^2}\right)}{\log\left(\frac{(1+g_2^2)(1+(g_1+g_2)^2)}{(1+g_2^2)^2}\right)}$$

For multiplexing gains less than 0.5, both QMF and DDF are DMT-optimal for this network, but the plots in Fig. 1.4a clearly demonstrate the edge that DDF has over even optimized QMF in finite SNRs at these rates. The situation changes around for Fig. 1.4b however, as in this regime DDF is not DMT-optimal [6] and is outperformed by CSIR-optimal QMF.

As proved in Section 1.4.3, the hybridization of CSIR-optimal QMF and DDF consistently outperforms both the schemes in the two settings shown.

## 2 Finite-SNR QMF Optimizations for Multiple-Relay Networks

In this chapter, we demonstrate how the insights from the single-relay network in the previous chapter can be utilized to provide a *scalable* solution for networks having more than one relays, the simplest example being that of an  $N$ -relay diamond network. We demonstrate the following two results that are of particular significance to diamond network operation at moderate SNRs: (i) We prove that an *universal* quantizer distortion level at all relays can be appropriately chosen (without the need for CSI) to improve the additive approximation gap of QMF from the conventional  $\Theta(N)$  [3] [7] to within  $\Theta(\log N)$  bits/s/Hz—an exponential improvement<sup>1</sup>. We demonstrate that as the number of relays in the network grows, this translates to significant finite SNR benefits as compared to using noise-level quantization, and (ii) We show how CSIR at the relay can be used to invoke a hybrid strategy involving DF and universal QMF that provably improves the outage performance of the latter, with simulations demonstrating a 5 dB gain over QMF, and a diversity order gain over DF in asymmetric diamond networks. We also provide analytical characterizations of global CSI-aware optimal quantizers for the 2-relay network as well as the symmetric  $N$ -Relay network, to benchmark the performance of the strategies we propose.

### 2.1 System Model

The  $N$ -Relay diamond network we consider is shown in Fig. 2.1. In this model, the source  $S$  communicates with the destination  $D$  via  $N$  relay nodes capable of causal signal processing. The signals transmitted by the source  $S$  and the relay nodes  $A_i \in \{A_1, A_2, \dots, A_N\}$  are denoted by  $X$  and  $X_i$ . The received signal at the destination and the relay nodes are denoted by  $Y$  and  $Y_i$ ,  $i \in \{1, 2, \dots, N\}$ . The received signals as a function

---

<sup>1</sup>A version of the  $\Theta(\log(N))$  gap result was also presented in [9] independently at the same conference as our work [10].

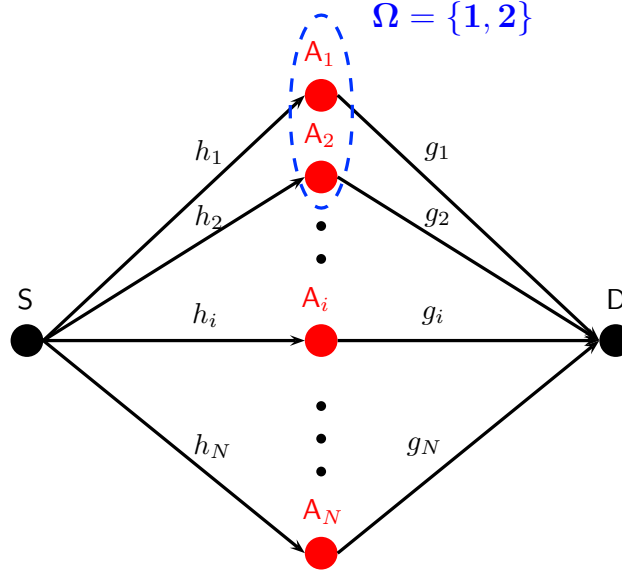


Figure 2.1: Diamond Network Communication Model

of the transmitted signals are as follows:

$$Y_i = h_i X + Z_i, \quad Y = \sum_{i=1}^N g_i X_i + Z$$

where  $h_i$  represents the complex channel coefficient between S and  $A_i$  and  $g_i$  denotes that between  $A_i$  and D.  $Z_i, i \in \{1, 2, \dots, N\}$  and  $Z$  are i.i.d  $\mathcal{CN}(0, 1)$  random variables. The transmitted signals are normalized to have an average power constraint of unity at the source and the relays, i.e.,  $\mathbb{E}(|X|^2) \leq 1$  and  $\mathbb{E}(|X_i|^2) \leq 1, i \in \{1, 2, \dots, N\}$ . Again, for notational convenience, we let  $h_i := |h_i|, g_i := |g_i|$  for  $i = \{1, 2, \dots, N\}$ .

## 2.2 Rate Expressions and Upper Bounds

We denote by  $\Omega$ , a partition of the index set  $[1 : N] := \{1, 2, \dots, N\}$  of the relay nodes  $\{A_1, \dots, A_N\}$ . Therefore, for any  $\Omega \subseteq [1 : N]$ ,  $\{S\} \cup \{A_i : i \in \Omega\}$  is a *cut* of the network (see Fig. 2.1 for illustration). Moreover, let  $X_\Omega := \{X_i : i \in \Omega\}$ .

### 2.2.1 QMF Achievable Rates

The achievable rate for QMF relaying over the  $N$ -relay diamond network is evaluated using the single-letter characterization<sup>2</sup> in [7].

$$R_{\text{QMF}} = \max_{\Omega} \min_{\Omega} \left\{ I(X, X_\Omega; \hat{Y}_{\Omega^c}, Y | X_{\Omega^c}) - I(Y_\Omega; \hat{Y}_\Omega | X, X_{[1:N]}, \hat{Y}_{\Omega^c}, Y) \right\}$$

<sup>2</sup>The Gaussian version was proved in [11] using lattice vector quantizers.

where the maximum is taken over all distributions  $p(X)\prod_{i \in [1:N]} p(X_i) p(\hat{Y}_i|Y_i, X_i)$ . Here  $\hat{Y}_i$  denotes the quantizer output of relay  $A_i$ . Generating the Gaussian vector quantization codebooks with the following independent single-letter probability distributions  $\hat{Y}_i = Y_i + \hat{Z}_i$ ,  $\hat{Z}_i \sim \mathcal{CN}(0, \Delta_i)$ ,  $i = 1, \dots, N$ , the above achievable rate is evaluated as

$$R_{\text{QMF}}(\Delta_{[1:N]}) = \min_{\Omega} \{R(\Omega; \Delta_{[1:N]})\}$$

where  $\Delta_J := \{\Delta_j | j \in J\}$ , and  $R(\Omega; \Delta_{[1:N]})$  is as follows:

$$R(\Omega; \Delta_{[1:N]}) = \left[ \log \left( 1 + \sum_{i \in \Omega} g_i^2 \right) + \log \left( 1 + \sum_{j \in \Omega^c} \frac{h_j^2}{1 + \Delta_j} \right) - \sum_{i \in \Omega} \log \left( \frac{1 + \Delta_i}{\Delta_i} \right) \right]^+ \quad (2.1)$$

### 2.2.2 DF Achievable Rates

The DF achievable rate is given by:

$$R_{\text{DF}} = \max_{\Omega} \left\{ \min \left\{ \log \left( 1 + \sum_{i \in \Omega} g_i^2 \right), \min_{i \in \Omega} \log(1 + h_i^2) \right\} \right\}$$

### 2.2.3 Upper Bounds on Capacity

The cutset upper bound on the capacity of the network is given by:

$$\bar{C}_{\text{cut}} \leq \min_{\Omega} \left\{ \log \left( 1 + \left( \sum_{i \in \Omega} g_i \right)^2 \right) + \log \left( 1 + \sum_{j \in \Omega^c} h_j^2 \right) \right\} \quad (2.2)$$

## 2.3 Achieving Capacity within $\Theta(\log(N))$ Bits

Following the reasoning in [7], we can further obtain a better *universal* quantizer distortion (in the sense of *worst-case* gap over all possible channel realizations in the network) independent of channel coefficients. Setting the quantizer distortions to be the same as  $\Delta$ , we have the following achievable rate: ( $R(\Omega; \Delta_{[1:N]})$  is defined in (2.1))

$$R(\Omega; \Delta_{[1:N]} = (\Delta, \dots, \Delta)) = \left[ \log \left( 1 + \sum_{i \in \Omega} g_i^2 \right) + \log \left( 1 + \sum_{j \in \Omega^c} \frac{h_j^2}{1 + \Delta} \right) - |\Omega| \log \frac{1 + \Delta}{\Delta} \right]^+$$

With a term-by-term comparison with the upper bound (2.2), we see that the worst-case gap is upper bounded by

$$\begin{aligned} \text{gap}^*(\Delta; N) &\leq \max \left\{ \begin{array}{l} \log(N) + N \log\left(\frac{1+\Delta}{\Delta}\right), \\ \left\{ \log(N-i) + (N-i) \log\left(\frac{1+\Delta}{\Delta}\right) + \log(1+\Delta) \right\}_{i \in \{1, 2, \dots, N\}} \end{array} \right\} \\ &= \max \left\{ \begin{array}{l} \log(N) + N \log\left(\frac{1+\Delta}{\Delta}\right), \\ \log(N-1) + (N-1) \log\left(\frac{1+\Delta}{\Delta}\right) + \log(1+\Delta) \end{array} \right\} \end{aligned} \quad (2.3)$$

Also, one can observe that the bound on the worst-case gap in (2.3) is indeed achieved for certain configurations of the network. The first term in the maximization is achieved when  $\Omega = \emptyset$  is the mincut in both the cutset and QMF rate expressions. A configuration of the following type makes this possible: Let  $g_i^2 = \rho^\alpha \quad \forall i, h_i^2 = \rho^\beta \quad \forall i$  with  $\alpha < \beta$  and  $\rho \rightarrow \infty$ . The second term can be achieved with a configuration of the following type: Let  $h_1^2 = \rho^\alpha, h_{i,i \in \{2, \dots, N\}}^2 = \rho^{\alpha'}, g_1^2 = \rho^{\beta'}, g_{i,i \in \{2, \dots, N\}}^2 = \rho^\beta$  with  $\alpha < \alpha', \beta < \beta'$  and  $\rho \rightarrow \infty$ . Thus, the expression in (2.3) can be interpreted as the worst-case gap for a given universal quantizer distortion  $\Delta$ , as opposed to simply a upper bound on it.

For the above, we now wish to find an optimal  $\Delta = \Delta_{\text{opt}}$  that solves the following problem:

$$\Delta_{\text{opt}} = \arg \min_{\Delta} \text{gap}^*(\Delta; N)$$

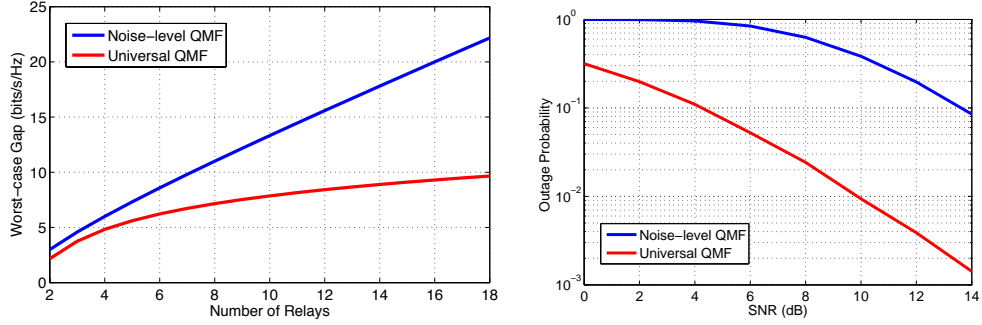
We note when  $\Delta < \frac{N}{N-1}$ , the first term inside the max in (2.3) is larger, and when  $\Delta \geq \frac{N}{N-1}$ , the second term dominates. Taken separately, we see that the first term is monotonically decreasing in  $\Delta$  and the second term has exactly one minima which occurs at  $\Delta = N-1$ . We observe that if this minima occurs before (in the order of increasing  $\Delta$ )  $\Delta = \frac{N}{N-1}$ , the optimizing  $\Delta$  is  $\Delta_{\text{opt}} = \frac{N}{N-1}$ . If however, the minima occurs after  $\Delta = \frac{N}{N-1}$ ,  $\Delta_{\text{opt}} = N-1$ . Combining all these, we have the following:

$$\Delta_{\text{opt}} = \begin{cases} \frac{N}{N-1}, & \frac{N}{N-1} > N-1 \Rightarrow N < 2.618 \Rightarrow N = 2 \\ N-1, & \frac{N}{N-1} < N-1 \Rightarrow N > 2.618 \Rightarrow N > 2 \end{cases}$$

This choice of  $\Delta_{\text{opt}}$  leads to the following result on the *best* worst-case gap in an  $N$ -relay diamond network with universal quantizers:

$$\text{gap}^*(N) = \begin{cases} 2\log(3) - 1, & N = 2 \quad (\Delta_{\text{opt}} = 2) \\ N \log\left(\frac{N}{N-1}\right) + 2\log(N-1), & N > 2 \quad (\Delta_{\text{opt}} = N-1) \end{cases}$$

One can see that for large  $N$ , the worst-case gap with optimized universal quantizers



(a) Comparison of worst-case gaps with number of relays. (b) Outage Performance of noise-level and universal QMF over a 4-relay network. All channels are i.i.d.  $R = 0.3 \log_2(\text{SNR})$ .

Figure 2.2: Illustration of benefits obtained from universal quantizers.

grows approximately logarithmically in  $N$ , as

$$\lim_{N \rightarrow \infty} N \ln \frac{N}{N-1} = \lim_{N \rightarrow \infty} \frac{1/N - 1/(N-1)}{-1/N^2} = \lim_{N \rightarrow \infty} \frac{N}{N-1} = 1.$$

In contrast, the worst-case gap with noise-level quantization is dominated by a linear term in  $N$ . Fig. 2.2a makes the benefits of using an optimized universal quantizer derived above explicit, in terms of the gap performance achieved. The moderate SNR outage benefits obtained from this choice of quantizers is illustrated in Fig. 2.2b, where even for a 4-relay diamond network, we see that universal quantizers provide a 9 dB gain over noise-level QMF.

## 2.4 Global CSI-aware Quantizer Optimization

With global CSI at the relays, the optimization problem can be stated as:

$$R_{\text{QMF}}^* = \max_{\Delta_{[1:N]} \geq 0} R_{\text{QMF}}(\Delta_{[1:N]}) = \max_{\Delta_{[1:N]} \geq 0} \min_{\Omega} \{R(\Omega; \Delta_{[1:N]})\}. \quad (2.4)$$

We note that this optimization is not convex, as within the minimization part of (2.4), for  $\Omega = \emptyset$ , the function  $R(\Omega; \Delta_{[1:N]})$  is not concave in  $\Delta_{[1:N]}$ . Instead, we provide an analytical characterization of the optimizing distortions and the corresponding achievable rates for the 2-relay network, and for symmetric  $N$ -Relay networks.

### 2.4.1 Solution for the 2-Relay Network

In order to solve the optimization problem in (2.4) for the case  $N = 2$ , we consider the following equivalent formulation:

$$\begin{aligned} R_{\text{QMF,G}}^* &= \max_{\Delta_2 > 0} \left\{ \max_{\Delta_1 > 0} \min_{\Omega} R(\Omega; \Delta_1, \Delta_2) \right\} \\ &:= \max_{\Delta_2 > 0} R_{\text{QMF,G}}^*(\Delta_2) \end{aligned} \quad (2.5)$$

with  $R_{\text{QMF,G}}^*(\Delta_2) = \max_{\Delta_1 > 0} \min_{\Omega} R(\Omega; \Delta_1, \Delta_2)$ ,  $\Delta_2 > 0$ .

We shall first characterize  $R_{\text{QMF,G}}^*(\Delta_2)$  and then optimize it over  $\Delta_2$  to obtain the solution. The following lemma and theorem summarize the main result.

**Lemma 2.4.1** (Characterization of  $R_{\text{QMF,G}}^*(\Delta_2)$ ). *Let us define the following intervals of  $\Delta_2$ :*

$$I_1 := (0, \delta_1)$$

$$I_2 := [\delta_1, \delta_2)$$

$$I_3 := [\delta_2, \infty)$$

where  $\delta_1 := \frac{(1+g_1^2+g_2^2)(1+h_1^2+h_2^2)+(1+g_2^2)h_1^2h_2^2}{g_2^2(1+g_1^2+g_2^2)(1+h_1^2)}$ , and  $\delta_2 := \frac{(1+g_1^2)(1+h_2^2)}{g_2^2}$ . In each range of  $\Delta_2$ , the optimizing  $\Delta_1^*$  and  $\Omega^*$  in the max-min problem  $\max_{\Delta_1 > 0} \min_{\Omega} R(\Omega; \Delta_1, \Delta_2)$  is given as follows:

- $\Delta_2 \in I_1$  :

$$\Delta_1^* = \frac{(1+g_2^2)(1+h_1^2)}{g_1^2}$$

$$\Omega^* = \{1, 2\} \text{ or } \{2\}$$

- $\Delta_2 \in I_2$  :

$$\Delta_1^* = \frac{(1+h_1^2)\Delta_2 + (1+h_1^2+h_2^2)}{(g_1^2+g_2^2)\Delta_2 - (1+h_2^2)}$$

$$\Omega^* = \{1, 2\} \text{ or } \emptyset$$

- $\Delta_2 \in I_3$  :

$$\Delta_1^* = \frac{(1+h_1^2)\Delta_2 + (1+h_1^2+h_2^2)}{g_1^2(\Delta_2 + (1+h_2^2))}$$

$$\Omega^* = \{1\} \text{ or } \emptyset$$

Moreover we always have  $0 < \delta_1 < \delta_2$ , and hence the three intervals  $I_1, I_2, I_3$  are not empty.

*Proof.* See Appendix A.2 □

**Theorem 2.4.2.** Let  $A := h_1^2(1+h_1^2) - h_2^2(1+h_1^2+g_1^2+g_2^2)$ ,  $B := 2h_1^2(1+h_1^2)$ ,  $C := h_1^2(1+h_1^2+h_2^2)$ , and  $\delta_3 := \frac{-B-\sqrt{B^2-4AC}}{2A}$ .

The solution to the maximization problem in (2.5), is summarized below:

1)  $A \geq 0$  or  $\delta_3 \in I_3$ : The optimal solution is

$$\begin{aligned}\Delta_2^* &= \delta_2 \\ \Delta_1^* &= \frac{(1+h_1^2)\delta_2 + (1+h_1^2+h_2^2)}{(g_1^2+g_2^2)\delta_2 - (1+h_2^2)} \\ &= \frac{(1+h_1^2)\delta_2 + (1+h_1^2+h_2^2)}{g_1^2(\delta_2 + (1+h_2^2))}\end{aligned}$$

2)  $A < 0$  and  $\delta_3 \in I_1$ : The optimal solution is

$$\begin{aligned}\Delta_2^* &= \delta_1 \\ \Delta_1^* &= \frac{(1+h_1^2)\delta_1 + (1+h_1^2+h_2^2)}{(g_1^2+g_2^2)\delta_1 - (1+h_2^2)} \\ &= \frac{(1+g_2^2)(1+h_1^2)}{g_1^2}\end{aligned}$$

3)  $A < 0$  and  $\delta_3 \in I_2$ : The optimal solution is

$$\begin{aligned}\Delta_2^* &= \delta_3 \\ \Delta_1^* &= \frac{(1+h_1^2)\delta_3 + (1+h_1^2+h_2^2)}{(g_1^2+g_2^2)\delta_3 - (1+h_2^2)}\end{aligned}$$

*Proof.* See Appendix A.3 □

### 2.4.2 Solution for the Symmetric $N$ -Relay Network

We consider the case where  $h_i = h$  and  $g_i = g$  for all  $i = 1, \dots, N$ . By symmetry, the optimal distortion level  $\Delta_i = \Delta$  for all  $i = 1, \dots, N$ , and the optimization becomes

$$R_{\text{QMF}}^* = \max_{\Delta \geq 0} \min_{k \in [0:N]} R_k(\Delta),$$

where  $R_k(\Delta) := \log\left(1 + (N-k)\frac{h^2}{1+\Delta}\right) + \log(1 + kg^2) - k \log\left(\frac{1+\Delta}{\Delta}\right)$ . By plotting the  $R_k(\Delta)$ 's for  $k \in [0:N]$  as a function of  $\Delta$  for various  $N, h$  and  $g$  combinations, one can observe that the max min optimum appears to occur at the value of  $\Delta$  where the curves  $R_0(\Delta)$  and  $R_N(\Delta)$  intersect. A demonstrative plot is shown for a 5-relay network in Fig. 2.3. This observation can in fact be proved, for which the following lemmas are necessary (proofs in Appendix A.4):

**Lemma 2.4.3.** *There exists exactly one positive  $\Delta = \Delta_{ij}^*$  satisfying  $R_i(\Delta) = R_j(\Delta)$ ,  $\forall i, j \in [0:N]$  and  $i \neq j$ .*

**Lemma 2.4.4.**  $\lim_{\Delta \rightarrow 0} \{R_i(\Delta) - R_{i+1}(\Delta)\} \geq 0 \quad \forall i \in [0:N-1]$ .

**Lemma 2.4.5.** *Let  $\Delta_{(i)(i+1)}^*$  be the unique positive solution of  $R_i(\Delta) = R_{i+1}(\Delta) \quad \forall i \in [0:N-1]$ . Then,  $\Delta_{(i)(i+1)}^*$  is non-decreasing in  $i$ , i.e.,  $\Delta_{01}^* \leq \Delta_{12}^* \leq \dots \leq \Delta_{(N-1)(N)}^*$ .*

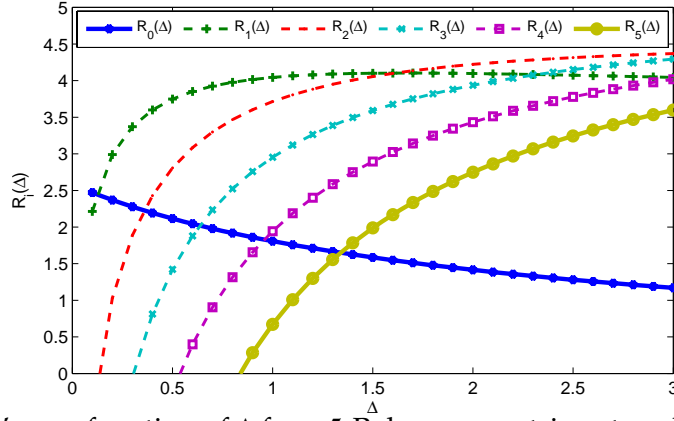


Figure 2.3:  $R_i(\Delta)$ 's as a function of  $\Delta$  for a 5-Relay symmetric network with  $|h| = 1$  and  $|g| = 3.16$ .

These lemmas ensure that each  $R_k(\Delta)$ ,  $k \in [1 : N]$  intersects  $R_0(\Delta)$  *before* (in the order of increasing  $\Delta$ ) any other curve. Since  $R_0(\Delta)$  is a *decreasing* function of  $\Delta$ , the initial observation is validated and can be crystalized as follows:

**Theorem 2.4.6.**  $(R_0(\Delta_{0N}^*), \Delta_{0N}^*)$  attains optimum, where  $\Delta_{0N}^*$  is the root of  $R_0(\Delta) = R_N(\Delta)$ .

## 2.5 CSIR limited Hybrid DF/QMF Relaying

In the spirit of the hybrid scheme that we proposed for the single relay network, a CSIR-limited hybrid scheme for the diamond network is illustrated in this subsection. In this scheme, the relays individually decide whether or not they can decode the source message, depending on the incoming source-to-relay channel  $h_i$  for the  $i^{th}$  relay. For the relays where the incoming channel supports decoding, the relays decode and transmit the re-encoded message. The relays that cannot decode apply QMF, i.e., they quantize, map and forward their received signals to the destination. Each relay sends a 1-bit flag (in a possibly orthogonalized preamble, so that these do not interfere) to let the destination know whether it used DF or QMF mode of operation.

In the following, we will demonstrate that this strategy, strictly improves upon the outage performance of QMF for all possible choices of quantizer distortions. In fact, as we illustrate in the next section, simulations even demonstrate significant benefits of this hybrid scheme over the DF scheme alone, which is known to not achieve optimal DMT or constant-gap performance for all channel configurations of the diamond network.

Writing out the probability of outage for the hybrid scheme, we have:

$$P_{\text{out}}(R) = \sum_{\Omega} \Pr\{R > R_{\text{HYB}}(\Omega_D) | \Omega_D = \Omega\} \cdot \Pr\{\Omega_D = \Omega\}$$

where  $\Omega_D$  denotes the subset of nodes that can decode the source message, and  $\Omega$

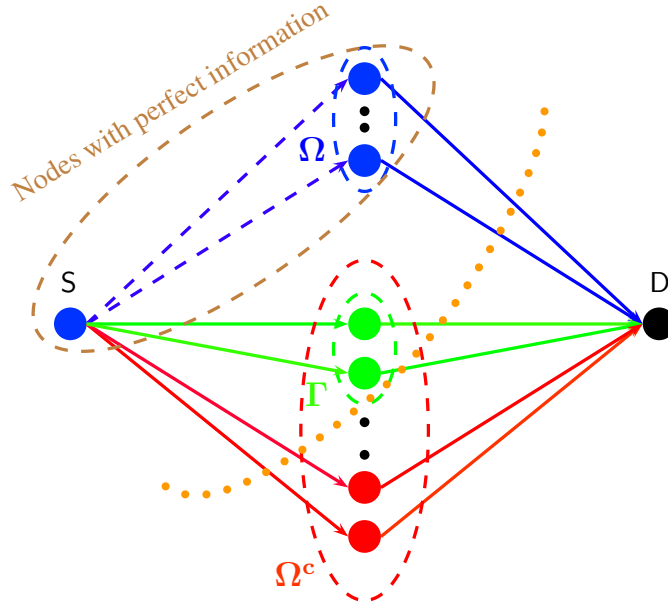


Figure 2.4: The cut in the above diagram depicts the information transfer across nodes for a given choice of  $\Gamma$ .  $I_D(\Omega)$  is the minimum of all such cut values computed over every possible choice of  $\Gamma$ .

denotes an arbitrary partition on the set of relays.

It is important to note that the supportable rate for the hybrid scheme,  $R_{\text{HYB}}(\Omega_D)$  is dependent on the set of nodes that can decode. For instance, in the term corresponding to  $\Omega_D = \emptyset$ , i.e., no relay can decode,  $R_{\text{HYB}}(\Omega_D = \emptyset) = R_{\text{QMF}}$ .

One can observe that the events  $\{R > R_{\text{HYB}}(\Omega_D) | \Omega_D = \Omega\}$  and  $\{R > I_D(\Omega_D = \Omega)\}$  are equivalent, where  $I_D(\Omega_D = \Omega)$  is given by the following expression (see Fig. 2.4 for illustration):

$$I_D(\Omega_D = \Omega) = \min_{\Gamma} \left\{ \begin{aligned} &\log(1 + \sum_{i \in (\Omega \cup \Gamma)} g_i^2) + \\ &\log\left(1 + \sum_{j \in (\Omega \cup \Gamma)^c} \frac{h_j^2}{1 + \Delta_j}\right) - \sum_{k \in \Gamma} \log\left(\frac{1 + \Delta_k}{\Delta_k}\right) \end{aligned} \right\} \quad (2.6)$$

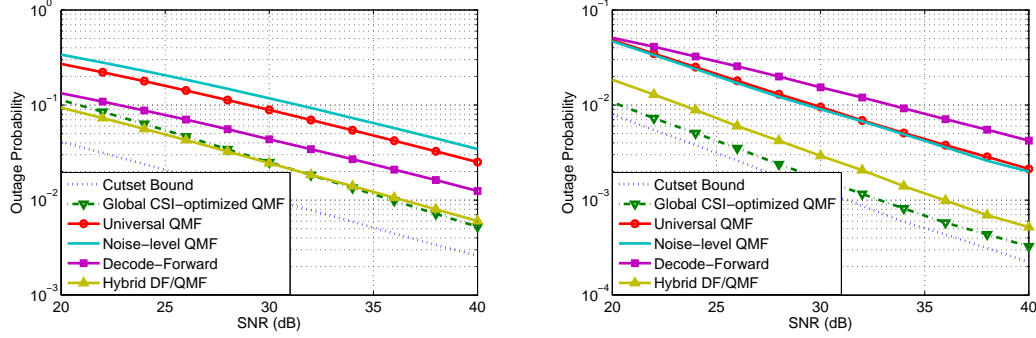
where  $\Gamma$  denotes a partition on the set  $\Omega^c$ .

We observe that to show HYB outperforms QMF, it is sufficient to show that  $I_D(\Omega) > R_{\text{QMF}}$ ,  $\forall \Omega$ . This is because the QMF rate expression does not depend on the choice of  $\Omega_D$ , the set of nodes that can decode the message.

To show this, we note that for every  $\Omega$  and every  $\Gamma$  (for a given  $\Omega$ ) in eq. (2.6), we can find a partition  $\Omega_{\text{QMF}} = \Omega \cup \Gamma$  for which the QMF mutual information,  $I_Q(\Omega_{\text{QMF}})$ , is less than the corresponding term inside the minimization expression for  $I_D(\Omega)$  by an amount  $\sum_{\omega \in \Omega} \log\left(\frac{1 + \Delta_{\omega}}{\Delta_{\omega}}\right)$ . Also, since  $R_{\text{QMF}} = \min_{\Omega_{\text{QMF}}} I_Q(\Omega_{\text{QMF}})$ , we can conclude that

$I_D(\Omega) > R_{\text{QMF}}, \forall \Omega$ , which proves the result.

## 2.6 Numerical Evaluations



(a) All channels are i.i.d. The rate scales as:  $R = 0.7 \log_2(\text{SNR})$ .  
 (b)  $\mathbb{E}\{|h_1|^2\} = \mathbb{E}\{|g_2|^2\} = \frac{\mathbb{E}\{|g_1|^2\}}{25} = \frac{\mathbb{E}\{|h_2|^2\}}{10}$ ;  $x$ -axis:  $\mathbb{E}\{|h_1|^2\}, R = 0.7 \log_2(\text{SNR})$ .

Figure 2.5: Outage Performance in Rayleigh faded channels over the 2-relay diamond network.

Fig. 2.5 shows the outage performance of the relaying schemes we consider for the diamond network under different channel configurations. Fig. 2.5a depicts the performance for i.i.d channels, whereas Fig. 2.5b looks at an antisymmetric network configuration. As we can see, in both the above settings, if global CSI of the channel strengths is available to the relays, QMF consistently provides very good performance. In the absence of global CSI however, we see that for i.i.d channels, DF provides a significant advantage over universal QMF, and the noise-level QMF is even worse. This is as per expectations, as the benefits of QMF are more pronounced in asymmetric settings, i.e., when one of the relays is closer to the source while the other is closer to the destination. Indeed, in Fig. 2.5b, where we have asymmetric channel configurations, we see that universal QMF outperforms DF in the diversity order (slope of the curve) itself.

It was shown in section 2.5 that the hybrid scheme can provably outperform the universal QMF scheme for the diamond network. What is even more interesting to note from the plots is that not only does it outperform universal QMF, it also significantly outperforms DF in both i.i.d and asymmetric network configurations. It strikes a balance between extracting the multiple-input single-output (MISO) gains of the DF scheme and the optimal DMT performance of QMF to achieve excellent finite SNR performance, even rivaling that of global-CSI optimal QMF.

## Related Work

Cooperative relaying over slow fading networks have been extensively studied in the literature. For full-duplex networks, the optimal DMT is found for the single relay channel [12] and then for arbitrary relay networks [3]. For half-duplex networks, [8] proposed the Dynamic Decode-and-Forward (DDF) scheme, which is later slightly improved by superposition coding in [13]. In [6], it is shown that QMF relaying achieves the optimal DMT for the single-antenna relay channel. For finite-SNR outage performance, most works in the literature were focused on DF and AF, eg., [14, 15, 16, 17, 18]. The outage performance of QMF over the half-duplex relay channel is recently studied in [19] but the optimization of schedules and performance of dynamic relaying protocols are not further pursued. The idea of hybridizing QMF with AF for half-duplex relays was reported in [20], while hybridizing QMF and DF has been reported in an independent archive submission [21], where the treatment is limited to full-duplex relay networks.



# Low-Complexity Codes **Part II**



# 3 Graph-based Codes for QMF Relaying

In this chapter, we translate the QMF principles to a practical coding scheme for the full-duplex 2-relay diamond network. Our source codebook and the relay mappings employ LDPC ensembles that allow a sparse factor graph representation, while the decoder implements a message passing algorithm on a compound graph. We here focus on the diamond network, however our designs extend to more general configurations.

## 3.1 Model and Metrics

### 3.1.1 2-Relay Diamond Network

As in the previous chapter, we consider the (two-relay) diamond network, where a source  $S$  wants to communicate to a destination node  $D$  with the help of two full-duplex relays  $R_1$  and  $R_2$ . The signal  $x_s$  transmitted by the source is broadcast to the relays. The received signals at  $R_1$  and  $R_2$  are given by

$$\begin{aligned} y_{R1} &= h_1 x_s + n_{R1} \\ y_{R2} &= h_2 x_s + n_{R2}, \end{aligned}$$

where  $h_1$  and  $h_2$  are the channel coefficients for the  $S$ -to- $R_1$  and  $S$ -to- $R_2$  channels, and  $n_{R1}$  and  $n_{R2}$  are i.i.d complex Gaussian random variables  $\mathcal{CN}(0, 1)$ . The destination  $D$  observes a superposition of the transmissions from  $R_1$  and  $R_2$ , corrupted by its receiver noise,

$$y = g_1 x_{R1} + g_2 x_{R2} + n_D,$$

where  $g_1$  and  $g_2$  are the channel coefficients for the  $R_1$ -to- $D$  and  $R_2$ -to- $D$  channels. The noise  $n_D$  has the same distribution as  $n_{R1}$ ,  $n_{R2}$ , and is independent of  $n_{R1}$  and  $n_{R2}$ . The transmitted signals from the source and the relays are subject to an average power constraint  $\mathcal{P}$ .

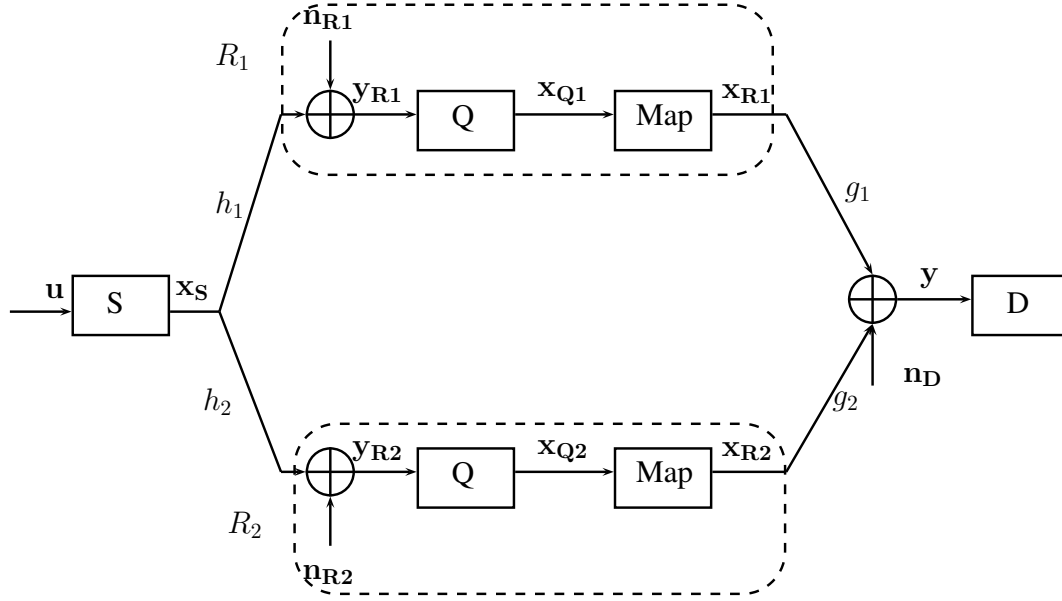


Figure 3.1: QMF Strategy for the 2-Relay Diamond Network

We consider a block-fading model for the channel coefficients, where  $h_1, h_2, g_1, g_2$  are independent circularly symmetric Gaussian random variables that are fixed during a transmission block.

### 3.1.2 Traditional Cooperative Strategies

To demonstrate the cooperation benefits of QMF and evaluate the performance of our design (detailed in section 3.2), we compare ourselves to the following traditional cooperative schemes for the parallel relay network.

- **Routing:** Without transmit CSI, one of the relays is arbitrarily chosen to decode and forward the incoming messages from the source node to the destination node, while the other relay remains silent.
- **Opportunistic Routing:** If the magnitude of the channel realizations are available at the relays, the routing strategy could be improved to use the stronger of the two available paths. This modification of the routing strategy that employs transmit CSI is referred to as opportunistic routing.
- **Amplify-and-forward:** The two relays amplify their received signals to their power constraint and transmit them. The destination node effectively observes a point-to-point channel and tries to recover the transmitted message from the source.
- **Amplify-and-forward with Beamforming:** If the phases of the channel realizations are available at the relays, the amplify-and-forward strategy could be improved by beamforming at the relays.

### 3.1.3 Outage Framework

As highlighted in the previous chapters, in fading wireless channels, an important performance metric is the outage probability of the system, defined as the probability that the network channel realizations do not support the transmitted rate. The trade-off between (multiplexing) rate and error probability (diversity order) for wireless systems can be characterized in the high-SNR regime through the diversity-multiplexing tradeoff. Here, we evaluate both the error performance (at a given rate) and spectral efficiency (the maximum supportable rate at given outage probability) of our QMF-based design, and compare it with the traditional cooperative schemes, in moderate SNR regimes.

## 3.2 QMF System Design

### 3.2.1 Encoding and Relaying

Fig. 3.1 shows the schematic diagram of the QMF strategy for the parallel relay network. The source  $S$  encodes the information vector  $\mathbf{u}$  into the signal vector  $\mathbf{x}_s \in \mathcal{A}_s^N$ , where  $\mathcal{A}_s$  represents the discrete channel-alphabet at the source and  $N$  denotes the transmission blocklength. The constellation  $\mathcal{A}_s$  is constrained to have average power equal to  $\mathcal{P}$ , i.e.,  $\frac{1}{|\mathcal{A}_s|} \sum_{a \in \mathcal{A}_s} \|a\|^2 = \mathcal{P}$

$R_1$  and  $R_2$  quantize their received vectors  $\mathbf{y}_{R1}$  and  $\mathbf{y}_{R2}$  into  $\mathbf{x}_{Q1}$  and  $\mathbf{x}_{Q2}$  respectively, where  $\mathbf{x}_{Q1}, \mathbf{x}_{Q2} \in \{\pm 1\}^{bN}$ , with  $b$  denoting the average number of quantized bits per symbol. Subsequently, the relays map  $\mathbf{x}_{Q1}$  to  $\mathbf{x}_{R1} \in \mathcal{A}_{R1}^N$  and  $\mathbf{x}_{Q2}$  to  $\mathbf{x}_{R2} \in \mathcal{A}_{R2}^N$ , and forward their signals to the destination. The transmit-alphabets at the relays,  $\mathcal{A}_{R1}$  and  $\mathcal{A}_{R2}$ , also satisfy the same power constraint  $\mathcal{P}$ .

We initially focus on the binary communication problem, i.e.  $\mathcal{A}_s = \{\pm 1\}$ . We also set  $\mathcal{A}_{R1} = \mathcal{A}_{R2} = \{\pm 1\}$ , and employ one-bit scalar quantizers at the relays. We defer the extension to non-binary constellations to section 3.2.3.

For our source codebook  $\mathcal{C}$ , we use an LDPC code of the desired rate with a code-membership function  $\mathbb{1}_{\{\mathbf{x}_s \in \mathcal{C}\}}$ . The theoretical development of the QMF scheme in [3] suggests that the mappings at the relays should provide sufficient and independent mixing of the incoming information streams. For the mapping at the relays, we also choose LDPC codes which induce the desirable mixing properties. The mappings can be thought of as encoding  $\mathbf{x}_Q$  with a rate  $\frac{1}{2}$  code, and letting the parity bits be the transmit sequence  $\mathbf{x}_R$ . In this setting the map-membership functions at the relays can be represented as  $\mathbb{1}_{\{(\mathbf{x}_{Q1} \cup \mathbf{x}_{R1}) \in \mathcal{M}_1\}}$  and  $\mathbb{1}_{\{(\mathbf{x}_{Q2} \cup \mathbf{x}_{R2}) \in \mathcal{M}_2\}}$ , where  $\mathcal{M}_1, \mathcal{M}_2$  represent the corresponding LDPC codebooks at the relays. These membership functions have a sparse factor-graph representation, which make them suitable components in iterative decoder structures.

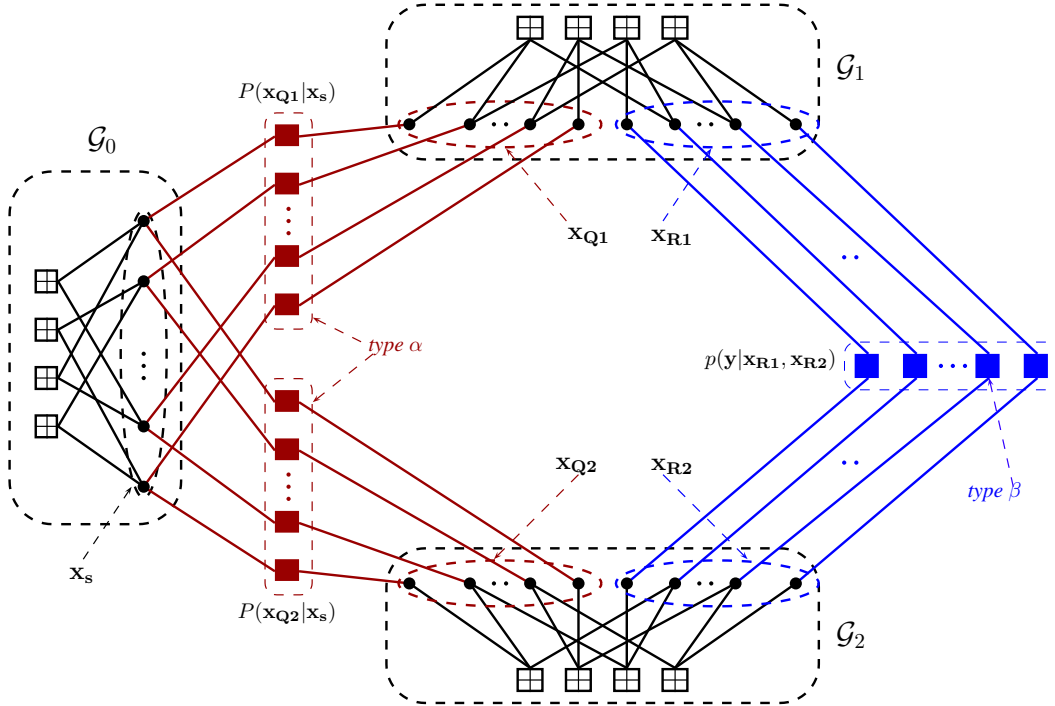


Figure 3.2: Decoding Graph for binary signaling with 1-bit scalar quantizers

### 3.2.2 Iterative QMF Decoder

We derive a compound graphical model to perform iterative decoding of the source bits  $\mathbf{x}_s$ . In contrast to point-to-point decoding, the network graphical model for our iterative QMF decoder has to incorporate the following additional features: (i) It should possess an explicit characterization of the function-nodes representing the quantization and multiple-access operations, together with their own set of message passing rules, and (ii) It should have a well defined information-exchange algorithm among the component LDPC Tanner-graphs corresponding to  $\mathcal{C}$ ,  $\mathcal{M}_1$  and  $\mathcal{M}_2$ . In the following, we detail the derivation and key features of the graphical model.

#### Sum-Product decomposition of a *posteriori* probability

The decoding rule for the bit-wise MAP decoder reads:

$$\hat{x}_{s,i}^{MAP}(\mathbf{y}) = \operatorname{argmax}_{x_{s,i} \in \{\pm 1\}} \sum_{\mathbf{x}_{s,i}} p(\mathbf{x}_s | \mathbf{y})$$

The *a posteriori* probability,  $p(\mathbf{x}_s | \mathbf{y})$ , can be expressed as:

$$\begin{aligned}
 p(\mathbf{x}_s|\mathbf{y}) &= \frac{1}{p(\mathbf{y})} \sum_{\sim \mathbf{x}_s, \mathbf{y}} p(\mathbf{x}_s, \mathbf{x}_{Q1}, \mathbf{x}_{Q2}, \mathbf{x}_{R1}, \mathbf{x}_{R2}, \mathbf{y}) \\
 p(\mathbf{x}_s|\mathbf{y}) &\stackrel{(a)}{\propto} \sum_{\sim \mathbf{x}_s, \mathbf{y}} p(\mathbf{x}_s) \cdot p(\mathbf{x}_{Q1}|\mathbf{x}_s) \cdot p(\mathbf{x}_{Q2}|\mathbf{x}_s) \cdot \\
 &\quad p(\mathbf{x}_{R1}|\mathbf{x}_{Q1}) \cdot p(\mathbf{x}_{R2}|\mathbf{x}_{Q2}) \cdot p(\mathbf{y}|\mathbf{x}_{R1}, \mathbf{x}_{R2}) \\
 &\stackrel{(b)}{\propto} \sum_{\sim \mathbf{x}_s, \mathbf{y}} p(\mathbf{x}_{Q1}|\mathbf{x}_s) \cdot p(\mathbf{x}_{Q2}|\mathbf{x}_s) \cdot p(\mathbf{y}|\mathbf{x}_{R1}, \mathbf{x}_{R2}) \cdot \\
 &\quad \mathbb{1}_{\{\mathbf{x}_s \in \mathcal{C}\}} \cdot \mathbb{1}_{\{(\mathbf{x}_{Q1} \cup \mathbf{x}_{R1}) \in \mathcal{M}_1\}} \cdot \mathbb{1}_{\{(\mathbf{x}_{Q2} \cup \mathbf{x}_{R2}) \in \mathcal{M}_2\}}
 \end{aligned}$$

where (a) follows from the fact that  $\mathbf{x}_s \leftrightarrow (\mathbf{x}_{Q1}, \mathbf{x}_{Q2}) \leftrightarrow (\mathbf{x}_{R1}, \mathbf{x}_{R2}) \leftrightarrow \mathbf{y}$  and  $\mathbf{x}_{R1} \leftrightarrow \mathbf{x}_{Q1} \leftrightarrow \mathbf{x}_s \leftrightarrow \mathbf{x}_{Q2} \leftrightarrow \mathbf{x}_{R2}$  form Markov chains, and (b) follows from the uniform distribution on the source codeword, and the code and map membership constraints. Also, from the memoryless property of the channel, the terms  $p(\mathbf{x}_{Q1}|\mathbf{x}_s)$ ,  $p(\mathbf{x}_{Q2}|\mathbf{x}_s)$  and  $p(\mathbf{y}|\mathbf{x}_{R1}, \mathbf{x}_{R2})$  further factorize on a symbol-by-symbol basis as shown in the decoder graph in Fig. 3.2. The decoding problem thus reduces to computing the marginal of a factorized function and choosing the value that maximizes the marginal.

### Structure of the decoder

As shown in Fig. 3.2, the compound graph contains the graphs corresponding to the source codebook ( $\mathcal{G}_0$ ), and the relay maps ( $\mathcal{G}_1$  and  $\mathcal{G}_2$ ) are constituents of the overall graphical structure. We observe that in addition to the variable and check nodes in  $\mathcal{G}_0$ ,  $\mathcal{G}_1$  and  $\mathcal{G}_2$ , two other types of function nodes enter the graph structure:

- (i) The source-to-relay (type  $\alpha$ ) function nodes, which connect the  $\mathbf{x}_s$  and  $\mathbf{x}_Q$  variable nodes, and represent the functions  $p(\mathbf{x}_{Q1}|\mathbf{x}_s)$  at  $R_1$  and  $p(\mathbf{x}_{Q2}|\mathbf{x}_s)$  at  $R_2$ . These nodes correspond to the quantization operation at the relays and facilitate soft-information exchange between  $\mathcal{G}_0$  and  $\{\mathcal{G}_1, \mathcal{G}_2\}$ .
- (ii) The multiple-access (type  $\beta$ ) function nodes, connecting the  $\mathbf{x}_{R1}$  and  $\mathbf{x}_{R2}$  variable nodes, and representing the function  $p(\mathbf{y}|\mathbf{x}_{R1}, \mathbf{x}_{R2})$ . The information-exchange between  $\mathcal{G}_1$  and  $\mathcal{G}_2$  that occurs via these nodes is an important ingredient in harnessing the benefits of co-operation from the relays.

### Message passing rules

The decoding proceeds via a message-passing algorithm on the decoding graph. We set all messages flowing through the edges to be in *log-likelihood ratio* form, i.e. of the form  $\ln \frac{p(x=+1)}{p(x=-1)}$ . The messages passed from every variable node and also from the check nodes in  $\mathcal{G}_0$ ,  $\mathcal{G}_1$  and  $\mathcal{G}_2$  follow usual belief propagation (BP) message passing rules as summarized in [22]. However, we need to illustrate the message passing rules for the

type  $\alpha$  and type  $\beta$  function nodes that are new to the network graphical model.

Each *type*  $\alpha$  function node  $c$  is connected to a variable node  $v_0$  in  $\mathcal{G}_0$  and to another node  $v_i$  in either  $\mathcal{G}_1$  or  $\mathcal{G}_2$ . The messages passed from the *type*  $\alpha$  function node to node  $v_0$  in  $\mathcal{G}_0$  and to node  $v_i$  in  $\mathcal{G}_i, (i \in \{1, 2\})$  are given by

$$\begin{aligned} m_{c \rightarrow v_0}^{\alpha \rightarrow \mathcal{G}_0} &= \ln \frac{p_{+1|+1} \cdot p(v_i = +1) + p_{-1|+1} \cdot p(v_i = -1)}{p_{+1|-1} \cdot p(v_i = +1) + p_{-1|-1} \cdot p(v_i = -1)} \\ &= \ln \frac{p_{+1|+1} e^{m_{v_i \rightarrow c}^{\mathcal{G}_i \rightarrow \alpha}} + p_{-1|+1}}{p_{+1|-1} e^{m_{v_i \rightarrow c}^{\mathcal{G}_i \rightarrow \alpha}} + p_{-1|-1}} \end{aligned} \quad (3.1)$$

$$\begin{aligned} m_{c \rightarrow v_i}^{\alpha \rightarrow \mathcal{G}_i} &= \ln \frac{p_{+1|+1} \cdot p(v_0 = +1) + p_{+1|-1} \cdot p(v_0 = -1)}{p_{-1|+1} \cdot p(v_0 = +1) + p_{-1|-1} \cdot p(v_0 = -1)} \\ &= \ln \frac{p_{+1|+1} e^{m_{v_0 \rightarrow c}^{\mathcal{G}_0 \rightarrow \alpha}} + p_{+1|-1}}{p_{-1|+1} e^{m_{v_0 \rightarrow c}^{\mathcal{G}_0 \rightarrow \alpha}} + p_{-1|-1}} \end{aligned} \quad (3.2)$$

where  $p_{\pm 1|\pm 1}$  denote the transition probabilities,  $p(v_i|v_0)$ , where  $v_0 \in \mathbf{x}_s$  and  $v_i \in \mathbf{x}_Q$ , and are obtained from the channel statistics.

Each *type*  $\beta$  function node  $c$  is connected to a variable node  $v_1$  in  $\mathcal{G}_1$  and to  $v_2$  in  $\mathcal{G}_2$ . Using similar marginalizations of the corresponding functions as in the case of *type*  $\alpha$  nodes, the messages passed from the *type*  $\beta$  nodes are derived as

$$m_{c \rightarrow v_1}^{\beta \rightarrow \mathcal{G}_1} = \ln \frac{p_{+1,+1} e^{m_{v_2 \rightarrow c}^{\mathcal{G}_2 \rightarrow \beta}} + p_{+1,-1}}{p_{-1,+1} e^{m_{v_2 \rightarrow c}^{\mathcal{G}_2 \rightarrow \beta}} + p_{-1,-1}} \quad (3.3)$$

$$m_{c \rightarrow v_2}^{\beta \rightarrow \mathcal{G}_2} = \ln \frac{p_{+1,+1} e^{m_{v_1 \rightarrow c}^{\mathcal{G}_1 \rightarrow \beta}} + p_{-1,+1}}{p_{+1,-1} e^{m_{v_1 \rightarrow c}^{\mathcal{G}_1 \rightarrow \beta}} + p_{-1,-1}} \quad (3.4)$$

where  $p_{\pm 1,\pm 1}$  represents  $p(y|v_1, v_2)$  where  $y$  is the channel observation,  $v_1 \in \mathbf{x}_{R1}$  and  $v_2 \in \mathbf{x}_{R2}$ .

#### Decoding Schedule

Having defined the message-passing rules for the variable and function nodes, it remains to specify the schedule for information exchange in the compound graphical model. From a computational standpoint, it is efficient to perform message-passing rounds within  $\mathcal{G}_1$  and  $\mathcal{G}_2$  in parallel, once they receive the corresponding incoming messages from the *type*  $\alpha$  and *type*  $\beta$  function nodes. This simultaneously updates the messages

$m_{v \rightarrow c}^{G_i \rightarrow \alpha}$  and  $m_{v \rightarrow c}^{G_i \rightarrow \beta}$  ( $i = 1, 2$ ). In the next step  $G_0$  performs local message-passing rounds with its inputs from the type  $\alpha$  nodes, and subsequently updates  $m_{v \rightarrow c}^{G_0 \rightarrow \alpha}$ . This in turn updates  $m_{c \rightarrow v}^{\alpha \rightarrow G_i}$ . Also  $G_1$  and  $G_2$  update their information via the type  $\beta$  update equations to have new estimates for the subsequent global iteration. Such a schedule makes good use of the parallelism inherent in the network structure and is illustrated in the algorithm below.

---

**Algorithm 1** Decoding Schedule
 

---

**Initialize:**  $m_{c \rightarrow v}^{\alpha \rightarrow G_1} = m_{c \rightarrow v}^{\alpha \rightarrow G_2} = 0$   
**Initialize:**  $m_{c \rightarrow v}^{\beta \rightarrow G_1}, m_{c \rightarrow v}^{\beta \rightarrow G_2}$  from channel observations  
**for**  $l = 1$  to  $max\_iter$  **do**  
     **for**  $i = 1, 2$  in parallel **do**  
         1. Run  $\omega_i$  rounds of BP on  $G_i$  with  $m_{c \rightarrow v}^{\alpha \rightarrow G_i}$  and  $m_{c \rightarrow v}^{\beta \rightarrow G_i}$  as inputs.  
         2. Update  $m_{v \rightarrow c}^{G_i \rightarrow \alpha}, m_{v \rightarrow c}^{G_i \rightarrow \beta}$ .  
     **end for**  
     Compute  $m_{c \rightarrow v}^{\alpha \rightarrow G_0}$  using (3.1).  
     Run  $\omega_0$  rounds of BP on  $G_0$  with  $m_{c \rightarrow v}^{\alpha \rightarrow G_0}$  as input.  
     Update  $m_{v \rightarrow c}^{G_0 \rightarrow \alpha}$ .  
     Compute  $m_{c \rightarrow v}^{\alpha \rightarrow G_1}, m_{c \rightarrow v}^{\alpha \rightarrow G_2}$  using (3.2).  
     Compute  $m_{c \rightarrow v}^{\beta \rightarrow G_1}, m_{c \rightarrow v}^{\beta \rightarrow G_2}$  using (3.3), (3.4).  
**end for**

---

After a fixed number of global iterations, a hard decision is taken on the value of the source bits  $\mathbf{x}_s$ , based on the sign of the corresponding messages at the variable nodes which is obtained by adding the messages from all incident edges. Note that as in the original QMF strategy, no hard decisions are made on the relay transmissions.

### 3.2.3 Non-binary signaling

To extend our scheme to higher order constellations, we adopt a 2-step procedure—namely coding in binary, followed by modulating the coded bits to the transmit constellation. The (non-binary) code and membership functions then factorize as

$$\mathbb{1}_{\{\mathbf{x}_s \in C\}} = \mathbb{1}_{\{\mathbf{c}_s \in C'\}} \cdot \mathbb{1}_{\{\Psi_v^s(\mathbf{c}_s) = \mathbf{x}_s\}}$$

$$\mathbb{1}_{\{(\mathbf{x}_Q \cup \mathbf{x}_R) \in \mathcal{M}\}} = \mathbb{1}_{\{(\mathbf{x}_Q \cup \mathbf{c}_R) \in \mathcal{M}'\}} \cdot \mathbb{1}_{\{\Psi_v^R(\mathbf{c}_R) = \mathbf{x}_R\}}$$

where  $\mathbf{c}_s$  and  $\mathbf{c}_R$  denote the *binary* coded and mapped vectors at the source and relays respectively, and  $\Psi_v^s$  and  $\Psi_v^R$  are the vector extensions of the constellation maps.  $C'$  and  $\mathcal{M}'$  denote the binary codebooks at the source and the relays.

From the perspective of the decoder, each *type*  $\alpha$  node now has  $k_s$  connecting edges to  $G_0$  and  $b$  connecting edges to  $G_i$  while each *type*  $\beta$  check node has  $k_{R1}$  and  $k_{R2}$  connecting edges to  $G_1$  and  $G_2$  respectively, where  $k_s$ ,  $k_{R1}$  and  $k_{R2}$  represent the number of bits-per-

symbol of the constellations  $\mathcal{A}_s$ ,  $\mathcal{A}_{R1}$  and  $\mathcal{A}_{R2}$ .

In general  $k_s$ ,  $k_{R1}$ ,  $k_{R2}$  may be chosen to be different from each other. In our setup, we restrict  $k_{R1}$  and  $k_{R2}$  to be greater than or equal to  $k_s$ . At the  $i^{th}$  relay, if the constellation has  $k_{Ri} > b$  we use a rate  $\frac{b}{k_{Ri}}$  LDPC code to encode  $\mathbf{x}_Q$  to  $\mathbf{c}_R$ . The encoding algorithm is the one in [22], which retains the input word as a subset of the codeword. In this case, the following equivalence holds at the relay:  $\mathbb{1}_{\{(\mathbf{x}_Q \cup \mathbf{c}_R) \in \mathcal{M}'\}} \equiv \mathbb{1}_{\{\mathbf{c}_R \in \mathcal{M}'\}}$ .

### 3.3 Numerical Evaluations

For the QMF simulations, the codebook  $\mathcal{C}'$  at the source is chosen from the ensemble designed for the AWGN channel [23] with maximum degree of variable nodes set to 8. The mapping codebooks at the relays,  $\mathcal{M}'_1$  and  $\mathcal{M}'_2$  are samples from a (1,2)-regular LDPC ensemble<sup>1</sup>. For signaling, we consider QAM constellations with *gray-code labeling*.

We note that the network is parameterized by the 4 Signal-to-Noise-Ratios (SNRs)  $S_{hi} = \mathbb{E}\{|h_i|^2\} \cdot \mathcal{P}$  and  $S_{gi} = \mathbb{E}\{|g_i|^2\} \cdot \mathcal{P}$ ,  $i \in \{1, 2\}$ .

To quantify the performance of our QMF design, we examine the following aspects of the system: (i) Error performance with fading links, which quantify the cooperative diversity achieved, and (ii) Rates achieved for a given outage/BER, which quantifies spectral efficiency

**Cooperative Diversity** Since the individual links are fading, wireless relay networks obtain cooperative diversity by providing multiple transmission paths from source to destination. Fig. 3.3a-3.3b, show that the performance of QMF is within 2–3 dB of the outage performance of the information-theoretic cut-set bound, at moderate SNR. More importantly it performs as well or better than AF-BEAM and OR schemes, which require transmit CSI at the relays. This demonstrates that our implementable designs behave similar to the information-theoretic predictions. Statistically symmetric fading channels seem to be more unfavorable to QMF than statistically asymmetric channels. This is not unexpected since information theory predicts that rate advantages of QMF over other schemes is more pronounced in asymmetric conditions [3].

**Spectral efficiency** A consequence of the approximate optimality of QMF is that it achieves the optimal multiplexing rate for a given error performance (diversity order). In Fig. 3.4a-3.4b we explore performance at higher spectral efficiencies through non-binary signaling. We see that our LDPC-based design achieves spectral efficiency within 3 dB

---

<sup>1</sup> Although a (1,2)-regular code does not by itself exhibit good performance, we found it to work better as component codes than most *ad-hoc* choices, including the (3,6)-regular ensemble, repeat-accumulate codes, and also the specially designed ensemble for the MAC channel in [22].

of optimal in asymmetric channels at moderate SNRs, without transmit CSI. We believe that the deterioration in performance for high-rates (3 bits/transmission) in symmetric channels is primarily because we have not optimized the LDPC designs.

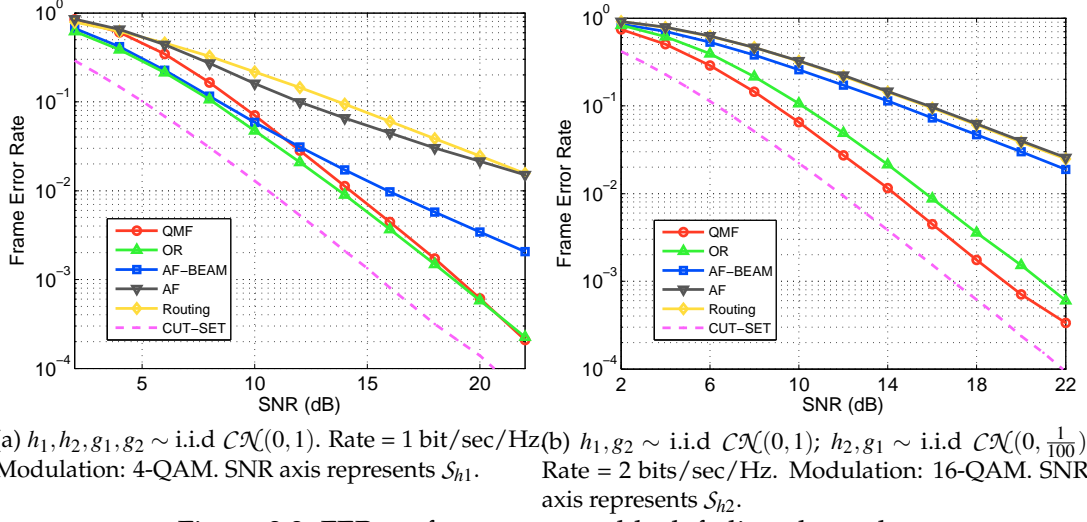


Figure 3.3: FER performance over block fading channels.

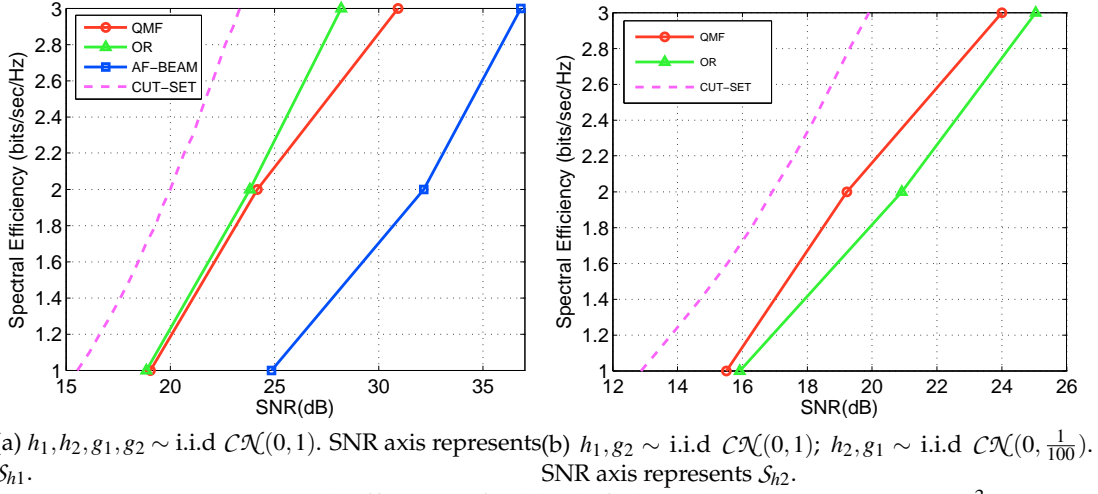


Figure 3.4: Spectral Efficiency for block-fading channels at FER =  $10^{-3}$ .



## Related Work

Lattice codes for QMF were studied in [11]. These allow polynomial-time complexity for the relay operation, however, similar to the original construction in [3], the decoding complexity is exponential in blocklength. In [24], a QMF LDPC-based coding scheme for the half-duplex single-relay network was presented. This scheme, to simplify the decoding problem, orthogonalizes the interfering signals by invoking a one-block delay at the relay, followed by successive interference cancelation at the destination. This approach does not maintain the desired universality property of the QMF strategy. In particular, it does not naturally extend to larger configurations since it relies on simplifying the QMF strategy, specifically for the case of a single half-duplex relay.



# Testbed Implementation **Part III**



## 4 QMF Relaying: First Experimental Study

We present in this chapter the first system design, deployment and experimental comparison of QMF, AF and DF relaying. We compare these results to a baseline direct transmission (DT) which does not employ a relay. Our system design emulates the 802.11 physical layer procedures, such as the frame structure, use of Orthogonal Frequency Division Multiplexing (OFDM) and use of standardized LDPC encoders. We implement all schemes and deploy them simultaneously on the same network to offer a fair comparison. We find that relaying schemes significantly outperform the baseline DT. We also find that QMF is a competitive scheme to DF and AF, offering in some cases up to 12% throughput benefits and up to 60% improvement in frame error-rates over the next best scheme. However, we also see that in a single-relay network, there are scenarios where DF does better than QMF.

### 4.1 Model and Preliminaries

We consider a network that consists of three wireless nodes: a source  $S$  communicates with a destination  $D$  with the help of a relay  $R$  (see Fig. 4.1). The relay  $R$  is half-duplex in nature, i.e., it cannot simultaneously listen and transmit over the same frequencies.

At a high level, the communication over our network depends on three choices: (i) the physical layer signaling; we emulate the physical layer operation prescribed by 802.11. We highlight the parts we need to describe our relaying schemes in Section 4.1.1 and give specific details in Section 4.3. (ii) the network operation; that is, whether we use the relay and in what network topology. For example, we may use the relay only when direct transmissions fail, or we may use it to form a two-hop path that connects the source to the destination. We describe our choices in Section 4.1.2. (iii) the relaying scheme; that is, if we do use the relay, which relaying strategy we deploy? We discuss several strategies and how we optimize their system implementation in Section 4.2.

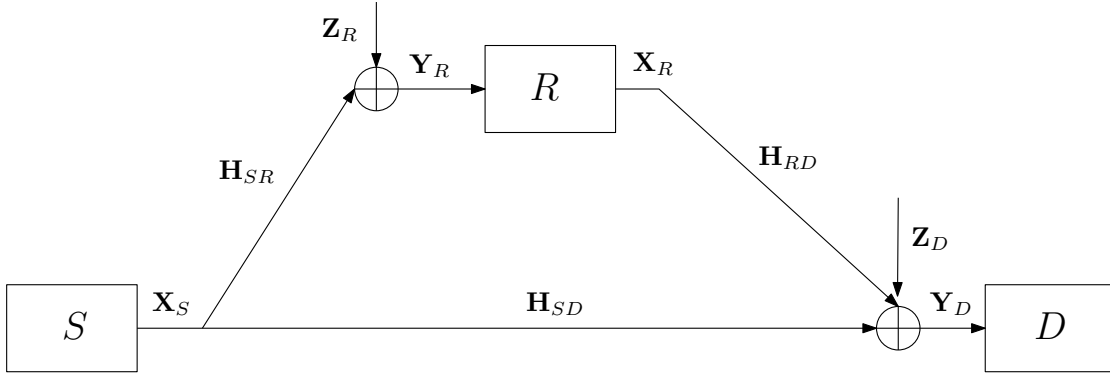


Figure 4.1: The 3-node network considered in this work: the source  $S$  communicates with the destination  $D$  with the help of the relay  $R$ .

#### 4.1.1 Signal Model

The communication happens in frames. We work with coded systems, i.e., to improve the error resiliency, the source encodes the information bits using the 802.11 standard LDPC codes (we give more details on the codes we implement in Section 4.4). After encoding, the codeword bits are first mapped to constellation symbols (we use QAM constellations supported in WiFi), and then modulated using OFDM. We employ OFDM modulation as specified in the WiFi physical layer to combat channel frequency selectivity. We denote by  $\mathbf{X} = [X_1, X_2, \dots, X_m]^T$  an input vector to an OFDM modulator and by  $\mathbf{Y} = [Y_1, Y_2, \dots, Y_m]^T$  the output vector of the corresponding OFDM demodulator, where the subscript denotes the inputs and outputs at subcarrier  $l \in \{1, \dots, m\}$ , with  $m$  being the total number of subcarriers (we use  $m = 64$ ). The inputs  $X_l$  are complex numbers corresponding to the signal constellation used. With OFDM, the point-to-point signal model [25] for each subcarrier is:

$$Y_l = H_l X_l + Z_l, \quad (4.1)$$

where  $Z_l$  is the additive Gaussian noise and  $H_l$  is the channel for subcarrier  $l \in \{1, \dots, m\}$ .

In our network, both the source and the relay may transmit at the same time. From the superposition property of wireless channels, if the two transmitters  $S, R$  each emit an OFDM symbol  $\mathbf{X}_i = [X_{i1}, X_{i2}, \dots, X_{im}]^T$ , where  $i \in \{S, R\}$ , then the demodulated OFDM symbol at node  $D$ , denoted by  $\mathbf{Y}_D = [Y_{D1}, Y_{D2}, \dots, Y_{Dm}]^T$ , is given by [25]

$$Y_{Dl} = H_{SD,l} X_{Sl} + H_{RD,l} X_{Rl} + Z_{Dl}, \quad (4.2)$$

where  $H_{SD,l}$  is the channel from  $S$  to destination  $D$  and  $H_{RD,l}$  is the channel from  $R$  to destination  $D$ .

### 4.1.2 Network Operation

Even in a small network with a single relay, there are several possibilities for the *network operation*, i.e., which links of the network we use and when we use them. We explore the following four choices in our experimentation.

**1. Direct Transmission (DT):** In the DT mode, we do not use the relay, i.e., the source  $S$  and destination  $D$  communicate directly using only the  $S$ – $D$  direct link. The failure recovery is simply through retransmission of the same frame. We deploy the DT mode in our experiments to assess how useful the relay and physical layer cooperation are in our scenario.

**2. Direct Transmission at Half Rate (DTHR):** This scheme also uses the  $S$ – $D$  direct link only, but incorporates a failure recovery mechanism through rate adaptation as advocated in the WiFi standard [26]. More specifically, we first attempt a direct transmission using a 16 QAM constellation. If this fails, we retransmit the same frame at half the rate. This is implemented by using a constellation of half the rate for the second transmission, i.e., 4 QAM<sup>1</sup>. As a result, the time duration of the second transmission doubles. Note that we need to account for the change in the rate when comparing the throughput performance with the other schemes. DTHR offers a recovery mechanism well suited to a direct link that is in general strong, but may infrequently experience deep fades.

**3. Link Switching (LS):** In LS we employ all three links: in a first attempt we employ broadcasting from the source, i.e., the  $S$ – $D$  and the  $S$ – $R$  links; in a second attempt we employ only the  $R$ – $D$  link. First, the source broadcasts a frame that is intended for the destination. The relay  $R$  also overhears the source transmission. If the destination successfully decodes the frame through the direct link, we declare success and proceed with the next frame. However, if the first attempt fails and the destination cannot decode, then in a second attempt, the relay retransmits the frame it has overheard from the source, while the source remains silent. The operation for LS is summarized in Table 4.1, and the corresponding signal model is:

$$\begin{aligned} \mathbf{Y}_R^{(1)} &= \mathbf{H}_{SR}^{(1)} \mathbf{X}_S^{(1)} + \mathbf{Z}_R^{(1)} \\ \mathbf{Y}_D^{(1)} &= \mathbf{H}_{SD}^{(1)} \mathbf{X}_S^{(1)} + \mathbf{Z}_D^{(1)} \\ \mathbf{Y}_D^{(2)} &= \mathbf{H}_{RD}^{(2)} \mathbf{X}_R^{(2)} + \mathbf{Z}_D^{(2)}, \end{aligned} \tag{4.3}$$

where the superscript  $(k)$ ,  $(k \in \{1, 2\})$ , denotes the attempt, and  $\mathbf{H}_{ij}^{(k)} = \text{diag}(H_{ij,1}^{(k)}, \dots, H_{ij,m}^{(k)})$  denotes the (sub-carrier) channels from node  $i$  to node  $j$  at attempt  $k$ . Note that since the transmissions from the source and the relay are orthogonalized in time, LS does not

<sup>1</sup>Clearly, adaptation to different rates is possible; we use this to get an indicative performance benchmark and because it ties well with 802.11 rate adaptation mechanisms.

require synchronized transmissions.

Attempt	Source	Relay	Destination
T1	Transmit	Receive	Receive
T2	Silent	Transmit	Receive

Table 4.1: Schedule for Link Switching

LS can be interpreted as trying to utilize two paths: first the direct  $S$ – $D$  link and then, if this fails, the  $S$ – $R$ – $D$  path. When the relay uses DF (Decode-Forward is described in Section 4.2) the LS mode of failure recovery is the single-relay analog of *routing* over larger networks.

**4. Link Cooperation (LC):** In LC as well, we employ all three links. Similar to LS, in a first attempt we employ broadcasting from the source, i.e., the  $S$ – $D$  and the  $S$ – $R$  links; however, if we fail, we then simultaneously employ both the  $S$ – $D$  and  $R$ – $D$  links. More specifically, if the destination fails to decode the first direct transmission of the source, in the second attempt both the source and relay cooperatively transmit. The schedule for LC is summarized in Table 4.2, and the corresponding signal model is:

$$\begin{aligned}
 \mathbf{Y}_R^{(1)} &= \mathbf{H}_{SR}^{(1)} \mathbf{X}_S^{(1)} + \mathbf{Z}_R^{(1)} \\
 \mathbf{Y}_D^{(1)} &= \mathbf{H}_{SD}^{(1)} \mathbf{X}_S^{(1)} + \mathbf{Z}_D^{(1)} \\
 \mathbf{Y}_D^{(2)} &= \mathbf{H}_{RD}^{(2)} \mathbf{X}_R^{(2)} + \mathbf{H}_{SD}^{(2)} \mathbf{X}_S^{(2)} + \mathbf{Z}_D^{(2)},
 \end{aligned} \tag{4.4}$$

where the notation is similar to (4.3).

Attempt	Source	Relay	Destination
T1	Transmit	Receive	Receive
T2	Transmit	Transmit	Receive

Table 4.2: Schedule for Link Cooperation

LC is the mode of operation that is the most promising: it puts in use all the network resources—both broadcasting and transmit cooperation to forward the information and thus, if we use a “good” relaying scheme, it has the potential to offer the best performance no matter which of the network links are stronger. The question is whether one of the relaying schemes (that we describe in the next Section) makes this possible.

**Discussion** The focus of our work is in evaluating the potential of PHY-layer cooperation; we leave open what a well-matched MAC-layer protocol would be. However, we do not think that heavy MAC-layer redesign would be required; there exist schemes in the literature that already implement the simple functionalities we would need. For instance, the modes that use a relay (LS and LC) operate *on-demand*, i.e., the relay is invoked only when the first attempt to communicate with the destination has failed.

MAC-layer protocols for activating on-demand relaying in 802.11-like networks have been discussed in [27, 28, 29].

## 4.2 Relaying Schemes

In this section we describe the three relaying schemes we will compare: Decode-Forward (DF), Amplify-Forward (AF) and Quantize-Map-Forward (QMF). We first give the high level operation and then describe our system design choices. The relaying schemes are only relevant for the LS and LC network operations (since in DT and DTHR we do not employ the relay at all).

### 4.2.1 Relay Operation

**Decode Forward (DF):** Once the relay receives a frame, it attempts to decode it and retrieve the information bits. If decoding is successful (i.e., the CRC passes *after* running the LDPC decoder), the relay can re-encode the decoded information, remodulate and forward the frame to the destination. If correct decoding is possible, it is an optimal relay operation, as it removes the  $S$ – $R$  link noise. If decoding at the relay fails however, the relay remains silent and cannot cooperate for that frame.

**Amplify Forward (AF):** The relay does not attempt to decode; rather it simply amplifies its received signal to the maximum transmit power of its radio (by multiplying with an appropriate amplification factor  $A$ ) and retransmits it. This is advantageous in cases where the relay cannot decode, but the destination can do so with the help of both the source and relay transmissions.

**Quantize-Map-Forward (QMF):** The relay quantizes the received symbols, collects a sequence of quantized values, and operates on the entire sequence to produce a transmit sequence. This is distinct from DF since the relay does not decode and is distinct from AF since it operates on a *sequence* of quantized symbols.

### 4.2.2 System Design

#### Cooperative Transmissions

In the LC mode, effectively we have the source and relay cooperating like a *distributed*  $2 \times 1$  transmit antenna system to the destination. For point-to-point links with 2 transmit and 1 receive antennas, the WiFi standard recommends an Alamouti space-time code [30, 26], as it gives the best rate-reliability tradeoff for the  $2 \times 1$  MISO channel, asymptotically in SNR (*i.e.*, it is diversity-multiplexing-tradeoff optimal). Accordingly, to optimize the performance of AF and DF, we implement a *distributed* Alamouti code in the LC mode.

QMF cannot take advantage of Alamouti coding, because of the random mapping at the relay. We describe in the following, the transmissions for all schemes.

**Decode Forward (DF):** In the LC mode, if the relay successfully decodes the source frame, then we can exactly create a  $2 \times 1$  multiple transmit antenna situation. That is, we can implement a distributed Alamouti scheme by using the decoded symbols at the relay in cooperation with the source. If  $S_1$  and  $S_2$  are two QAM symbols transmitted on a particular subcarrier  $l$  over two OFDM symbols, then the transmission scheme for the distributed Alamouti scheme is given in Table 4.3. Using the OFDM signal model of (4.2), the demodulated symbols at the destination  $D$  for that subcarrier  $l$  are

$$\begin{aligned} Y_{Dl}^{(2,1)} &= H_{RD,l}^{(2)} S_1 + H_{SD,l}^{(2)} S_2 + Z_{Dl}^{(2,1)} \\ Y_{Dl}^{(2,2)} &= -H_{RD,l}^{(2)} S_2^* + H_{SD,l}^{(2)} S_1^* + Z_{Dl}^{(2,2)}, \end{aligned} \quad (4.5)$$

where  $Y_{Dl}^{(2,k)}$  is the demodulated signal on subcarrier  $l$  at  $D$  across two OFDM symbols,  $k = 1, 2$  and  $H_{RD,l}^{(2)}$ ,  $H_{SD,l}^{(2)}$  denote the channels on subcarrier  $l$  in attempt 2. Standard Alamouti combining at  $D$  [30] results in the following effective point-to-point channels per subcarrier:

$$\begin{aligned} \tilde{Y}_{Dl}^{(2,1)} &= S_1 \sqrt{|H_{RD,l}^{(2)}|^2 + |H_{SD,l}^{(2)}|^2} + \tilde{Z}_{Dl}^{(2,1)} \\ \tilde{Y}_{Dl}^{(2,2)} &= S_2 \sqrt{|H_{RD,l}^{(2)}|^2 + |H_{SD,l}^{(2)}|^2} + \tilde{Z}_{Dl}^{(2,2)}, \end{aligned} \quad (4.6)$$

where  $\tilde{Z}_{Dl}^{(2,k)}$ ,  $k = 1, 2$  is Gaussian noise of the same variance as the noise in (4.5).

	OFDM Symbol 1	OFDM Symbol 2
Relay	$S_1$	$-S_2^*$
Source	$S_2$	$S_1^*$

Table 4.3: Transmitted signals from source and relay per subcarrier for DF LC

**Amplify Forward (AF):** For AF, since the relay does not decode, the distributed Alamouti scheme of Table 4.3 is modified by using the amplified received signal at subcarrier  $l$ , instead of the decoded symbols as in DF (see Table 4.4).

	OFDM Symbol 1	OFDM Symbol 2
Relay	$AY_{Rl}^{(1,1)}$	$AY_{Rl}^{(1,2)}$
Source	$S_2$	$S_1^*$

Table 4.4: Transmitted signals from source and relay per subcarrier for AFLC

where

$$\begin{aligned} Y_{RI}^{(1,1)} &= H_{SR,l}^{(1)} S_1 + Z_R^{(1,1)} \\ Y_{RI}^{(1,2)} &= -H_{SR,l}^{(1)} S_2^* + Z_R^{(1,2)} \end{aligned}$$

The received signals are modified from (4.5) as:

$$\begin{aligned} Y_{DI}^{(2,1)} &= H_{RD,l}^{(2)'} S_1 + H_{SD,l}^{(2)} S_2 + Z_{DI}^{(2,1)'} \\ Y_{DI}^{(2,2)} &= -H_{RD,l}^{(2)'} S_2^* + H_{SD,l}^{(2)} S_1^* + Z_{DI}^{(2,2)'} \end{aligned} \quad (4.7)$$

where  $H_{RD,l}^{(2)'} = AH_{RD,l}^{(2)}H_{SR,l}^{(1)}$ . Note that the noise-variances corresponding to  $Z_{DI}^{(2,k)'}$  are larger than  $Z_{DI}^{(2,k)}$  in (4.5) since we are forwarding noise in AF. Using the same Alamouti combining at  $D$  as in (4.6), we get

$$\begin{aligned} \check{Y}_{DI}^{(2,1)} &= S_1 \sqrt{|H_{RD,l}^{(2)'}|^2 + |H_{SD,l}^{(2)}|^2} + \check{Z}_{DI}^{(2,1)} \\ \check{Y}_{DI}^{(2,2)} &= S_2 \sqrt{|H_{RD,l}^{(2)'}|^2 + |H_{SD,l}^{(2)}|^2} + \check{Z}_{DI}^{(2,2)}, \end{aligned} \quad (4.8)$$

where  $\check{Z}_{DI}^{(2,k)}$ ,  $k = 1, 2$  is still Gaussian noise with same (larger) variance as  $Z_{DI}^{(2,k)'}$  in (4.7).

**Quantize-Map-Forward (QMF):** We implement it as outlined in the previous chapter: the relays employ a scalar quantizer (symbol-by-symbol on a QAM symbol level) to quantize the received signals from the source (as proposed in [31, 32]). Instead of the random mapping operation proposed in [3], we use a permutation mapping (randomly chosen bit-interleaver) on the quantized bits corresponding to each codeword in the frame. After mapping, the relay re-modulates the frame as per the 802.11 specifications, and if the direct transmission in the first time slot fails, forwards it to the destination.

### Decoding at the Receiver

In attempt 2 of the LC mode, as we already described in (4.2), the destination receives a superposition of the source and relay transmissions

$$Y_{DI} = H_{SD,l} X_{SI} + H_{RD,l} X_{RI} + Z_{DI}.$$

For AF and DF, we have already seen that effectively we have point-to-point channels with parameters that take into account the operations at the relay. Thus, standard point-to-point LDPC decoders are sufficient for decoding AF and DF frames.

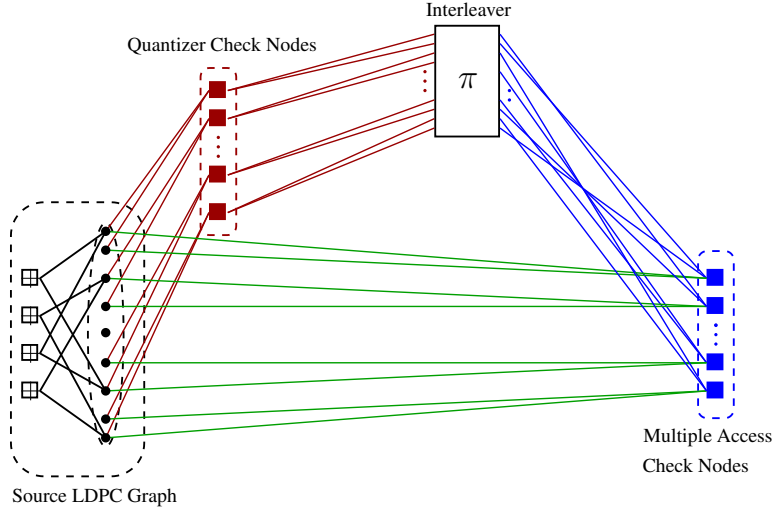


Figure 4.2: LDPC-based joint decoder for QMF

QMF, on the other hand, uses non-linear operations (quantization) at the relay and hence a point-to-point decoder does not suffice for decoding. Similar to the decoder for the diamond network in the previous chapter, Fig. 4.2 outlines the graphical structure of the decoder for one codeword with QMF LC. As highlighted before, this is *not* a standard structure for iterative (LDPC) codes due to two reasons: (i) the quantization at the relay which takes the received signal  $Y_{RI}$  and quantizes it to  $\hat{Y}_{RI}$ . (ii) the superposition of the two streams  $X_{SI}$ ,  $X_{RI}$ . The decoding algorithm over the graphical structure is as described in Chapter 3.

In addition, to reduce the occurrence of low-weight error events, we use a further *enhancement layer* for the LDPC decoders of all three schemes, QMF, AF and DF, that treats LLR magnitudes above a certain pre-determined threshold as correct, and others as *erasures* (lost bits) after a fixed number of iterations. Then another erasure correction round of iterations is performed to clean up the residual errors.

### 4.3 System Implementation

**Overall system** The source, relay, and destination nodes were implemented using the WARP SDR platform [33]. We used the WARPLab framework, which allows interaction with the WARP hardware via a host PC running MATLAB (see Fig. 4.3). The host PC was used to control real-time over-the-air transmission and reception.

We implemented the four network operation methods described in Section 4.1.2 coupled with the three relaying strategies defined in Section 4.2.1. Table 4.5 summarizes the implemented schemes when the relay is active; additionally, we implemented Direct Transmission (DT) and Direct Transmission Half Rate (DTHR).

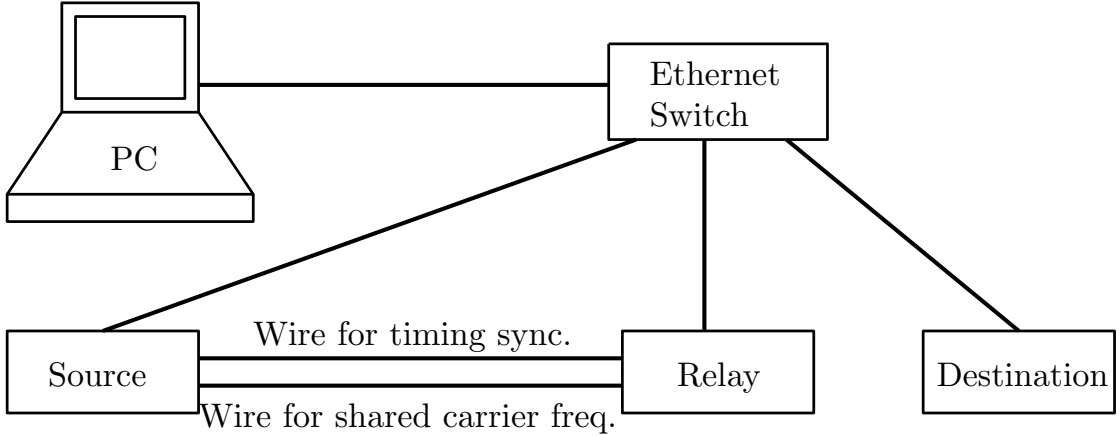


Figure 4.3: Node and host PC configuration

	Amplify-Forward	Decode-Forward	Quantize-Map-Forward
Link Switching	AFLS	DFLS	QMFLS
Link Cooperation	AFLC	DFLC	QMFLC

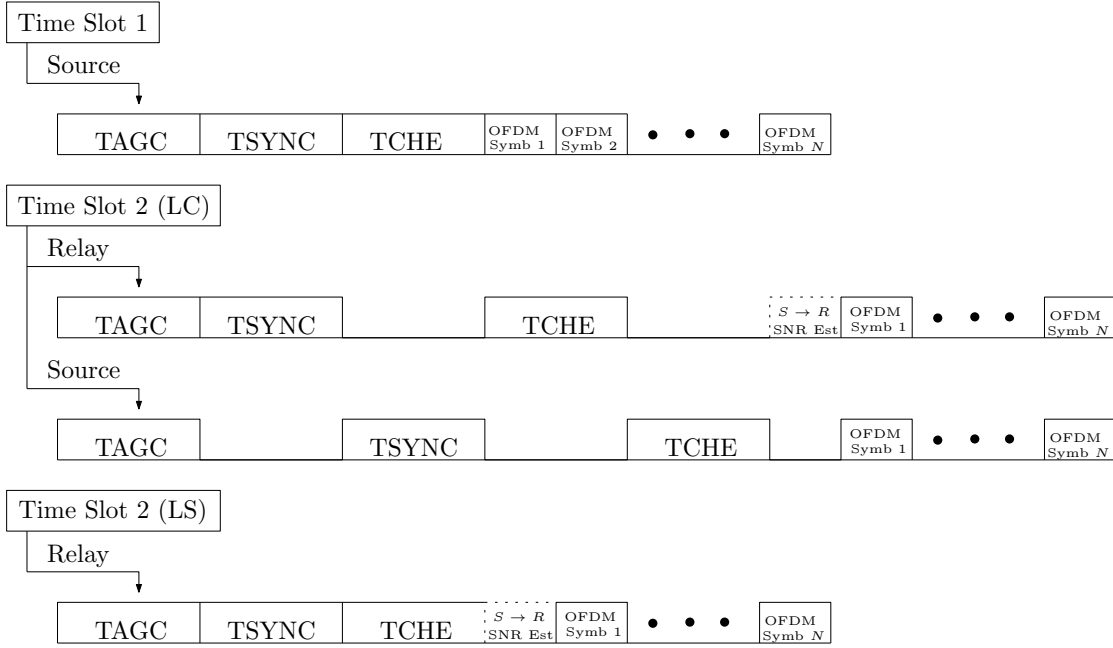
Table 4.5: Implemented schemes when the relay is active. The network modes (rows) are described in Section 4.1.2 and the relaying strategies (columns) in Section 4.2.1.

#### 4.3.1 Frame Structure and Operation

We use a frame structure specified in the 802.11 standard [26], which stipulates that we first transmit training for Automatic Gain Control (TAGC), followed by training for timing synchronization (TSYNC), training for channel estimation (TCHE) and then the payload. We use the signal that the 802.11 standard defines as long training symbols for timing synchronization and channel estimation. Our experiments correspond to a 20 MHz bandwidth system with 64 subcarriers. During the payload transmission, for each OFDM symbol transmitted, 48 subcarriers are data subcarriers, 4 subcarriers carry pilots, and the rest of the subcarriers are unused, as per the 802.11 payload structure. The signals transmitted over-the-air were centered at a frequency of 2.4 GHz in a 20MHz bandwidth. Next, we give more specific details of the frame structures for each scheme for the attempts over the two time-slots.

**Time-slot operation:** To make a fair comparison between schemes with and without cooperation, we allow a maximum of two attempts for every source information frame to be successful, as described in Section 4.1.2. We send each attempt over a *time slot*, which is one frame in length. If the communication is not successful after two attempts then the frame is declared in error and the source moves on to the first attempt for the next information frame.

**First Time Slot:** For all schemes, the first attempt is always only via the direct link from source to destination. The source transmits using the standard frame structure we previously described; the frame structure is shown in Fig. 4.4. If the destination is



TAGC: Training for AGC, TSYNC: Training for Synchronization

TCHE: Training for Channel Estimation

$S \rightarrow R$  SNR Est: SNR estimate of the  $S \rightarrow R$  channel sent to  $D$  for AF and QMF

Figure 4.4: Time-slot frame structure for LS and LC.

able to decode successfully, we proceed with the first attempt of a new frame. If the transmission attempt fails, then we move to the next attempt in the second time-slot described below.

**Second Time Slot:** The source re-transmits at lower rate in DTHR mode. In LS mode, only the relay transmits, using a standard frame structure. In the LC mode, both the source and the relay transmit. The different relaying operations for each of the modes are described in Section 4.2.1. The frame structures for the second attempt are shown in Fig. 4.4. As noted in Fig. 4.4, in AFLC/AFLS and QMFLC/QMFLS, the relay sends one more OFDM symbol than in DFLC/DFLS. This extra OFDM symbol is only sent by the relay and it is used to forward an estimate of the source to relay SNR. This estimate is used by the iterative decoder at the destination. The SNR estimate is not forwarded by DFLC/DFLS because the bits are decoded at the relay before forwarding them.

### 4.3.2 Timing and Carrier Synchronization

The WARPLab framework allows a coarse timing synchronization of the nodes involved in communication. However, for 20MHz OFDM time scales this coarse synchronization is not accurate enough; more elaborate mechanisms that enable the required timing and carrier frequency synchronization are required both at the receivers and distributed

transmitters.

**Operation at a receiver:** A node in receiver mode can solve timing synchronization by exploiting the autocorrelation properties of the training sent for timing synchronization. The signal used for channel estimation, labeled as TCHE in Fig. 4.4, is also used for time-domain estimation and correction of the carrier frequency offset (CFO). The time domain correction is applied to the training for channel estimation and to the OFDM symbols before performing the FFT for conversion to the frequency domain. To correct for residual phase noise present, another level of estimation and correction of CFO and a phase noise correction is applied in the frequency domain. The frequency domain CFO and phase noise are estimated based on the four known pilot subcarriers that are included in each OFDM symbol. Since DT/DTHR/LS modes effectively create single-transmitter, single-receiver (point-to-point) channels, we distinguish its operation from the LC modes.

*Link Cooperation (LC):* In order for the destination to be able to set the AGC correctly for the reception of the sum signal, the source and relay send training for AGC simultaneously. The waveform for AGC sent by the source is similar to the one sent by the relay, with the only difference being that it is cyclically shifted in order to avoid accidental nulling. The source and relay both send training for timing synchronization and channel estimation and these training signals are orthogonal in time. This orthogonality ensures that the two node diversity is also present in the timing synchronization phase, since the destination can solve timing synchronization from any of the two copies it receives. The orthogonal training for channel estimation is needed in order to compute clean channel estimates from each of the links; these two channel estimates are needed for decoding in the LC mode. To implement the orthogonality of training/timing in link cooperation mode, the four pilot subcarriers are split and alternated between the source and the relay in the following way. In odd OFDM symbols the relay transmits pilots 1 and 3 and the source transmits pilots 2 and 4. In even OFDM symbols the relay transmits pilots 2 and 4 and the source transmits pilots 1 and 3. This is the same method for pilot assignment proposed in [34, 35].

The mechanism described above for CFO correction enables a receiver to solve for only one CFO. However, in LC mode, at the destination there would be two CFOs to correct for—one due to the  $R-D$  link and another due to the  $S-D$  link. In [36, 35] this issue of two CFOs is solved by having the relay lock on to the carrier of the source by estimating its CFO with respect to the source and applying a time domain correction so that the destination observes only one CFO. Although feasible to implement, this was not the focus of our study. Consequently, for our implementation, we used a wire to share the carrier frequency clock of the source between the source and the relay, as shown in Fig. 4.3.

**Distributed synchronization:** In LC, in the second time slot, the relay and the source

transmit synchronously to ensure required orthogonality in the training phase and avoid intersymbol interference when receiving the payload. Thus, the synchronization mechanism must be accurate enough to ensure that at the destination, the time of arrival of the signals from the source and the relay is within the cyclic prefix of the OFDM symbols. In our implementation, the duration of cyclic prefix is  $0.8 \mu s$ , which is the exact same duration of the cyclic prefix specified in 802.11 for a 20 MHz bandwidth system. Recent work [36, 35, 37] has demonstrated that one can design protocols that achieve accurate timing synchronization (between 20 ns and 100 ns accuracy) for distributed OFDM communication enabled by implementing a large part of the distributed timing synchronization mechanisms in real time in the FPGA. Incorporating this fast turnaround time to the WARPLab framework, although feasible, was not the focus of our study. Consequently, we synchronized the time of transmission of distributed transmitters via a wired connection between source and relay, as shown in Fig. 4.3, for all schemes.

### 4.3.3 Estimation of Effective Noise

To decode, all our schemes require an estimate of the effective noise variance in the digital (sampled) domain. This estimate is used to compute the log likelihood probabilities that serve as the input to the decoders, and thus an accurate estimation is important for the iterative (LDPC) decoder performance. However, accurate estimation of the noise variance can be a challenging and complex task, since there are many sources of noise in a hardware implementation. For example, there is additive noise, quantization noise at ADC and DAC, IQ imbalance, channel estimation errors, carrier frequency offset errors and timing synchronization inaccuracy. Also, the noise added by the radios is a function of the gains set by the AGC and the received signal power. To balance the need for an accurate estimate and the system need for low complexity, we developed the following simple algorithm that builds on four components: (i) the (analog) RSSI measurement provided by the radios (ii) the approximate (calibrated) noise level of the radios we use (iii) the channel estimates per subcarrier (iv) the model for the received signal. We describe how we put these together in the following two steps.

- *Step 1 - Computation of the Analog SNR:* We compute the SNR in the analog domain as

$$\text{SNR-analog (dB)} = \text{PayloadRSSI (dBm)} - N_0 \text{ (dBm)} \quad (4.9)$$

The analog thermal noise value  $N_0$  is initialized with the calibrated value for the WARP boards. The receiver radio path is shown in Fig. 4.5. The RSSI reading is made after downconversion to baseband and the radios provide the value of the receiver RF Gain and the mapping of RSSI readings to RSSI at the receiver antenna. Hence, from the RSSI reading we actually get the RSSI of the signal at the receiver antenna. This is the PayloadRSSI that we use to compute the SNR-analog in (4.9). The analog RSSI values are reported every  $0.1 \mu s$  by the radios or 40 RSSI readings per OFDM symbol. Hence, for a payload of  $L$  OFDM symbols we have  $40L$  RSSI readings that are averaged to get

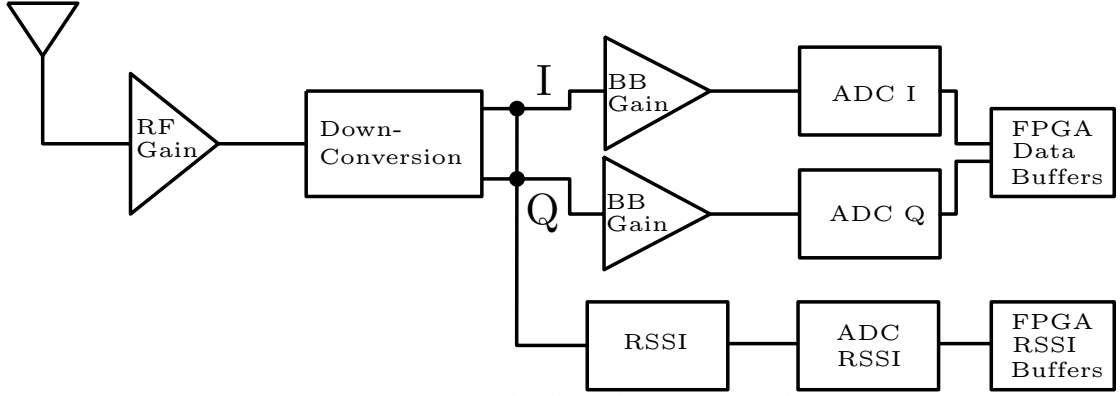


Figure 4.5: Radio board receiver path

the payload RSSI represented in (4.9).

• *Step 2 - Solve for the effective digital noise variance:* In the digital domain, we model the received signal as shown in (4.1). Since we have  $m$  subcarriers, the SNR in the digital domain can be estimated as

$$\text{SNR-digital} = \frac{\sum_{l=1}^m |H_l|^2}{m\sigma^2}, \quad (4.10)$$

where  $\sigma^2$  is effective (digital) noise power per subcarrier (the signal power is normalized to 1). We estimate that the SNR computed in the digital domain is the same as the SNR computed in the analog domain minus an estimate  $\Delta$  of effects like imperfect channel estimation and imperfect CFO correction.

$$\text{SNR-digital (dB)} = \text{SNR-analog (dB)} - \Delta \text{ (dB)} \quad (4.11)$$

From (4.9), (4.10) and (4.11) we solve for the effective noise variance  $\sigma^2$ , which is used in the iterative decoder. Guided by the WARP radio calibrations, we use values of  $N_0 = -95 \text{ dBm}$  and  $\Delta = 5 \text{ dB}$ .

As for any estimator, the method for  $\sigma^2$  estimation described in the two steps above can have errors that affect the decoder performance. To the best of our knowledge, there is currently no work on the comparison of DF, AF and QMF schemes under errors in  $\sigma^2$ . We leave the development and implementation of more robust estimators for future work.

For AF and QMF, the decoding at the destination needs the SNR-digital computed for the source to relay link. The relay computes this information and forwards it to the destination using one extra OFDM symbol, as shown in Fig. 4.4. To do so, we first quantize the SNR estimate to one out of 40 possible values ranging from  $-10$  to  $30 \text{ dB}$  (in steps of  $1 \text{ dB}$ ). We can describe these 40 values using 6 bits. We repeat these 6 bits

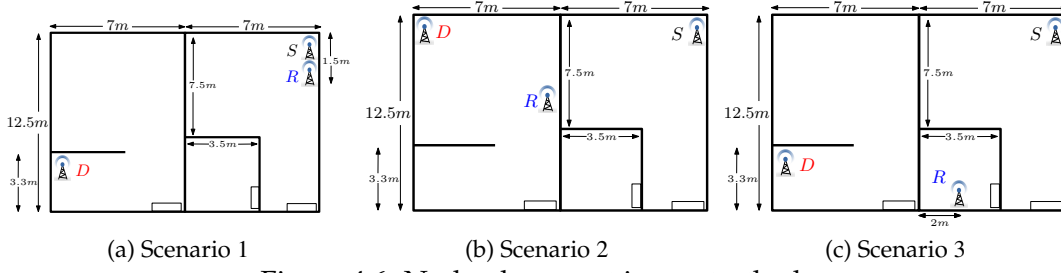


Figure 4.6: Node placement in our testbeds

8 times, modulate them with BPSK and allocate them to the 48 data subcarriers in the OFDM symbol used to forward the SNR information.

### 4.4 Experimentation

**Setup** Our testbed covers a rectangular area of  $175 \text{ m}^2$ , and spans across three rooms. We report the results for three scenarios, which we describe in terms of the average Received Signal Strength Indicator (RSSI) in dBm. We note that the RSSI values not only depend on the distance between devices, but also on the multipath effects in our indoor environment. Moreover, in addition to the relative positioning, we also needed to adjust the transmit power of the radios in some cases, in order to achieve the RSSI values for our scenarios that are typical for 802.11 systems and recommended for the modulation we employ. The RSSI values for all the scenarios is given in Fig. 4.7.

- **Scenario 1** captures the case where the source and the relay are close: we deployed the relay at a distance of 1.5m from the source as depicted in Fig. 4.6a. As a result, the  $S-R$  link is much stronger than the  $S-D$  and  $R-D$  links, which is reflected in the average RSSI values we measure at our receivers.
- **Scenario 2** captures the case where all three links have approximately equal strength. The node placement is shown in Fig. 4.6b.
- **Scenario 3** captures the case where the  $S-R$  and  $R-D$  links are much stronger than the  $S-D$  direct link. The nodal arrangement is depicted in Fig. 4.6c.

In all our experiments we used 16 QAM modulation, an LDPC code of rate  $3/4$  with codeword length of 1944 bits and the parity matrix defined in the 802.11 standard. Each frame encapsulated four codewords, leading to 5184 information bits (payload) per frame. For each experiment we transmitted at least 1600 frames, which corresponds to at least 8294400 information bits transmitted per experiment.

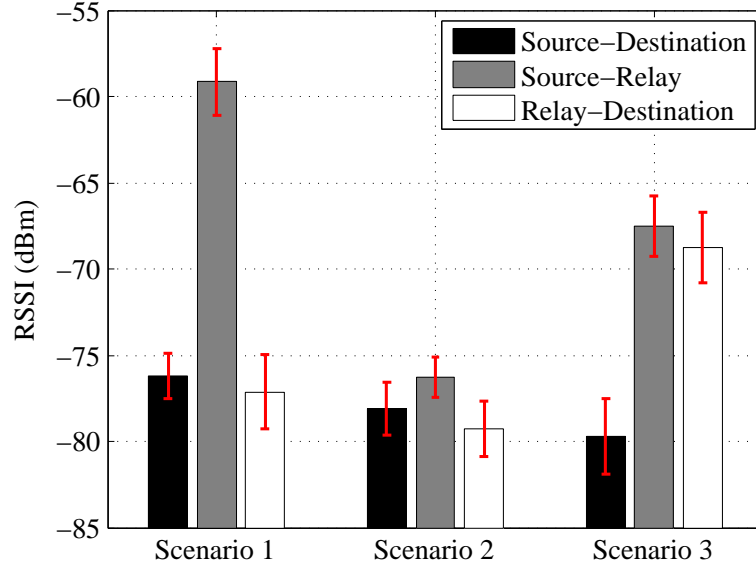


Figure 4.7: Average measured RSSI values per scenario.

**Metrics:** We use two performance metrics:

- (i) *Frame Error Rate (FER)* quantifies the error probability our frame transmissions have with each scheme.
- (iii) *Throughput* quantifies the amount of successfully decoded information bits that reach the destination, normalized by the total over-the-air transmission time and bandwidth used. Thus, we count the amount of decoded information bits per channel use in bps/Hz.

**Discussion of results** The following observations are based on the FER results shown in Fig. 4.8 and the throughput results shown in Fig. 4.9.

**(1) Relaying helps over DT:** In all three scenarios, LC schemes significantly outperform DT. The FER gains of relay transmission ranged from a factor of 10 in Scenarios 1 and 2, to nearly a factor of 100 in Scenario 3, where the direct path was very weak. The throughput gains were 20-40% in Scenarios 1 & 2, and was nearly a factor of 15 in Scenario 3. DTHR<sup>2</sup> can improve the throughput performance with respect to DT, for example in Scenarios 2 and 3. However, in all the scenarios the performance of DTHR was always worse than all of the LC schemes. This is because the reliability benefit of transmitting at a lower rate does not offset the diversity gain obtained with link cooperation.

**(2) Link Cooperation (LC) helps:** In Scenarios 1 and 2, link cooperation gives a factor of 10-40 gain in FER and a 40-70% gain in throughput over link switching. In Scenario 3, link switching performs marginally better than link cooperation. There are two main reasons why in Scenario 3 LC does not improve performance over LS. First, at an average

<sup>2</sup>For DTHR, we only compared throughput since the transmission rate was lower than the other schemes. This implied that the FER was not directly comparable.

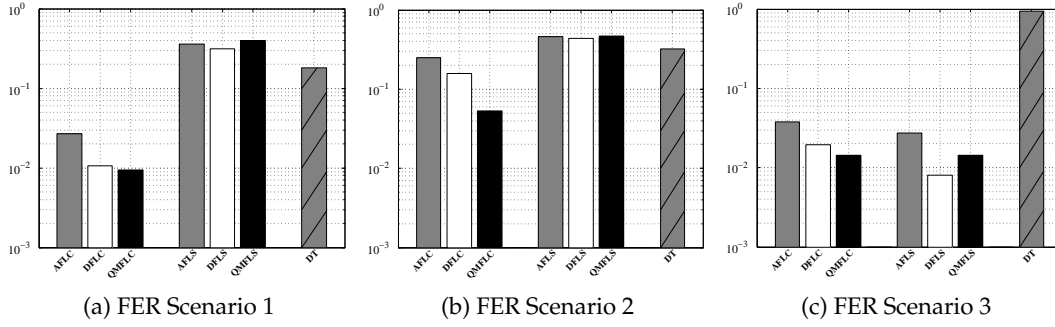


Figure 4.8: Frame error rates.

RSSI of  $-80$  dBm, the  $S$ - $D$  link in Scenario 3 is 13 dB weaker than the  $R$ - $D$  link. Hence, the contribution from the  $S$ - $D$  link is minimal. Second, in LC mode, the pilots for frequency domain CFO and phase noise corrections are split between the source and the relay as was explained in Section 4.3.2. However, since the  $S$ - $D$  link is very weak, the pilots assigned to the source are received with very weak power and hence do not help towards CFO or phase noise correction. Consequently, in Scenario 3, the last hop in LC is effectively a single  $R$ - $D$  link, reminiscent of LS, with the added disadvantage of having only half the pilots as compared to LS.

**(3) Universality of QMF:** QMFLC shows the most competitive performance across all the scenarios. QMF outperforms AF because the frames it sends in the second time-slot are less noisy since the quantization removes some of the noise. In Scenarios 1 and 3 there is very little difference between the performance of QMF and DF. In these two scenarios, since the  $S$ - $R$  link is at a medium-to-high RSSI ( $-60$  dBm in Scenario 1 and  $-67$  dBm in Scenario 3), DF can decode most of the time and hence exhibits good performance. In Scenario 2, the  $S$ - $R$  link is at a low RSSI ( $-78$  dBm); hence decoding at the relay fails more often, affecting the performance of DF negatively. As a result, the gains from QMF are most pronounced in Scenario 2, as the relay always transmits a reasonable quantized signal that the destination can exploit in decoding. Scenario 2 shows a 12% throughput benefit for QMFLC and up to 60% improvement in FER over the next best scheme (DFLC).

**Note:** Although we observe that cooperation helps and QMF outperforms the other schemes in scenarios 1 & 2, we neither believe nor expect that this is true for all possible scenarios; for example, if the direct link  $S$ - $D$  is much stronger than the rest, we expect DT to do best; and if this link essentially does not exist (effectively creating a line network as seen in scenario 3) DFLS (*i.e.*, routing) does better than all others schemes. Here, we focused on scenarios where the outcome of the comparison is not obvious, and thus more interesting.

**Why frames are lost:** We grouped frame failures in categories: failed due to timing, or a certain number of bit errors between  $[a, b]$  remained in the decoded frame (and thus the

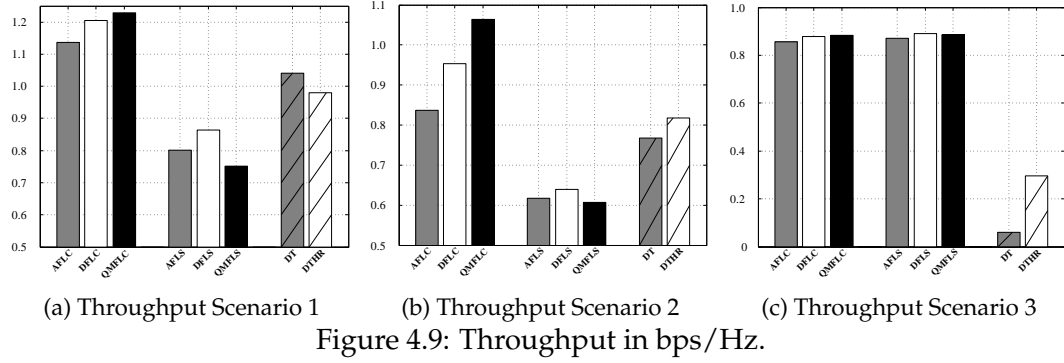
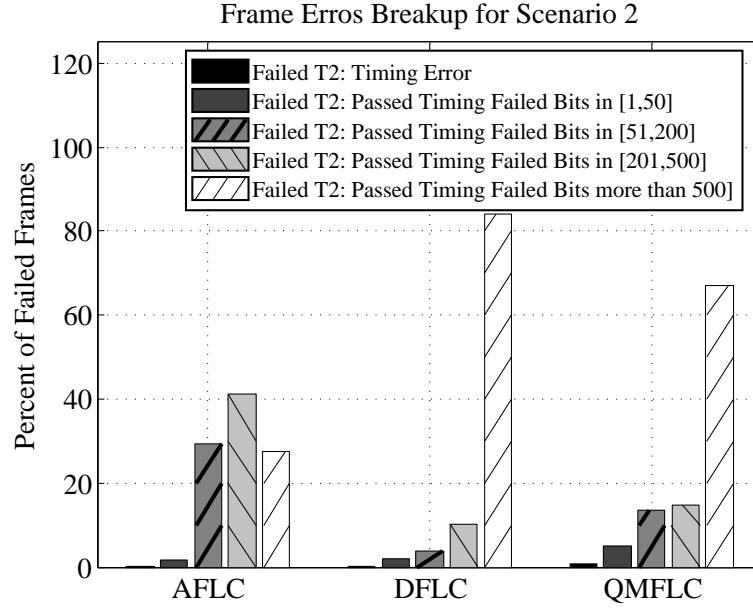


Figure 4.9: Throughput in bps/Hz.

Figure 4.10: Distribution of percentage of frames that fail in  $T_2$ .

CRC check failed). We plot an example of this analysis for Scenario 2 in Fig. 4.10. We observe that for DF and QMF, frame errors primarily occur when a *large* fraction of the bits are in error, indicating that relay processing reduces low-weight error patterns. In contrast, in AF we see frames failing even with a small number of bit errors: a plausible explanation being that since AF does not process its received signal at the relay (DF decodes, QMF quantizes and remaps), the amplified noisy signals propagate to the destination resulting in a (relatively) less sharp threshold behavior in the LDPC decoder.



## 5 QUILT: An Advanced Architecture for PHY-layer cooperation

This chapter proposes and evaluates QUILT, a system for physical-layer relaying that seamlessly adapts to the underlying network configuration to achieve competitive or better performance as compared to the best current approaches. The core component of QUILT is that the relay decides opportunistically whether to use DF or QMF to recover the source sequence, on a frame-by-frame granularity and with no coordination or awareness from the source. Thus QUILT synthesizes on-demand relaying and opportunistic selection of DF or QMF to achieve a consistently good performance across variable configurations.

In addition to the novel relay operation, QUILT is also equipped with improved decoding techniques at the destination. The main improvement in the decoder builds on the following observation: even if both the first (unaided) and the second (cooperative) source transmission fail to be decoded by the destination, it is likely that each of them brings some useful information to the decoder and thus, if jointly processed, they may lead to successful decoding. In a sense, this approach is the relay-network equivalent of the hybrid-ARQ schemes for point-to-point channels that are fast becoming part of standards [26]. We thus term this “hybrid decoding” and present a low complexity implementation that makes it possible.

### 5.1 QUILT System Overview

QUILT prescribes physical layer operations for a three-node network that consists of a source, a relay and a destination, building on top of the physical layer procedures of WiFi IEEE802.11. The relay is half-duplex, i.e., it can either transmit or receive. QUILT can essentially be thought of as a more refined approach to QMF-based relaying in systems, based on the insights gained from the first implementations presented in Chapter 4. We describe its main components in the following and also depict it schematically in Fig. 5.1.

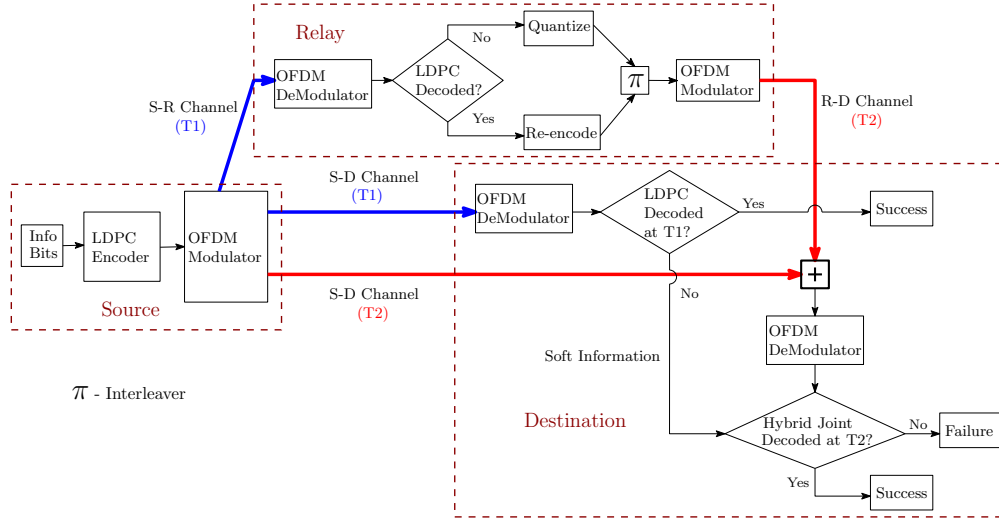


Figure 5.1: Schematic diagram of QUILT illustrating the various components of the system.  $T_1$  and  $T_2$  indicate the first and second phase, respectively.

### 5.1.1 Source Operation

The source operation is essentially the same as in Chapter 4: each information packet is encoded using an LDPC code (compliant with the IEEE802.11 specifications). Also, OFDM modulation is employed as specified in the WiFi physical layer to combat channel frequency selectivity. After LDPC encoding, the codeword bits are first mapped to QAM symbols and then modulated using OFDM. Each coded packet the source creates results in several OFDM symbols.

### 5.1.2 On Demand Relaying: Two Phase Operation

The two-phase operation is essentially the Link Cooperation mode described in the previous chapter, with structural refinements made to the relay processing and destination decoding.

To recap briefly, the source first attempts to directly transmit a packet to the destination. The relay also overhears this transmission. If the direct transmission is successful, the source proceeds with the transmission of a new packet; if unsuccessful, the source and the relay cooperatively transmit to try to help the destination decode.

### 5.1.3 Relay Operation in Phase 2

The relay operates as follows:

- Attempts to recover the source information in a packet, using an LDPC decoder and soft information from its received signal. It infers success through the CRC

check.

- If successful, it re-encodes the source information to create the same signal vectors as the source.
  - If unsuccessful, it quantizes the elements of its received vectors to their closest constellation points, and creates a (noisy, with discrete errors) version of the signal vectors the source has.
- Maps the elements of the recovered vectors to bits, interleaves the resulting bit sequence with a randomly selected bit-interleaver, maps the interleaved bit sequence to signal constellation points, passes it through an OFDM modulator, and transmits it synchronously with the source.

**Discussion** We here discuss the reasons for selecting our particular method for sequence recovery, and for interleaving at the relay.

To recover the source sequence, if the relay can successfully decode, this is the optimal operation it can do, as it perfectly cleans up the noise. If the relay fails to decode, our symbol quantization attempts to recover a sequence that is close to the source transmission and conveys information to the destination. To achieve this, symbol quantization is not the only option: infact, the insight from the information theoretic form of QMF is that we should be using sequence quantization. For instance, a possible choice could be to select the codeword an ML decoder would identify, even if this is not the correct one; that is, use the closest codeword to the receiver signal, which amounts to quantizing to the codeword sequences. We were not able to experiment with this option, as it leads to impractical complexity both at the relay and the destination. We opted for symbol quantization that still identifies a sequence close to the transmitted one, yet has viable complexity.

Interleaving is a key component of our relay operation for two independent reasons. The first is specific to OFDM modulation: because of interleaving, the relay assigns signals received through weak or interfered subcarriers in the source-relay channel to potentially strong or cleaner subcarriers in the relay-destination channel and also induces mixing of signals from distributed terminals across subcarriers, thus achieving frequency-space diversity and significant performance benefits (see Section 5.4). This benefit is present irrespective of quantization or decoding at the relay. The second reason is specific to QMF: as our theoretical analysis in Section 5.2 shows, the mapping that interleaving implements, outperforms random mappings for the QMF operation, offering significant benefits (see Section 5.2) even when we operate on a single subcarrier; i.e., these benefits are independent of OFDM.

### 5.1.4 Hybrid Decoding at the Destination

In phase 1, the destination attempts to decode using a standard LDPC decoder. If it fails, at the end of phase 2, QUILT takes advantage of the received signals in both phases to decode the source packet. For this, the destination employs a graphical structure that captures the streams received in phases 1 and 2, and adapts to whether decoding or quantization were employed at the relay. The decoder for QUILT is an adaptation of the QMF-LC decoder in Chapter 4, wherein the stochastic quantizer nodes become deterministic perfect connections if the relay decoding succeeds, and are the same as in Chapter 4 otherwise. The decision is guided by a 1-bit flag that the relay transmits, to inform the destination whether the relay-decoding succeeded. Further, the log-likelihood ratio computations take into account the received soft information from both transmission phases.

## 5.2 Theoretical Analysis

We here provide theoretical analysis that substantiates our design choices in QUILT. We show that we gain:

- Benefits from interleaving over the conventional random mapping operation in QMF.
- Benefits from hybrid decoding at the destination.
- Benefits from opportunistic relay decoding/quantization.

For our performance evaluations, we compared information theoretical metrics, such as outage probability, through simulations over narrowband (single-carrier) flat Rayleigh-fading channels that assume infinite complexity processing at the source, the relay and the destination.

### 5.2.1 Performance Metric: Outage Probability

We evaluate the error performance using the classical notion of outage probability [25], i.e., the probability that a (fixed) transmission rate  $R$  is not supported by a scheme. For our calculations we assume 4-QAM constellations at the source and relay. We also assume that the channels are fading i.i.d. over the two phases<sup>1</sup>, independently across the three links, but the distributions in the three links may not be identical. The target rate of the transmit packet is  $R = 1$  bit/s/Hz. Adapting for our two-phase on-demand

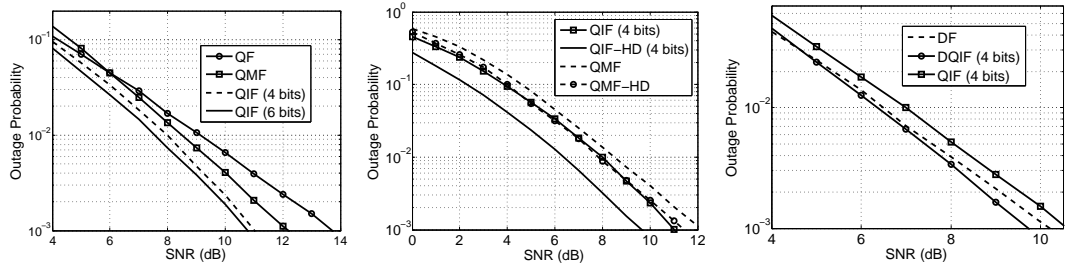
---

<sup>1</sup>A situation commonly encountered when the two phases occur sufficiently far apart, larger than the coherence time of the channel.

relaying protocol, we have that

$$\begin{aligned} \mathbb{P}[\text{Outage}] &= \mathbb{P}\left[\left\{R > C_{\text{P2P}}\left(H_{SD}^{(1)}\right)\right\} \cap \left\{R > C_R\left(H_{SD}^{(1)}, H_{SR}^{(1)}, H_{SD}^{(2)}, H_{RD}^{(2)}\right)\right\}\right] \\ &= \mathbb{P}\left[R > C_{\text{P2P}}\left(H_{SD}^{(1)}\right)\right] \mathbb{P}\left[R > C_R(\cdot) | R > C_{\text{P2P}}\left(H_{SD}^{(1)}\right)\right], \end{aligned}$$

where  $C_{\text{P2P}}(H_{SD}^{(1)})$  is the single-user capacity supported by channel  $H_{SD}^{(1)}$  and QAM constellation, and  $C_R(H_{SD}^{(1)}, H_{SR}^{(1)}, H_{SD}^{(2)}, H_{RD}^{(2)})$  is the capacity of the cooperative scheme, which depends on the particular strategy under consideration. For strategies that do not use hybrid decoding,  $C_R$  is just a function of  $H_{SR}^{(1)}, H_{SD}^{(2)}$  and  $H_{RD}^{(2)}$ . We evaluate numerically the outage probability by using analytical expressions for  $C_R(H_{SR}^{(1)}, H_{SD}^{(2)}, H_{RD}^{(2)})$  for each strategy, that we derived by modifying the arguments in [3, 7].



(a) Outage performance for QF, QMF, and QIF. All channels are i.i.d. (b) Outage performance for QMF and QIF with and without hybrid decoding. All channels are i.i.d. (c) Outage performance for QIF, DF, and DQIF.  $\text{SNR}_{RD} = 4\text{SNR}_{SD} = 4\text{SNR}_{SR}$ . X-axis denotes  $\text{SNR}_{SD}$ .

Figure 5.2: Outage performance of different relaying schemes.

### 5.2.2 Benefits of Interleaving

We compare the following schemes: (i) QMF: scalar quantization followed by random mapping at the relay, as in [3], (ii) QIF: scalar quantization followed by bit-level interleaving at the relay and (iii) QF (Quantize-Forward): only scalar quantization at the relay.

The plot in Fig. 5.2a is generated with all three links having i.i.d. Rayleigh fading channels with the same SNR. We observe that QIF outperforms QMF, even for very short interleaver lengths<sup>2</sup>. This can be intuitively explained as follows: in the original QMF relaying scheme, the random mapping at relay results in independence between the transmissions of the source and the relay. Hence the original QMF cannot harness

<sup>2</sup>Due to a multi-letter vector channel representation, it is only feasible to numerically evaluate the expressions for short length interleavers. However, we do see that performance improves with length of the interleaver. Thus the theoretical plots for QIF in this section are much more pessimistic than the long-length interleavers that we use in our over-the-air experiments.

the coherent combining power gain that may increase the performance in the moderate SNR regime. Instead, in QIF the interleaver preserves the weight of the quantized codeword and hence retains certain correlation with the transmission from the source, while providing enough mixing across source and relay terminals to guarantee spatial diversity. Indeed, we observe that QIF outperforms QF significantly, since with no mapping, QF cannot extract the full spatial diversity.

### 5.2.3 Benefits of Hybrid Decoding

In Fig. 5.2b (where again all three links have i.i.d. Rayleigh fading channels) we verify that hybrid decoding leads to a significantly improved performance for QIF and QMF. The versions of QMF and QIF with hybrid decoding are labeled QMF-HD and QIF-HD respectively. The gain observed is well expected as the signal received in Phase 1 contains information that can improve the decoding performance. Interestingly, the gain for hybrid decoding in QIF, roughly 1.5dB, is almost double of that in QMF.

### 5.2.4 Benefits of Opportunistic Decoding or Quantization

We compare the following schemes: (i) DF: relay decodes and forwards if it can, else does not cooperate (ii) QIF: as mentioned above, and (iii) DQIF (Decode/Quantize-Interleave-Forward): the relay opportunistically decodes and forwards if possible, else performs QIF.

In Fig. 5.2c, where all three links have Rayleigh fading channels, but the SNR in the relay-destination link is four times stronger than that in the source-destination and source-relay links, we observe the benefit of opportunistic decoding when the reception at the relay is weak. In particular, while DF slightly outperforms QIF, DQIF is also shown to extract the combined benefits of both DF and QIF. Moreover, we must point out that the theoretical demonstrations for QIF are carried out with short length interleavers and the performance of QIF improves with interleaver length (see Fig. 5.2a). In real-world experiments, we use long interleavers that will provide better performance than the demonstrations in this section show. The relative superiority of DF and QIF will of course vary with channel conditions, but a combination of the two appears to be a promising scheme in terms of universality.

## 5.3 System Implementation

### 5.3.1 Cooperative Schemes Implemented

Below we give a description and motivation of the schemes we analyze via experiments using our deployed testbed.

The relay operations we consider in our experiments are:

- *Quantize-Forward (QF)*: Scalar quantization and subsequent forwarding by the relay.
- *Quantize-Interleave-Forward (QIF)*: Scalar quantization followed by bit-level interleaving of the quantized sequences by the relay and subsequent forwarding.
- *Decode-Forward (DF)*: Decoding at the relay if possible and transmit a  $2 \times 1$  Alamouti jointly with the source. If decoding at the relay is not possible it remains silent.
- *Decode-Interleave-Forward (DIF)*: Decoding at the relay if possible and transmit bit-level interleaved signal. If decoding at the relay is not possible it remains silent.
- *Decode-Interleave-Quantize-Interleave-Forward (DIQIF)*: DIF if relay decoding succeeds; QIF otherwise.

We note that DIF was not considered in our single-carrier theoretical analysis. We implemented this for our (OFDM-based) over-the-air experiments to provide DF an option to exploit the frequency diversity across subcarriers that the interleaver in QIF was inherently providing.

For Phase 2, the destination operations we consider are:

- *No Hybrid Decoding*: The decoding at destination only uses the signal received in Phase 2.
- *Hybrid Decoding (-HD)*: The destination attempts to decode with both the signals received in Phase 1 and Phase 2.

To further demonstrate the utility of cooperation, we implement the baseline Direct Transmission (DT) scheme as described in the previous chapter. Also, note that, in the nomenclature used, QUILT refers to DIQIF-HD, which is essentially the all-encompassing system that is the cornerstone of this chapter.

#### 5.3.2 Frame Structure

We designed our system to emulate the physical layer procedures of WiFi (IEEE802.11). Each transmitted frame consists of a preamble and the payload. The frame structure is identical to the one described in the previous chapter.

## 5.4 Experimental evaluation

In this section, we experimentally evaluate QUILT and compare it with alternative cooperative communication strategies.

### 5.4.1 Performance Metrics

As in Chapter 4, we consider the following metrics:

- *Frame-Error Rate (FER)*: The percentage of source packets that were not decoded after both phases.
- *Throughput*: The number of information bits successfully delivered to the destination per channel use (bps/Hz).

### 5.4.2 Testbed

As in Chapter 4, we used the WARP SDR hardware to implement the source, relay and destination nodes in our testbed and used the WARPLab framework to interact with the WARP hardware via a host PC running MATLAB.

We evaluated the performance of the protocols for different experiment scenarios which were obtained by keeping the source fixed and varying the relay and destination placement and source and relay powers. The node locations for each of the three scenarios considered are shown in Fig. 5.3 and the Received Signal Strength Indicator (RSSI) for each link for each scenario is shown in Fig. 5.4.

For each setting, we ran the experiment for at least 2500 coded frames. In all experiments, we used randomly chosen bit-interleavers of length equal to that of an LDPC codeword. We used 16-QAM constellations with a coding rate of 3/4.

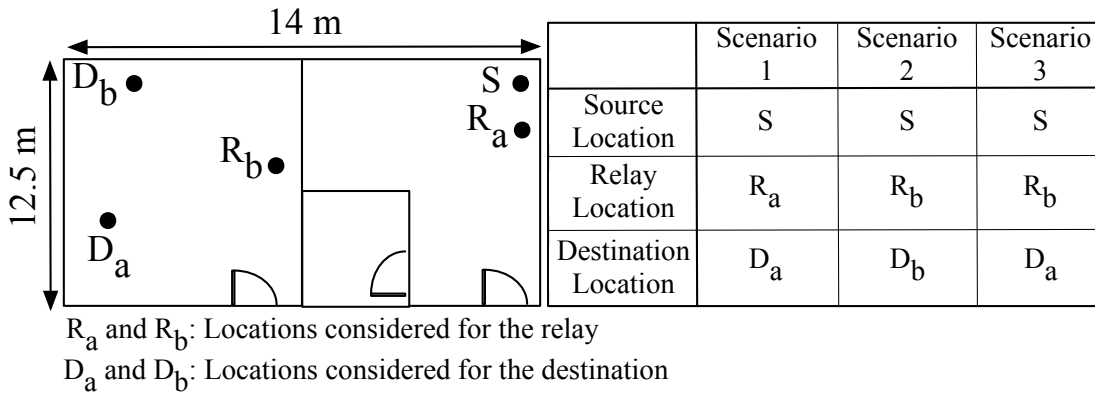


Figure 5.3: Node placement illustrating the topologies considered.

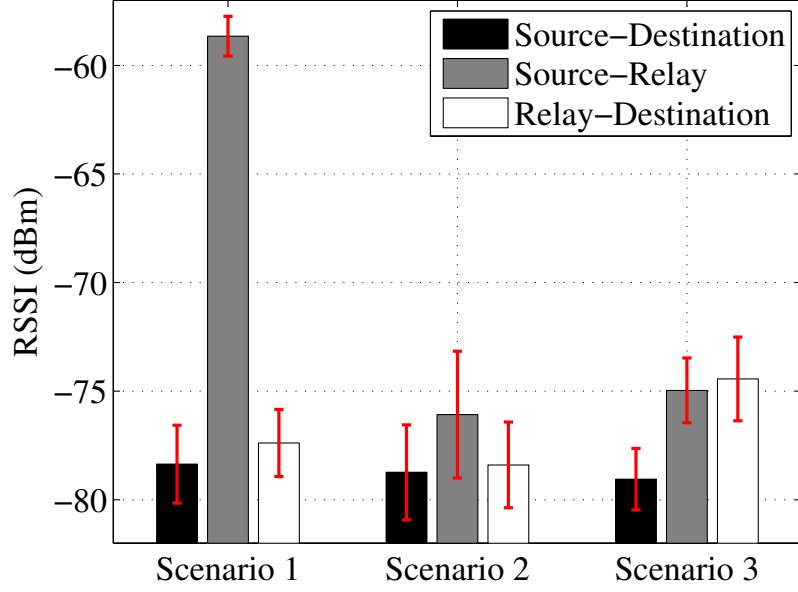


Figure 5.4: RSSIs for the different settings considered.

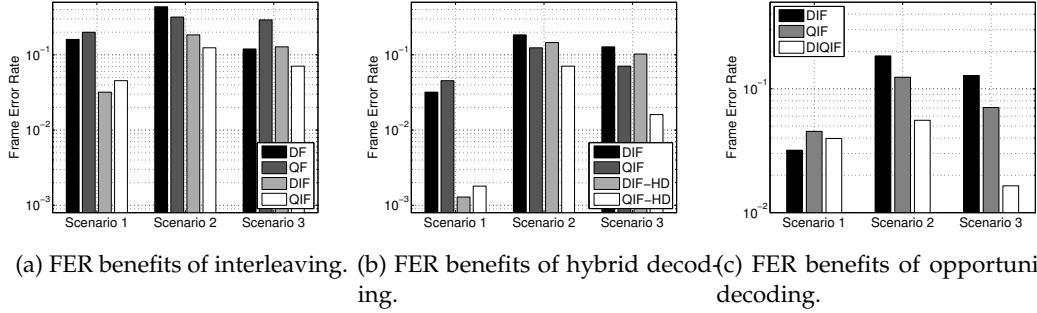


Figure 5.5: FER benefits of interleaving, hybrid decoding, and opportunistic decoding.

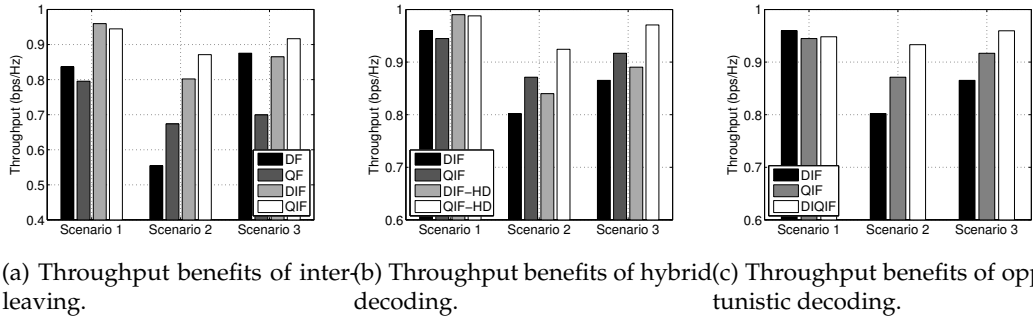


Figure 5.6: Throughput benefits of interleaving, hybrid decoding, and opportunistic decoding/quantizing.

### 5.4.3 Evaluation of Interleaving

We observed in Section 5.2 that interleaving can significantly improve the outage probability of QIF vs. QF<sup>3</sup> (see Figure 5.2a). The theoretical evaluation was only possible for short interleavers, and across a single subcarrier. The question is: how much interleaving helps when we use long interleavers across subcarriers?

Fig. 5.5a and 5.6a present the performance of DF, QF, DIF and QIF. We note that for these experiments, we allowed DF to implement an Alamouti code when the source and the relay cooperatively transmit in the phase 2, thus achieving full spatial diversity. We make the following observations.

First, QIF outperforms QF in all three scenarios, with **throughput gains** ranging from **15% to 30%**. We expected significant benefits, as interleaving enables to capture space-frequency diversity. Infact, it was shown in [31] that interleaving is sufficient to extract full spatial diversity from distributed transmissions for single carrier systems; here, we have the additional benefit of capturing frequency diversity through mixing signals across OFDM subcarriers.

Second, although DF achieves full spatial diversity due to the Alamouti code, DIF still offers benefits, up to an impressive **45%** throughput gain (Scenario 2, Fig. 5.6a). This reflects the additional frequency diversity gain from interleaving.

Third, Scenario 1 provides evidence that DIF can in some cases outperform QIF.

### 5.4.4 Evaluation of Hybrid Decoding

Next, we investigate the effect of relay-assisted hybrid decoding. Fig. 5.5b and 5.6b compare the performance of DIF and QIF, which in the second phase utilize only the second transmission for decoding, with that of DIF-HD and QIF-HD, which combine the received signals in both phases 1 and 2 when decoding. We observe that:

First, hybrid decoding consistently offers benefits for both QIF and DIF across all the three scenarios, for instance up to **25 times** FER improvement (in Scenario 1, Fig. 5.5b).

Second, hybrid decoding makes a more significant difference when the channels are less noisy, i.e., we start with lower FER, as is the case in Scenario 1. This is because there are comparatively fewer errors in the erroneous codewords, which can be corrected with hybrid decoding.

Third, hybrid decoding can help QIF more than DIF, as we see in Scenarios 2 and 3.

---

<sup>3</sup>We emphasize once again that the random mapping version of QMF in [3] is not an *implementable* strategy due to complexity limitations. Moreover, we have shown in Section 5.2 that QIF outperforms random mapping.

This is because with DIF, when the relay cannot decode it remains silent in phase 2; while with QIF the relay always transmits potentially useful information that can be leveraged through hybrid decoding across both phases, which is reflected in the QIF-HD performance.

#### 5.4.5 Evaluation of Opportunistic Decoding or Quantizing

To explore the performance of opportunistic decoding/quantizing at the relay, Fig. 5.5c and 5.6c compare the FER and throughput of DIF and QIF vs. DIQIF. We find that:

DIQIF, that implements opportunistic decoding/quantizing, has competitive or better performance than the next best scheme, as high as **a factor of 8** over DIF and **a factor of 5** over QIF (as in Scenario 3, Fig. 5.5c). The benefits of DIQIF are more pronounced when the source-to-relay link is weak, as is the case in Scenarios 2 and 3. This is because, in such cases the relay cannot decode, and DIF cannot exploit the relay-destination channel, while DIQIF can. Moreover, although QIF outperforms DIF in terms of FER, there exist frames where relay decoding is possible, and the opportunistic DIQIF decoding enables to clean them up from the source-relay noise, thus boosting the end-to-end performance. In Scenario 1, on the other hand, the source-relay link is very strong and supports relay decoding almost all the time; the DIQIF relay also performs decoding, but has the added requirement of communicating a 1-bit flag to inform the destination whether it decoded; we believe it is errors in this bit that result in the marginal penalty of the DIQIF performance over DIF.

#### 5.4.6 Putting it All Together: Evaluation of QUILT

We compare in Fig. 5.7a the FER performance of QUILT with (i) DIF-HD and QIF-HD, the most competing strategies implemented in this work, and (ii) DT-HD, direct transmissions with hybrid decoding, to benchmark the performance of a system without a relay. We observe the following:

First, we note FER gains of over **2 orders of magnitude** of our relaying strategies vs. DT-HD (in Scenario 1, Fig. 5.7a), clearly illustrating the benefits of relaying.

Second, QUILT has competitive or better performance than the next best scheme, up to **a factor of 5** over QIF-HD (in Scenario 3, Fig. 5.7a). In Scenario 1, where the source-relay link is very strong, we observed very few errors for DIF-HD, QIF-HD and QUILT (even after running the experiments in this scenario for over 4000 frames) as hybrid decoding cleans up most errors in this setup, leading to similar performance across the three schemes (marginally better for QUILT).

Since we operate at quite low FERs, we note that the vast majority of transmissions are

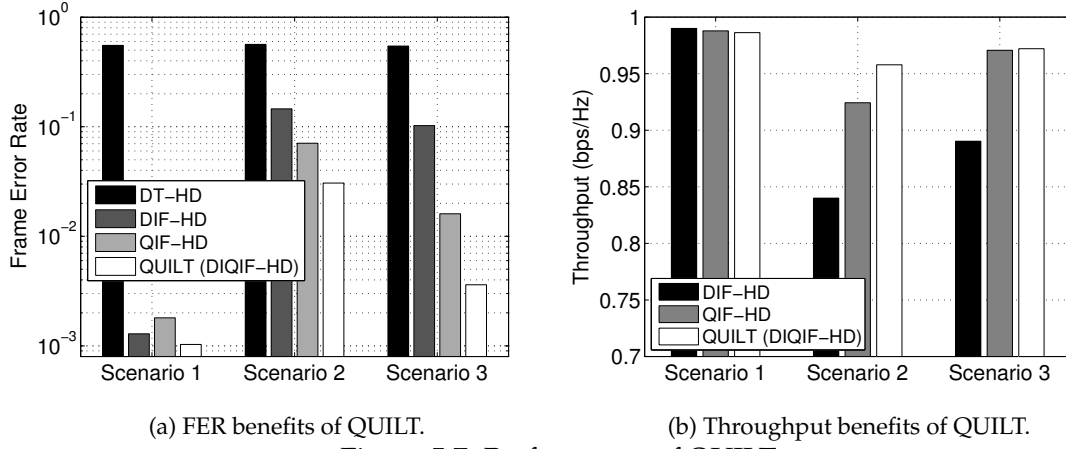


Figure 5.7: Performance of QUILT.

successful and thus, the difference in fraction of frames correctly decoded does not lead to discernible throughput differences in Fig. 5.7b. However, when operating at higher FERs, we believe that the FERs trends evidenced in Fig. 5.7a will lead to more significant throughput differences, as was the case in Fig. 5.6b, 5.6c.

Overall, we find that QUILT, by synthesizing opportunistic selection of decoding/quantizing and interleaving at the relay with hybrid decoding at the destination, achieves universally competitive performance across all the scenarios we examined.

## Related Work

The works in [38], [39] survey testbed implementations of physical layer relay schemes; the focus is on the implementation of either DF or AF schemes. A testbed based on uncoded DF in a single-relay system was investigated in [40]. A WARP radio testbed based on DF was implemented in [41]. None of these works implemented advanced error correction or broadband OFDM modulation. In [36] both (uncoded) AF and DF relaying along with distributed Alamouti-based transmission were implemented over broadband OFDM. However, this implementation lacked error correcting codes and distributed frequency-diversity coding. Apart from the relaying strategy, other issues related cooperative relaying have also been studied through implementation on testbeds; for example the experimental work in [35] and [27] focuses on the synchronization for multiple simultaneous transmissions.



# A Appendices

## A.1 Optimal Quantizer for Asymmetric Fades

When  $\lambda_1 \neq \lambda_2$ , we have,

$$Q'(\Delta) = \frac{1}{(\lambda_2 - \lambda_1)} \left\{ \begin{aligned} & \left( \lambda_2 e^{-(\lambda_1 \alpha_2 + (\lambda_2 - \lambda_1) \lceil \alpha_1 \rceil^+)} \right) \cdot \left( (\lambda_1 - \lambda_2) \lceil \alpha_1 \rceil^{+'} - \lambda_1 \alpha_2' \right) \\ & + \lambda_1 \lambda_2 \alpha_2' e^{-\lambda_2 \alpha_2} \end{aligned} \right\}$$

Similar to the case  $\lambda_1 = \lambda_2$ , we start by assuming  $\alpha_1 > 0$ . From the boundary values in Table A.1, we note that  $Q(0) = 0$  and  $Q(\infty) = e^{-\lambda_2(2^R - 1)}$ . Moreover, we observe that  $Q'(\infty) < 0$ , which implies that the function is decreasing just before attaining its limiting value. These conditions dictate that there must be *at least* one finite local maxima of  $Q(\Delta)$ , and the  $\Delta = \Delta^\S$  that maximises  $Q(\Delta)$  corresponds to the global maxima. The critical points can be found efficiently using numerical methods to find the roots of  $Q'(\Delta) = 0$ . From plotting  $Q(\Delta)$  for various parameter sets  $(h, R, \lambda_1, \lambda_2)$ , we conjecture that there is *exactly* one critical point of  $Q(\Delta)$ , but we cannot at this point prove the claim due to the general transcendental nature of the expression.

As before, if  $\Delta^\S > \Delta_t = \frac{h^2}{2^R - 1} - 1$ , our assumption on  $\alpha_1$  is validated, and  $\Delta^* = \Delta^\S$ . Otherwise, we set  $\lceil \alpha_1 \rceil^+ = 0$  in the  $Q(\Delta)$  expression. We also note that in this case, the maximizing  $\Delta^*$  will lie in the interval  $(0, \Delta_t]$ . In such a case,  $Q'(\Delta) = \frac{\lambda_1 \lambda_2 \alpha_2'}{\lambda_2 - \lambda_1} \{ e^{-\lambda_2 \alpha_2} - e^{-\lambda_1 \alpha_2} \} >$

Functions	$\lim_{\Delta \rightarrow 0^+}$	$\lim_{\Delta \rightarrow \infty}$
$\alpha_1 = 2^R - \frac{h^2}{1+\Delta} - 1$	$2^R - h^2 - 1$	$2^R - 1$
$\alpha_2 = 2^R \left(1 + \frac{1}{\Delta}\right) - 1$	$\infty$	$2^R - 1$
$\alpha_1' = \frac{h^2}{(1+\Delta)^2}$	$h^2$	$0^+$
$\alpha_2' = -\frac{2^R}{\Delta^2}$	$-\infty$	$0^-$

Table A.1: Limiting values of  $\alpha_1, \alpha_2, \alpha_1'$  and  $\alpha_2'$

## Appendix A. Appendices

---

0  $\forall \Delta \in (0, \Delta_t]$ , i.e.,  $Q(\Delta)$  is monotonically increasing in  $\Delta$ . Hence, the maximizing  $\Delta^* = \Delta_t$ .

Thus, similar to the case where  $\lambda_1 = \lambda_2$ , we have  $\Delta^* = \max \{\Delta^\S, \Delta_t\}$  for  $\lambda_1 \neq \lambda_2$ .

### A.2 Proof of Lemma 2.4.1

Throughout this proof we work under a fixed  $\Delta_2$ . Hence for notational convenience, let us drop the  $\Delta_2$  argument in  $R(\Omega; \Delta_1, \Delta_2)$ .

First observe that

$$\begin{aligned} R(\emptyset; \Delta_1) &:= \log \left( 1 + \frac{h_1^2}{1 + \Delta_1} + \frac{h_2^2}{1 + \Delta_2} \right) \\ R(2; \Delta_1) &:= \left[ \begin{array}{c} \log(1 + g_2^2) + \log \left( 1 + \frac{h_1^2}{1 + \Delta_1} \right) \\ -\log \left( \frac{1 + \Delta_2}{\Delta_2} \right) \end{array} \right]^+ \end{aligned}$$

are decreasing functions of  $\Delta_1$ , while

$$\begin{aligned} R(1; \Delta_1) &:= \left[ \begin{array}{c} \log(1 + g_1^2) + \log \left( 1 + \frac{h_2^2}{1 + \Delta_2} \right) \\ -\log \left( \frac{1 + \Delta_1}{\Delta_1} \right) \end{array} \right]^+ \\ R(1, 2; \Delta_1) &:= \left[ \begin{array}{c} \log(1 + g_1^2 + g_2^2) - \log \left( \frac{1 + \Delta_1}{\Delta_1} \right) \\ -\log \left( \frac{1 + \Delta_2}{\Delta_2} \right) \end{array} \right]^+ \end{aligned}$$

are increasing functions of  $\Delta_1$ . Besides, within the two curves  $R(1; \Delta_1)$  and  $R(1, 2; \Delta_1)$ , one will be no less than the other throughout all positive  $\Delta_1$ . Therefore to simplify the problem, let us first find the condition for one of them to be the dominant one, and for the remaining one can focus on the relations of the other two decreasing functions with this dominant increasing curve.

$$\begin{aligned} R(1; \Delta_1) &\leq R(1, 2; \Delta_1) \\ \iff \log(1 + g_1^2) + \log \left( 1 + \frac{h_2^2}{1 + \Delta_2} \right) - \log \left( \frac{1 + \Delta_1}{\Delta_1} \right) \\ &\leq \log(1 + g_1^2 + g_2^2) - \log \left( \frac{1 + \Delta_1}{\Delta_1} \right) - \log \left( \frac{1 + \Delta_2}{\Delta_2} \right) \\ \iff (1 + g_1^2)(1 + h_2^2 + \Delta_2) &\leq (1 + g_1^2 + g_2^2)\Delta_2 \\ \iff \Delta_2 &\geq \frac{(1 + g_1^2)(1 + h_2^2)}{g_2^2} = \delta_2 \end{aligned}$$

Below we discuss in two difference cases based on the above condition.

### A.2.1 $\Delta_2 \geq \delta_2$

In this case we have

$$R_{\text{QMF},G}^*(\Delta_2) = \max_{\Delta_1 > 0} \min \{R(1; \Delta_1), R(\emptyset; \Delta_1), R(2; \Delta_1)\}$$

Note that at the two extreme values of  $\Delta_1$ ,

$$\begin{aligned} R(1; \Delta_1 = 0) &= 0 \\ R(1; \Delta_1 = \infty) &= \log(1 + g_1^2) + \log\left(1 + \frac{h_2^2}{1 + \Delta_2}\right) \\ R(\emptyset; \Delta_1 = 0) &= \log\left(1 + h_1^2 + \frac{h_2^2}{1 + \Delta_2}\right) \\ R(\emptyset; \Delta_1 = \infty) &= \log\left(1 + \frac{h_2^2}{1 + \Delta_2}\right) \\ R(2; \Delta_1 = 0) &= \left[ \begin{array}{c} \log(1 + g_2^2) + \log(1 + h_1^2) \\ -\log\left(\frac{1 + \Delta_2}{\Delta_2}\right) \end{array} \right]^+ \\ R(2; \Delta_1 = \infty) &= \left[ \log(1 + g_2^2) - \log\left(\frac{1 + \Delta_2}{\Delta_2}\right) \right]^+ \end{aligned}$$

We conclude that  $R(1; \Delta_1)$  and  $R(\emptyset; \Delta_1)$  will always intersect at some positive  $\Delta_1$ , and using the monotonicity of these curves, the intersection occurs at only one point. On the other hand  $R(1; \Delta_1)$  and  $R(2; \Delta_1)$  may not. Moreover, using the monotonicity of these curves, we have

$$\begin{aligned} &\forall \Delta_1 > 0, R(1; \Delta_1) \leq R(2; \Delta_1) \\ &\iff R(1; \Delta_1 = \infty) \leq R(2; \Delta_1 = \infty) \\ &\iff \log(1 + g_1^2) + \log\left(1 + \frac{h_2^2}{1 + \Delta_2}\right) \\ &\quad \leq \log(1 + g_2^2) - \log\left(\frac{1 + \Delta_2}{\Delta_2}\right) \\ &\iff \Delta_2 \geq \frac{(1 + g_1^2)(1 + h_2^2)}{g_2^2 - g_1^2} \text{ and } g_2^2 > g_1^2 \end{aligned}$$

Hence, if  $g_2^2 > g_1^2$  and  $\Delta_2 \geq \frac{(1 + g_1^2)(1 + h_2^2)}{g_2^2 - g_1^2}$ , then  $\Delta_1^* = \Delta_1^*(1; \emptyset) :=$  the intersection of  $R(1; \Delta_1)$

## Appendix A. Appendices

---

and  $R(\emptyset; \Delta_1)$ :

$$\Delta_1^*(1; \emptyset) := \frac{(1 + h_1^2)\Delta_2 + (1 + h_1^2 + h_2^2)}{g_1^2(\Delta_2 + (1 + h_2^2))}$$

Otherwise, we use the monotonicity of these curves to arrive at  $\Delta_1^* = \min \{\Delta_1^*(1; \emptyset), \Delta_1^*(1; 2)\}$ , where  $\Delta_1^*(1; 2) :=$  the intersection of  $R(1; \Delta_1)$  and  $R(2; \Delta_1)$ :

$$\Delta_1^*(1; 2) := \frac{(1 + g_1^2)(1 + h_1^2)\Delta_2}{(g_1^2 - g_2^2)\Delta_2 + (1 + g_1^2)(1 + h_2^2)}$$

Next we introduce the following claim, the proof of which is at the end of this section.

**Claim 1.** *Within the range  $\Delta_2 \geq \delta_2$ , we always have  $\Delta_1^*(1; 2) > \Delta_1^*(1; \emptyset)$ .*

Therefore,  $\Delta_1^* = \Delta_1^*(1; \emptyset)$  is the optimal solution for  $\Delta_2 \geq \delta_2$ , and  $\Omega^* = \{1\}$  or  $\Omega^* = \emptyset$ .

### A.2.2 $\Delta_2 < \delta_2$

In this case we have

$$R_{\text{QMF},G}^*(\Delta_2) = \max_{\Delta_1 > 0} \min \{R(1, 2; \Delta_1), R(\emptyset; \Delta_1), R(2; \Delta_1)\}$$

Again, note that at the two extreme values of  $\Delta_1$ ,

$$\begin{aligned} R(1, 2; \Delta_1 = 0) &= 0 \\ R(1, 2; \Delta_1 = \infty) &= \left[ \log(1 + g_1^2 + g_2^2) - \log\left(\frac{1 + \Delta_2}{\Delta_2}\right) \right]^+ \\ R(\emptyset; \Delta_1 = 0) &= \log\left(1 + h_1^2 + \frac{h_2^2}{1 + \Delta_2}\right) \\ R(\emptyset; \Delta_1 = \infty) &= \log\left(1 + \frac{h_2^2}{1 + \Delta_2}\right) \\ R(2; \Delta_1 = 0) &= \left[ \begin{array}{c} \log(1 + g_2^2) + \log(1 + h_1^2) \\ -\log\left(\frac{1 + \Delta_2}{\Delta_2}\right) \end{array} \right]^+ \\ R(2; \Delta_1 = \infty) &= \left[ \log(1 + g_2^2) - \log\left(\frac{1 + \Delta_2}{\Delta_2}\right) \right]^+ \end{aligned}$$

We conclude that  $R(1, 2; \Delta_1)$  and  $R(2; \Delta_1)$  will always intersect at some positive  $\Delta_1$ , and using the monotonicity of these curves, the intersection occurs at only one point. On the other hand  $R(1, 2; \Delta_1)$  and  $R(\emptyset; \Delta_1)$  may not. Moreover, using the monotonicity of these

curves, we have

$$\begin{aligned}
 & \forall \Delta_1 > 0, R(1, 2; \Delta_1) \leq R(\emptyset; \Delta_1) \\
 & \iff R(1, 2; \Delta_1 = \infty) \leq R(\emptyset; \Delta_1 = \infty) \\
 & \iff \log(1 + g_1^2 + g_2^2) - \log\left(\frac{1 + \Delta_2}{\Delta_2}\right) \\
 & \leq \log\left(1 + \frac{h_2^2}{1 + \Delta_2}\right) \\
 & \iff \Delta_2 \leq \frac{1 + h_2^2}{g_1^2 + g_2^2}
 \end{aligned}$$

Hence, if  $\Delta_2 \leq \frac{1 + h_2^2}{g_1^2 + g_2^2}$ , then  $\Delta_1^* = \Delta_1^*(1, 2; 2) :=$  the intersection of  $R(1, 2; \Delta_1)$  and  $R(2; \Delta_1)$ :

$$\Delta_1^*(1, 2; 2) := \frac{(1 + g_2^2)(1 + h_1^2)}{g_1^2}$$

Otherwise, we use the monotonicity of these curves to arrive at

$$\Delta_1^* = \min\{\Delta_1^*(1, 2; \emptyset), \Delta_1^*(1, 2; 2)\}$$

where  $\Delta_1^*(1, 2; \emptyset) :=$  the intersection of  $R(1, 2; \Delta_1)$  and  $R(\emptyset; \Delta_1)$ :

$$\Delta_1^*(1, 2; \emptyset) := \frac{(1 + h_1^2)\Delta_2 + (1 + h_1^2 + h_2^2)}{(g_1^2 + g_2^2)\Delta_2 - (1 + h_2^2)}$$

Below we derive the necessary and sufficient condition for  $\Delta_1^*(1, 2; \emptyset) \geq \Delta_1^*(1, 2; 2)$ :

$$\begin{aligned}
 & \Delta_1^*(1, 2; \emptyset) \geq \Delta_1^*(1, 2; 2) \\
 & \iff g_1^2((1 + h_1^2)\Delta_2 + (1 + h_1^2 + h_2^2)) \\
 & \geq (1 + g_2^2)(1 + h_1^2)(g_1^2 + g_2^2)(\Delta_2 - (1 + h_2^2)) \\
 & \iff \Delta_2 \leq \frac{(1 + g_1^2 + g_2^2)(1 + h_1^2 + h_2^2) + (1 + g_2^2)h_1^2h_2^2}{g_2^2(1 + g_1^2 + g_2^2)} \\
 & = \delta_1
 \end{aligned}$$

The following claim concludes the discussion of this case.

**Claim 2.** For any nonzero  $\{h_1, h_2, g_1, g_2\}$ ,

$$\frac{1 + h_2^2}{g_1^2 + g_2^2} < \delta_1 < \delta_2$$

## Appendix A. Appendices

---

Therefore, for  $0 < \Delta_2 \geq \delta_1$ ,  $\Delta_1^* = \Delta_1^*(1, 2; 2)$  is the optimal solution, and  $\Omega^* = \{1\}$  or  $\Omega^* = \{2\}$ . For  $\delta_1 \leq \Delta_2 < \delta_2$ ,  $\Delta_1^* = \Delta_1^*(1, 2; \emptyset)$  is the optimal solution, and  $\Omega^* = \{1, 2\}$  or  $\Omega^* = \emptyset$ .

Combining the above two cases for  $\Delta_2 \geq \delta_2$  and  $\Delta_2 < \delta_2$ , we have the complete characterization of  $R_{\text{QMEG}}^*(\Delta_2)$ .

### A.2.3 Proof of Claim 1

Assume the contrary, that  $\Delta_1^*(1; 2) \leq \Delta_1^*(1; \emptyset)$ . After some manipulations, we have

$$\Delta_1^*(1; 2) \leq \Delta_1^*(1; \emptyset) \iff \left\{ \begin{array}{l} (1 + h_1^2)g_2^2(1 + g_1^2)\Delta_2^2 \\ + \left[ \begin{array}{l} (1 + h_1^2 + h_2^2)(g_2^2 - g_1^2) \\ + (g_1^2g_2^2 - 1)(1 + h_1^2)(1 + h_2^2) \end{array} \right] \Delta_2 \\ - (1 + g_1^2)(1 + h_2^2)(1 + h_1^2 + h_2^2) \end{array} \right\} \leq 0$$

Denote this quadratic function of  $\Delta_2$  by  $f(\Delta_2)$ . Now let's plug in  $g_2^2\Delta_2 \geq (1 + g_1^2)(1 + h_2^2)$  to give a lower bound on  $f(\Delta_2)$ :

$$\begin{aligned} f(\Delta_2) &\geq g_1^2 \left[ (1 + h_1^2)(1 + h_2^2)(2 + g_1^2 + g_2^2) - (1 + h_1^2 + h_2^2) \right] \Delta_2 \\ &> 0 \end{aligned}$$

which leads to contradiction.

### A.2.4 Proof of Claim 2

First of all,

$$\begin{aligned} &\delta_1 < \delta_2 \\ \iff &\frac{(1 + g_1^2 + g_2^2)(1 + h_1^2 + h_2^2) + (1 + g_2^2)h_1^2h_2^2}{g_2^2(1 + g_1^2 + g_2^2)(1 + h_1^2)} \\ &< \frac{(1 + g_1^2)(1 + h_2^2)}{g_2^2} \\ \iff &(1 + g_1^2 + g_2^2)(1 + h_1^2 + h_2^2) + (1 + g_2^2)h_1^2h_2^2 \\ &< (1 + g_1^2 + g_2^2)(1 + h_1^2)(1 + g_1^2)(1 + h_2^2) \\ \iff &(1 + g_2^2)h_1^2h_2^2 < (1 + g_1^2 + g_2^2)(1 + g_1^2)h_1h_2^2 \\ &\quad + g_1^2(1 + g_1^2 + g_2^2)(1 + h_1^2 + h_2^2) \end{aligned}$$

which is obviously true since  $(1 + g_2^2) < (1 + g_1^2 + g_2^2) < (1 + g_1^2 + g_2^2)(1 + g_1^2)$ .

Second,

$$\begin{aligned}
 & \frac{1 + h_2^2}{g_1^2 + g_2^2} < \delta_1 \\
 \iff & g_2^2(1 + g_1^2 + g_2^2)(1 + h_1^2)(1 + h_2^2) \\
 & < (g_1^2 + g_2^2)(1 + g_1^2 + g_2^2)(1 + h_1^2 + h_2^2) \\
 & \quad + (g_1^2 + g_2^2)(1 + g_2^2)h_1^2h_2^2 \\
 \iff & g_2^2(1 + g_1^2 + g_2^2)h_1^2h_2^2 \\
 & < g_1^2(1 + g_1^2 + g_2^2)(1 + h_1^2 + h_2^2) \\
 & \quad + (g_1^2 + g_2^2)(1 + g_2^2)h_1^2h_2^2,
 \end{aligned}$$

which is obviously true since  $g_2^2(1 + g_1^2 + g_2^2) < (g_1^2 + g_2^2)(1 + g_2^2)$ .

### A.3 Proof of Theorem 2.4.2

By the characterization in Lemma 2.4.1, (2.5) can be solved by finding the optimal solution in each of the above three ranges  $I_1, I_2, I_3$  of  $\Delta_2$  analytically, and then find the maximum of these three.

For  $\Delta_2 \in I_3$ , note that  $\Delta_1^*$  is an increasing function of  $\Delta_2$  and that  $R(\emptyset; \Delta_1, \Delta_2)$  decreases when both  $\Delta_1$  and  $\Delta_2$  increase. Hence we conclude that  $R_{\text{QMF,G}}^*(\Delta_2)$  is a decreasing function in this range. Hence

$$\Delta_2^* = \delta_2 \qquad \Delta_1^* = \frac{(1 + h_1^2)\delta_2 + (1 + h_1^2 + h_2^2)}{g_1^2(\delta_2 + (1 + h_2^2))}$$

in this range.

For  $\Delta_2 \in I_1$ , note that  $\Delta_1^*$  does not depend on  $\Delta_2$  and that  $R(1, 2; \Delta_1, \Delta_2)$  increases when  $\Delta_2$  increases. Hence we conclude that  $R_{\text{QMF,G}}^*(\Delta_2)$  is an increasing function in this range. Hence

$$\Delta_2^* = \delta_1 \qquad \Delta_1^* = \frac{(1 + g_2^2)(1 + h_1^2)}{g_1^2}$$

in this range.

For  $\Delta_2 \in I_2$ , unlike the previous two cases,  $R_{\text{QMF,G}}^*(\Delta_2)$  may not be monotone in this case.

## Appendix A. Appendices

---

Here

$$\begin{aligned} R_{\text{QMF,G}}^*(\Delta_2) &= \log \left( 1 + \frac{h_1^2}{1 + \Delta_1^*} + \frac{h_2^2}{1 + \Delta_2} \right) \\ &= \log(1 + g_1^2 + g_2^2) - \log \left( \frac{1 + \Delta_1^*}{\Delta_1^*} \right) - \log \left( \frac{1 + \Delta_2}{\Delta_2} \right) \end{aligned}$$

The derivative of the above function with respect to  $\Delta_2$  has the same sign as the quadratic function  $q(\Delta_2) := A\Delta_2^2 + B\Delta_2 + C$ , where

$$\begin{aligned} A &= h_1^2(1 + h_1^2) - h_2^2(1 + h_1^2 + g_1^2 + g_2^2) \\ B &= 2h_1^2(1 + h_1^2) \quad C := h_1^2(1 + h_1^2 + h_2^2) \end{aligned}$$

If  $A \geq 0$ , then the above quadratic is always positive, implying that  $R_{\text{QMF,G}}^*(\Delta_2)$  is an increasing function. Therefore

$$\begin{aligned} \Delta_2^* &= \delta_2 \\ \Delta_1^* &= \frac{(1 + h_1^2)\delta_2 + (1 + h_1^2 + h_2^2)}{(g_1^2 + g_2^2)\delta_2 - (1 + h_2^2)} \\ &= \frac{(1 + h_1^2)\delta_2 + (1 + h_1^2 + h_2^2)}{g_1^2(\delta_2 + (1 + h_2^2))} \end{aligned}$$

is the optimal solution.

If  $A < 0$ , since  $q(0) = C > 0$  and  $q(\infty) < 0$ , it has a only one positive root

$$\delta_3 := \frac{-B - \sqrt{B^2 - 4AC}}{2A}$$

If  $\delta_3 \in I_3$  then

$$\Delta_2^* = \delta_3 \quad \Delta_1^* = \frac{(1 + h_1^2)\delta_3 + (1 + h_1^2 + h_2^2)}{(g_1^2 + g_2^2)\delta_3 - (1 + h_2^2)}$$

is the optimal solution.

If  $\delta_3 < \delta_1$ , that is,  $\delta_3 \in I_1$ , then  $q(\Delta_2) < 0$  for  $\Delta_2 \in I_3$  and hence  $R_{\text{QMF,G}}^*(\Delta_2)$  is a decreasing function of  $\Delta_2$  in this range. Therefore,

$$\begin{aligned} \Delta_2^* &= \delta_1 \\ \Delta_1^* &= \frac{(1 + h_1^2)\delta_1 + (1 + h_1^2 + h_2^2)}{(g_1^2 + g_2^2)\delta_1 - (1 + h_2^2)} \\ &= \frac{(1 + g_2^2)(1 + h_1^2)}{g_1^2} \end{aligned}$$

is the optimal solution.

If  $\delta_3 \geq \delta_2$ , that is,  $\delta_3 \in I_3$ , then  $q(\Delta_2) > 0$  for  $\Delta_2 \in I_3$  and hence  $R_{\text{QMF,G}}^*(\Delta_2)$  is an increasing function of  $\Delta_2$  in this range. Therefore,

$$\begin{aligned}\Delta_2^* &= \delta_2 \\ \Delta_1^* &= \frac{(1+h_1^2)\delta_2 + (1+h_1^2+h_2^2)}{(g_1^2+g_2^2)\delta_2 - (1+h_2^2)} \\ &= \frac{(1+h_1^2)\delta_2 + (1+h_1^2+h_2^2)}{g_1^2(\delta_2 + (1+h_2^2))}\end{aligned}$$

is the optimal solution.

## A.4 Proof of Lemmas 2.4.3, 2.4.4 and 2.4.5

### A.4.1 Proof of Lemma 2.4.3

Without loss of generality, let  $N \geq i > j \geq 0$ . Note that

$$\log \left\{ \left( 1 + \frac{(N-i)h^2}{1+\Delta} \right) (1+ig^2) \left( \frac{\Delta}{1+\Delta} \right)^i \right\} = \log \left\{ \left( 1 + \frac{(N-j)h^2}{1+\Delta} \right) (1+jg^2) \left( \frac{\Delta}{1+\Delta} \right)^j \right\}$$

if and only if  $f(\Delta) = 0$ , where

$$\begin{aligned}f(\Delta) = & \left\{ \left( 1 - \frac{1+jg^2}{1+ig^2} \right) \Delta^{i-j+1} + \left( 1 + (N-i)h^2 - \left( \frac{1+jg^2}{1+ig^2} \right) (1 + (N-j)h^2 + i-j) \right) \Delta^{i-j} \right. \\ & \left. - \left( \frac{1+jg^2}{1+ig^2} \right) \sum_{p=1}^{i-j-1} \left\{ \binom{i-j}{p} (1 + (N-j)h^2) + \binom{i-j}{p-1} \right\} \Delta^p - \left( \frac{1+jg^2}{1+ig^2} \right) (1 + (N-j)h^2) \right\}\end{aligned}$$

We note that in  $f(\Delta)$ , the coefficient of  $\Delta^{i-j+1}$  is positive and that the coefficients of  $\Delta_{\{p \in [0:i-j-1]\}}^p$  are negative. The coefficient of  $\Delta^{i-j}$  may be positive or negative, depending on the channel configurations. Either way, the number of *sign changes* of the coefficients of  $f(\Delta)$  when written in descending order of powers is exactly 1. By the Descartes' sign scheme, the number of positive roots of such a polynomial equation is given by  $\alpha - 2m$ , where  $\alpha$  is the number of sign changes and  $m$  is a positive integer. Since  $f(\Delta)$  has *exactly* 1 sign change,  $f(\Delta)$  has *exactly* 1 positive root, which proves the lemma.

### A.4.2 Proof of Lemma 2.4.4

For  $i \in [0 : N-1]$ ,  $R_i(\Delta) - R_{i+1}(\Delta)$  can be simplified as,

$$R_i(\Delta) - R_{i+1}(\Delta) = \left\{ \log \left( \frac{1+\Delta}{\Delta} \right) + \log \left( \frac{1+\Delta+(N-i)h^2}{1+\Delta+(N-i-1)h^2} \right) + \log \left( \frac{1+ig^2}{1+(i+1)g^2} \right) \right\}$$

## Appendix A. Appendices

---

From the above, we note that for finite  $h$  and  $g$ ,  $\lim_{\Delta \rightarrow 0} \{R_i(\Delta) - R_{i+1}(\Delta)\} = +\infty$  due to the presence of the term  $\log\left(\frac{1+\Delta}{\Delta}\right)$  in the expression for  $R_i(\Delta) - R_{i+1}(\Delta)$ , which proves the lemma.

### A.4.3 Proof of Lemma 2.4.5

We define the sequence of polynomials  $f_m(\Delta) = \frac{(1+\Delta)^{m+2}}{\Delta^m} (2^{R_{m+1}(\Delta)} - 2^{R_m(\Delta)})$ . Further, let  $\Delta_m^*$  denote the unique positive root of  $f_m(\Delta)$  (which is also the unique positive solution of  $R_m(\Delta) = R_{m+1}(\Delta)$ ). Then,  $\Delta_m^*$  satisfies

$$g^2 \Delta_m^{*2} + (g^2 (1 + (N-m)h^2) - 1 - h^2 - g^2 h^2 + 2mg^2) \Delta_m^* - (1 + mg^2) (1 + (N-m)h^2) = 0.$$

For the required condition to hold true, i.e,  $\Delta_m^* \leq \Delta_{m+1}^*$ , we must have  $f_{m+1}(\Delta_m^*) < 0$ , since  $R_{m+1}(\Delta) > R_{m+2}(\Delta)$  for  $\Delta \in (0, \Delta_{m+1}^*)$  by the preceding lemma. For  $f_{m+1}(\Delta_m^*) < 0$ ,

$$\Delta_m^* \geq \frac{h^2 (1 + (m+1)g^2) - g^2 (1 + (N-m)h^2)}{g^2 (2 + h^2)} = \Delta_t.$$

What now remains to be shown in order for the lemma to hold is that  $f_m(\Delta_t) < 0$  for all values of  $h, g, N$  and all  $m \in [0 : N-1]$ . Substituting the value of  $\Delta_t$ , we obtain,

$$\begin{aligned} f_m(\Delta_t) = & -\frac{h^6}{(2+h^2)^2} \left[ \underbrace{m^2 g^2 + m(2 + (3-2N)g^2) + g^2(N-1)^2 - (N-2) + \frac{1}{g^2}}_{\Gamma} \right] \\ & - \frac{h^4}{(2+h^2)^2} \left[ N + 2(m+1) + g^2(N^2 + 2m - 1) + \frac{2}{g^2} \right] \\ & - \frac{h^2}{(2+h^2)^2} \left[ 2N + 3 + 4m + g^2(4m^2 + 4m + (2N-1)) + \frac{2}{g^2} \right] - \frac{[2+g^2]}{(2+h^2)^2}. \end{aligned}$$

From the above expression for  $f_m(\Delta_t)$ , it is clear that  $\Gamma > 0$  is a sufficient condition for  $f_m(\Delta_t) < 0$ .  $\Gamma$  can be viewed as a quadratic in  $m$  with a discriminant  $D_\Gamma = (5-4N)g^4 + 4(1-N)g^2$ . Since the coefficient of  $m^2$  is positive, the necessary and sufficient condition for  $\Gamma > 0$ ,  $\forall m, g, h, N$  is that  $D_\Gamma < 0$ , which is satisfied for  $N \geq 2$ . This proves the lemma.

# Bibliography

- [1] "Akamai's State of the Internet q1 2014 report, volume 7, number 1." Online: [http://www.akamai.com/dl/akamai/akamai-soti-a4-q114.pdf?WT.mc\\_id=soti\\_Q114](http://www.akamai.com/dl/akamai/akamai-soti-a4-q114.pdf?WT.mc_id=soti_Q114).
- [2] "Cisco Visual Networking Index: Global Mobile Data Traffic Forecast Update, 2013—2018." Online: [http://www.cisco.com/c/en/us/solutions/collateral/service-provider/visual-networking-index-vni/white\\_paper\\_c11-520862.pdf](http://www.cisco.com/c/en/us/solutions/collateral/service-provider/visual-networking-index-vni/white_paper_c11-520862.pdf).
- [3] A. S. Avestimehr, S. N. Diggavi, and D. N. C. Tse, "Wireless network information flow: A deterministic approach," *IEEE Transactions on Information Theory*, vol. 57, pp. 1872–1905, April 2011.
- [4] T. M. Cover and A. E. Gamal, "Capacity theorems for the relay channel," *IEEE Transactions on Information Theory*, vol. 25, pp. 572–584, September 1979.
- [5] L. Zheng and D. Tse, "Diversity and multiplexing: a fundamental tradeoff in multiple-antenna channels," *Information Theory, IEEE Transactions on*, vol. 49, pp. 1073–1096, May 2003.
- [6] S. Pawar, A. Avestimehr, and D. Tse, "Diversity-multiplexing tradeoff of the half-duplex relay channel," in *Communication, Control, and Computing, 2008 46th Annual Allerton Conference on*, pp. 27–33, Sept 2008.
- [7] S. H. Lim, Y.-H. Kim, A. E. Gamal, and S.-Y. Chung, "Noisy network coding," *IEEE Transactions on Information Theory*, vol. 57, pp. 3132–3152, May 2011.
- [8] K. Azarian, H. El Gamal, and P. Schniter, "On the achievable diversity-multiplexing tradeoff in half-duplex cooperative channels," *Information Theory, IEEE Transactions on*, vol. 51, pp. 4152–4172, Dec 2005.
- [9] B. Chern and A. Ozgur, "Achieving the capacity of the n-relay gaussian diamond network within logn bits," in *Information Theory Workshop (ITW), 2012 IEEE*, pp. 377–380, Sept 2012.

## Bibliography

---

- [10] A. Sengupta, I.-H. Wang, and C. Fragouli, "Optimizing quantize-map-and-forward relaying for gaussian diamond networks," in *Information Theory Workshop (ITW), 2012 IEEE*, pp. 381–385, Sept 2012.
- [11] A. Ozgur and S. Diggavi, "Approximately achieving gaussian relay network capacity with lattice-based qmf codes," *Information Theory, IEEE Transactions on*, vol. 59, pp. 8275–8294, Dec 2013.
- [12] M. Yuksel and E. Erkip, "Multiple-antenna cooperative wireless systems: A diversity x2013multiplexing tradeoff perspective," *Information Theory, IEEE Transactions on*, vol. 53, pp. 3371–3393, Oct 2007.
- [13] N. Prasad and M. Varanasi, "High performance static and dynamic cooperative communication protocols for the half duplex fading relay channel," *Wireless Communications, IEEE Transactions on*, vol. 9, pp. 328–337, January 2010.
- [14] A. Bletsas, H. Shin, and M. Win, "Cooperative communications with outage-optimal opportunistic relaying," *Wireless Communications, IEEE Transactions on*, vol. 6, pp. 3450–3460, September 2007.
- [15] K.-S. Hwang, Y. chai Ko, and M.-S. Alouini, "Outage probability of cooperative diversity systems with opportunistic relaying based on decode-and-forward," *Wireless Communications, IEEE Transactions on*, vol. 7, pp. 5100–5107, December 2008.
- [16] C. Conne and I.-M. Kim, "Outage probability of multi-hop amplify-and-forward relay systems," *Wireless Communications, IEEE Transactions on*, vol. 9, pp. 1139–1149, March 2010.
- [17] K. Tourki, H.-C. Yang, and M.-S. Alouini, "Accurate outage analysis of incremental decode-and-forward opportunistic relaying," *Wireless Communications, IEEE Transactions on*, vol. 10, pp. 1021–1025, April 2011.
- [18] H. Yu, I.-H. Lee, and G. Stuber, "Outage probability of decode-and-forward cooperative relaying systems with co-channel interference," *Wireless Communications, IEEE Transactions on*, vol. 11, pp. 266–274, January 2012.
- [19] S. Yao, T. Kim, M. Skoglund, and H. Poor, "Half-duplex relaying over slow fading channels based on quantize-and-forward," *Information Theory, IEEE Transactions on*, vol. 59, pp. 860–872, Feb 2013.
- [20] S. Yao and M. Skoglund, "Hybrid digital-analog relaying for cooperative transmission over slow fading channels," *Information Theory, IEEE Transactions on*, vol. 55, pp. 944–951, March 2009.
- [21] J. Hou and G. Kramer, "Short message noisy network coding," *CoRR*, vol. abs/1304.1692, 2013.

- 
- [22] T. Richardson and R. Urbanke, *Modern Coding Theory*. New York, NY, USA: Cambridge University Press, 2008.
- [23] T. Richardson, M. Shokrollahi, and R. Urbanke, "Design of capacity-approaching irregular low-density parity-check codes," *Information Theory, IEEE Transactions on*, vol. 47, pp. 619–637, Feb 2001.
- [24] V. Nagpal, I.-H. Wang, M. Jorgovanovic, D. Tse, and B. Nikolic, "Quantize-map-and-forward relaying: Coding and system design," in *Communication, Control, and Computing (Allerton), 2010 48th Annual Allerton Conference on*, pp. 443–450, Sept 2010.
- [25] D. Tse and P. Viswanath, *Fundamentals of Wireless Communication*. Cambridge University Press, May 2005.
- [26] "Local and metropolitan area networks-specific requirements part 11: Wireless LAN medium access control (MAC) and physical layer (PHY) specifications," *IEEE Std 802.11-2012*.
- [27] X. Zhang and K. G. Shin, "DAC: Distributed asynchronous cooperation for wireless relay networks," in *Proceedings of the IEEE INFOCOM*, pp. 1064–1072, March 2010.
- [28] C. Hunter, P. Murphy, and A. Sabharwal, "Real-time testbed implementation of a distributed cooperative MAC and PHY," in *Proceedings of the IEEE CISS*, pp. 1–6, March 2010.
- [29] Chang, K. et al., "Relay operation in 802.11ad," in *IEEE 802.11ad TGad 1-/0494r1*, 2010.
- [30] S. Alamouti, "A simple transmit diversity technique for wireless communications," *IEEE Journal on Select Areas in Communications*, vol. 16, pp. 1451–1458, October 1998.
- [31] A. Sengupta, S. Brahma, A. Ozgur, C. Fragouli, and S. Diggavi, "Graph-based codes for quantize-map-and-forward relaying," in *Proceedings of the IEEE Information Theory Workshop*, pp. 140–144, October 2011.
- [32] E. Atsan, R. Knopp, S. Diggavi, and C. Fragouli, "Towards integrating quantize-map-forward relaying into LTE," in *Proceedings of the IEEE Information Theory Workshop*, pp. 212–216, September 2012.
- [33] "WARP Project, <http://warpproject.org..>"
- [34] P. Murphy, *Design, Implementation, and Characterization of a Cooperative Communications System*. PhD thesis, Rice University, 2010.
- [35] H. Rahul, H. Hassanieh, and D. Katabi, "SourceSync: a distributed wireless architecture for exploiting sender diversity," in *Proceedings of the ACM SIGCOMM*, pp. 171–182, August 2010.

## Bibliography

---

- [36] P. Murphy and A. Sabharwal, "Design, implementation, and characterization of a cooperative communications system," *IEEE Transactions on Vehicular Technology*, vol. 60, pp. 2534–2544, July 2011.
- [37] H. V. Balan, R. Rogalin, A. Michaloliakos, K. Psounis, and G. Caire, "AirSync: Enabling distributed multiuser MIMO with full spatial multiplexing," *IEEE/ACM Transactions on Networking*, no. 99, 2013.
- [38] T. Korakis, M. Knox, E. Erkip, and S. Panwar, "Cooperative network implementation using open-source platforms," *IEEE Communications Magazine*, vol. 47, no. 2, pp. 134–141, 2009.
- [39] G. Bradford and J. N. Laneman, "A survey of implementation efforts and experimental design for cooperative communications," in *Proceedings of the IEEE ICASSP*, pp. 5602–5605, March 2010.
- [40] G. Bradford and J. N. Laneman, "An experimental framework for the evaluation of cooperative diversity," in *Proceedings of the IEEE CISS*, pp. 641–645, March 2009.
- [41] M. Knox and E. Erkip, "Implementation of cooperative communications using software defined radios," in *Proceedings of the IEEE ICASSP*, pp. 5618–5621, March 2010.

# Curriculum Vitae

AYAN SENGUPTA

EPFL IC ARNI

Building INR, Station 14

1015 Lausanne, Switzerland

Email: dilse.ayan@gmail.com

ayan.sengupta@epfl.ch

Phone: +41-78-926-58-70

## EDUCATION

---

- 2010–2014 **PhD in Computer, Communication and Information Sciences**  
École Polytechnique Fédérale de Lausanne (EPFL), Switzerland  
Advisor: Prof. Christina Fragouli
- 2006–2010 **B.Tech in Electronics and Electrical Communication Engineering**  
Indian Institute of Technology (IIT), Kharagpur, India  
GPA: 9.87/10.00

## AWARDS

---

1. **Swiss National Science Foundation Early Postdoc Mobility Fellowship** for 18 months, starting March 2015.
2. **Best Paper Award, ACM MobiHoc 2013** for the paper “Quantize Map and Forward (QMF) Relaying: An Experimental Study” co-authored with Melissa Duarte, Siddhartha Brahma, Christina Fragouli and Suhas Diggavi. The *acceptance rate* for this conference was 10 percent.
3. **President of India Gold Medal, 2010** on being adjudged to be the *best student in order of merit* among the graduating students of all **B.Tech (Hons.) & B.Arch (Hons.)** courses in IIT Kharagpur.
4. **National Talent Search (NTS) Scholarship** by the **National Council of Educational Research and Training (NCERT), India** in **2004**.

## PUBLICATIONS

---

1. S. Brahma, A. Sengupta, C. Fragouli, “**Switched Local Schedules for Diamond Networks**,” Accepted to IEEE Information Theory Workshop (ITW), 2014.
2. A. Sengupta, I.-H. Wang, C. Fragouli, “**Cooperative Relaying at Finite SNR – Role of Quantize Map and Forward**,” in IEEE Transactions on Wireless Communications, vol. 13, issue 9, pp. 4857–4870.
3. S. Brahma (*co-primary*), A. Sengupta (*co-primary*) and C. Fragouli, “**Efficient Sub-network Selection in Relay Networks**,” in IEEE International Symposium on Information Theory (ISIT), pp. 1927–1931, June 2014.
4. S. Brahma (*co-primary*), M. Duarte (*co-primary*), A. Sengupta (*co-primary*), I.-H. Wang, C. Fragouli and S. Diggavi, “**QUILT: A Decode/Quantize Interleave Transmit Approach to Cooperative Relaying**,” in Proceedings of IEEE International Conference on Computer Communications (INFOCOM), pp. 2508-2516, Apr. 2014. (*Acceptance Rate: 19%*)
5. M. Duarte, A. Sengupta, S. Brahma, C. Fragouli and S. Diggavi, “**Quantize Map Forward (QMF) Relaying: An Experimental Study**,” in Proceedings of the Fourteenth ACM International Symposium on Mobile Ad Hoc Networking and Computing (MobiHoc), pp. 227-236, Aug. 2013. (*Acceptance Rate: 10%*)
6. A. Sengupta, I.-H. Wang, and C. Fragouli, “**Optimizing Quantize Map and Forward in Slow Fading Relay Networks**,” in Proceedings of Annual Allerton Conference on Communications, Control, and Computing, pp. 1928-1934, Oct. 2012.
7. A. Sengupta, I.-H. Wang, C. Fragouli, “**Optimizing Quantize Map and Forward Relaying for Gaussian Diamond Networks**,” in IEEE Information Theory Workshop (ITW), pp. 381-385, 3-7 Sept. 2012.
8. A. Sengupta, S. Brahma, A. Ozgur, C. Fragouli and S. Diggavi, “**Graph-based Codes for Quantize Map and Forward Relaying**,” in IEEE Information Theory Workshop (ITW), pp. 140-144, Oct. 2011.

## REFERENCES

---

Prof. Christina Fragouli  
Department of Electrical Engineering  
University of California, Los Angeles  
Email: christina.fragouli@ucla.edu

Prof. Suhas Diggavi  
Department of Electrical Engineering  
University of California, Los Angeles  
Email: suhas@ee.ucla.edu